AEROSOL FORMATION FROM ORGANIC GASES BY ULTRAVIOLET RADIATION(Dissertation_全文)

AUTHOR(S):

Sekiya, Takashi

AEROSOL FORMATION FROM ORGANIC GASES BY ULTRAVIOLET RADIATION

by

Takashi SEKIYA

December 1986

Kyoto University

Kyoto, Japan

AEROSOL FORMATION FROM ORGANIC GASES BY ULTRAVIOLET RADIATION

by

Takashi SEKIYA

December 1986

Kyoto University

Kyoto, Japan

ACKNOWLEDGEMENTS

The author would like to express his sincere appreciation to Professor Toru Ogawa for his continuous guidance, many stimulating suggestions and discussions throughout the present work. The author is deeply grateful to Dr. Tsutomu Yabuzaki for many helpful discussions, educational suggestions and encouragements.

The author also wish to express his deep appreciation to Professors Susumu Kato and Iwane Kimura for their valuable comments and helpful suggestions.

It is a willingness of the author to acknowledge the helpful suggestions and the critical reading of the manuscript of Dr. Masao Kitano, especially to his comfortable textFOmatter.

Experiments in Chapters 2 and 3 were performed with the help of Messrs. Masanobu Watanabe, Yozo Nishiura and Hiromitu Ogura. It is a pleasure to acknowledge their help and cooperation.

The author appreciates the help and encouragements of Dr. Minoru Tsutsui and other staffs of Radio Atmospheric Science Center and Professor Kimura's group.

Numerical calculation in Chapters 3 and 4 were partly preformed at the Data Processing Center of Kyoto University.

ABSTRACT

This thesis concerns with aerosol formation from various kinds of organic gases, especially conditions of formation and particle size distribution under several experimental conditions.

The word aerosol means the state in which solid particles or liquid droplets, or mixture of them are floating in a certain gas. There are many kinds of aerosols in nature, e.g. dust risen by wind, sea spray, volcanic dust, rainy cloud, fog, etc.

The aerosols which take their origin from vegetation are estimated to reach 1/4 of all atmospheric aerosols. They are organic aerosol. Photochemical smog, which is believed to take its origin from human activities such as exhaust of factories and automobiles is important from the view point of environmental problems. They are believed to be more or less concerned with the photochemical aerosol production related to organic compounds.

Aerosols include many interesting subjects from the view points of physical and chemical studies. Especially knowledge about the aerosol formation related to photochemical processes with organic compounds are limited yet.

In this thesis, it will be reported that many kinds of organic compounds such as dichlorobenzene, pinene, etc. produce aerosols when exposed to ultraviolet (UV) radiation of wavelengths shorter than about 310 nm from a deuterium lamp (D_2 lamp). The effective wavelength is much shorter than that for photochemical smog. This thesis will be devoted to the study

about these organic aerosols.

These compounds can be classified according to whether they produce aerosol or not when exposed to the monochromatic UV radiation from a KrF excimer laser (λ=249 nm) or exposed to ozone in the absence of UV radiation. The compounds such as aniline, phenol and α-pinene are active with both stimulations. The compounds such as dichlorobenzene and toluene are active with only UV radiation. The compounds such as benzoic acid and camphene are inactive with both stimulations. The compound is not found which is active with only ozone. These differences are discussed.

Next the temporal change in the particle size distribution of the aerosol produced from p-dichlorobenzene by continuous exposure to UV radiation with wavelength 220 nm, with power density about 1 mW/cm^2 is optically measured. Two laser beams with different wavelengths are applied into the aerosol as probes, and the dependence of the scattered light intensity on the polarization and wavelength are measured. The measured dependence are compared with the theoretically calculated dependence, which are given by assuming the size distribution function which has several adjustable parameters. These parameters are adjusted so that the calculated and the measured dependence give good agreement.

As a result, most probable particle size distribution is obtained at each sampling time. Based on its temporal change, the process of aerosol growth is discussed in detail. First many particles of radii smaller than 0.1 μm are produced homogeneously. The peak number density is about 3×10^6 $particles/cm^3$. Then particles grow mainly by coalescence. In about 20 minutes,

the stable state is established. The most frequent radius is 0.2 μm, the number density is about 5×10^5 particles/cm^3 and the total volume density is about 1.5×10^4 μm^3/cm^3. The breadth of the distribution first becomes broader, but becomes narrower as coalescence progresses, and at the stable state, the distribution is near monodisperse.

By using the same technique, another temporal change of the particle size distribution is studied, where, unlike the previous measurement, the aerosol is rapidly produced by brief exposure to UV radiation from a KrF excimer pulse laser. The condensable species are produced by applying several UV light pulses from KrF laser at the beginning, then the temporal change of the particle size distribution is observed without applying any more UV light pulses.

The measured size distribution is largely different from that obtained in previous experiment. The sharpening of the distribution is not found. The distribution is developed rapidly in the initial brief time (about less than 30 sec), then it was spread broadly and its wing reached the radii of 0.3 μm.

The aerosol formation experiments using a fully airtight cell filled with pure argon (Ar) gas are also performed in order to study the influence of surrounding gas, especially oxygen (O_2), on aerosol formation. P-dichlorobenzene and α-pinene are tested. The UV light source used here is the D_2-lamp.

In both cases, the aerosol production is observed. However there is a significant difference as follows. In the absence of O_2, a large amount of aerosol is produced from p-dichlorobenzene and the products are fully stable. As to the aerosol formation from p-dichlorobenzene, the presence of O_2 plays no significant

role. On the other hand, the aerosol produced from α-pinene in the absence of O_2 is not stable and disappears soon. To stabilize it, the presence of O_2 in the surrounding gas is indispensable. The stability of products may be caused by oxidation.

From the attempt to identify the products by gas-chromatograph-mass-spectroscopy, two kinds of pinene-monoxide, α-campholene aldehyde and iso-pinocamphene are found in the products from α-pinene. On the other hand, the constituents of products from p-dichlorobenzene is not identified.

The aerosol producibility of p-dichlorobenzene is much higher than other compounds. Then in order to study the influence of chlorine (Cl) in a raw material molecule on the aerosol formation, aerosol producibilities of kinds of chlorobenzenes are studied. The result is as follows. The aerosol producibility of dichlorobenzene is the highest. Then those of mono- and trichlorobenzene follow. The aerosol producibilities of tetra- and hexachlorobenzene are much smaller than those of previous three. The number of Cl in a molecule seems not to correlate the aerosol producibility. The geometrical feature of molecule may be more dominant.

CONTENTS

CHAPTER 1

GENERAL INTRODUCTION

1.1 Aerosols

The word aerosol means the state in which solid particles or liquid droplets, or mixture of them are floating in a certain gas as shown in Fig. 1.1. Usually a group of particles whose radii are from 10^{-4} to 10^{2} μm is called aerosol. Rainy cloud, fog, smoke of cigarette etc. are examples of aerosols. There are many kinds of aerosols in nature, e.g. dust risen by wind, sea spray, meteoric dust, volcanic dust, dust from forest fire, rainy cloud,

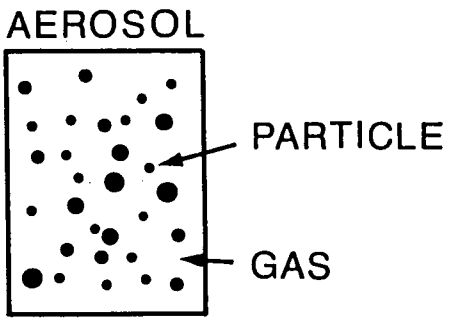

Fig. 1.1 The word aerosol means the state in which small particles are floating in a certain gas.

fog, haze of the mountain, etc. as shown in Fig. 1.2.[1~7)]

Since Went pointed out,[8)] it has been believed that volatile oils secreted from plants react with ozone and produce aerosols. Haze over a forest or a mountain is thought to be one of such organic aerosols.[9~14)] The aerosol which takes its origin from vegetation is estimated to reach 1/4 of all atmospheric

Fig. 1.2 Various aerosols.

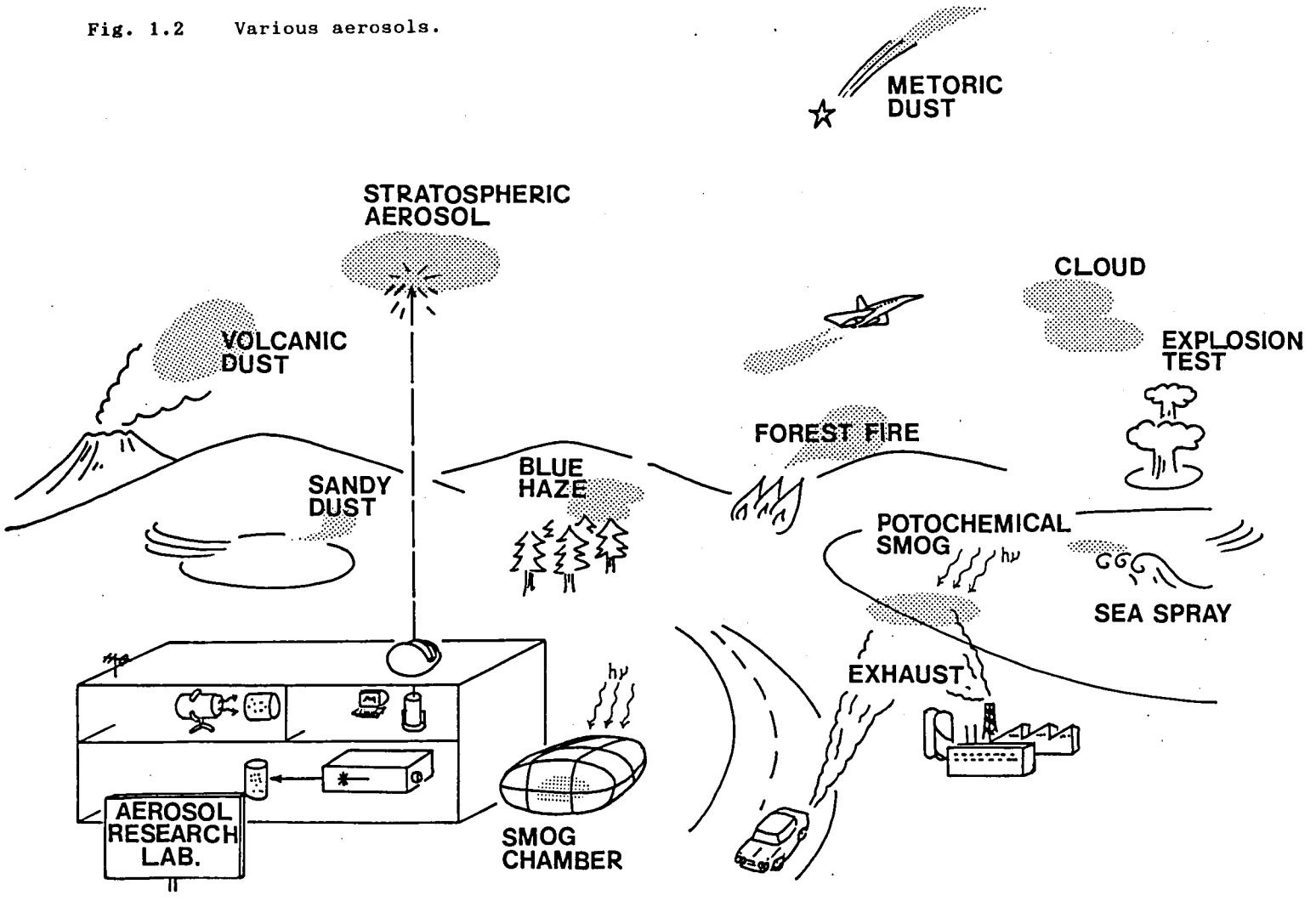

aerosols. On the other hand, there are many inorganic aerosols in nature such as sea spray, volcanic ash, sandy dust, etc.[1)]

Some of natural aerosols are produced by mechanical forces such as smashing and others are produced through chemical processes such as photochemical smog. So the natural aerosols are extremely diverse from both view points of origin and constituent.

On the other hand, there are aerosols which have their origin from human activity. Smoke or dust from industry or traffic decreases visibility and threatens our health.[3,14)] Radioactive aerosol from accident of nuclear reactor or nuclear explosion test are recognized as environmental problem. The photochemical smog is also believed to take its origin from exhaust of factories and automobiles.[14,16)] That is an annual threat in summer.

Recently there are many attempts to utilize various aerosols in pharmacy, medicine, and engineering. Spray of medicine and paint are popular.

A clean room for semiconductor industry or laboratory hardly hates the dust such as aerosol. In this field, the technique of aerosol handling is applied to monitor dust and remove it.

Fine particles of submicron size have large surface to volume ratio and sometimes show high chemical activity or other new characteristics which cannot be expected from the analogy of the characteristics in bulk. It may not be suitable to classify the fine particle into aerosols, for the word fine particle does not necessarily mean the state of particles floating in a certain gas. However, both have common characteristics. They are expected to be some new material in the next generation.

Cluster is a group of a number of atoms or molecules, which are bound with a weak force such as van der Waals' force. Cluster is one of aerosols, and its beam is utilized as a convenient method to transport materials onto a substratum such as silicon wafer. This may be one of the aerosol application.

As presented above, aerosols are very familiar to us. In addition, aerosols include many interesting subjects from the view points of physical and chemical studies.[3,4] When the diameter of aerosol particle becomes comparable with the mean free path of surrounding gas molecules, the hydrodynamics of aerosol becomes very complex, for the size of particle fall in the range where it becomes invalid to treat the surrounding gas as continuous medium.

In the gravity, aerosols are generally unstable because of the gravitational settling. However the life time of the submicron aerosol particles that go into the stratosphere reaches more than years. The stratospheric aerosols are believed to be concerned with the thermal balance of the earth and to have some influences upon the climate, for instance, cold weather caused by eruption of volcano.[1,5]

The diffusion of aerosol in the atmosphere is also complex problem. Recently the invention of a laser radar enable us to monitor the stratospheric aerosol continuously. In addition, the technology of deep space exploration such as Voyager Mission enable us to discuss the atmospheric aerosols on the planets or satellite other than the earth.[17] As to the behavior of aerosols on the earth and the influence upon the global climate, the researches have just started.

Since the size of aerosol particles become comparable with

the wavelengths of visible light, the characteristics of light scattering becomes peculiar. In this range, the treatment based on the Rayleigh scattering becomes invalid and the treatment based on the Mie theory is necessary.[3,4,18,19] If the shape of particle is not sphere, problem becomes more complex. The light scattering of aerosol in the air influence the visibility, in addition, is believed to be largely concerned with the thermal balance of the earth or other celestial bodies as mentioned before.

Our knowledge about those various features of aerosols are limited yet in spite of its long history of studies. Many questions remain to be studied, for instance, total amount of aerosol in nature, its origin, constituent, physical and chemical processes of formation and growth (including photochemical processes, gas-to-particle conversion, temporal change of particle size distribution and its driving force, etc.), hydrodynamical behavior, light scattering characteristics, influence upon human health or global climate, and applicability for new material engineering.

1.2 Photochemical Aerosols

Photochemical aerosol formation is one of the most important subjects in aerosol studies. The research on photochemical aerosols covers from photochemical smog, blue haze over a forest or a mountain, stratospheric aerosol on the earth and other planet or satellite, to some artificial aerosols.

The sunlight related to the photochemical smog (hereafter we will consider the aerosol on the earth) are limited in visible range.[20,21] Since the ultraviolet rays in solar radiation is cut

by thick air and ozone layer at upper atmosphere, it cannot reach so lower atmosphere near the ground level as to contribute to the photochemical aerosol formation. In this respect, nitrogen dioxide (NO_2) is the only absorber at the lower atmosphere related to photochemical smog.[21] NO_2 is included in exhaust from factories and automobiles. NO_2 absorbs the light of visible range and dissociates. As a result, O, O_3, NO, NO_3, N_2O_5 and HNO_3 are produced as

$$NO_2 + h\nu \longrightarrow NO + O \quad 290<\lambda<430 \text{ nm}, \quad (1.1)$$

$$O_2 + O + M \longrightarrow O_3 + M, \quad (1.2)$$

$$O_3 + NO_2 \longrightarrow NO_3 + O_2, \quad (1.3)$$

$$NO_2 + NO_3 \longrightarrow N_2O_5 \quad (1.4)$$

and

$$N_2O_5 + H_2O \longrightarrow 2HNO_3 . \quad [21] \quad (1.5)$$

If the atmosphere contains organic compounds, series of very complicated reactions take place, and, as a result, many kinds of radicals or active molecules such as CO, C_2H_5, HCO, OH, O, O_3 are produced. They attack organic compounds and produce condensable species of low vapor pressure, leading to be aerosol particles.[14] In addition, if the atmosphere includes SO_2, SO_2 is oxidized by reactions with these radicals, as a result, mist of sulfuric acid is produced. The mist of sulfuric acid is one of the causes of pungency of photochemical smog. SO_2 is also an absorber of sunlight other than NO_2 as follows,

$$SO_2 + h\nu \longrightarrow {}^1SO_2^* \quad 290<\lambda<330 \text{ nm}, \quad (1.6)$$

$$^1SO_2^* + M \longrightarrow {}^3SO_2^* + M \qquad (1.7)$$

$$^3SO_2^* + O_2 + M \longrightarrow SO_4 + M\ , \qquad (1.8)$$

$$^3SO_2^* + O_2 \longrightarrow SO_3 + O \qquad (1.9)$$

and

$$SO_3 + H_2O \longrightarrow H_2SO_4\ ,^{21)} \qquad (1.10)$$

where $^1SO_2^*$ and $^3SO_2^*$ represent the excited singlet state and the excited triplet state of SO_2 respectively. The photochemical oxidation of SO_2 described above is, however, too slow to contribute in production of sulfuric acid. The photooxidation of SO_2 is negligible compared with the oxidation by the reactions with other radicals.[21] This is the outline that has been recognized as processes of photochemical smog so far.[14,21,22] However, our knowledge is limited yet about the constituents of organic aerosols produced through these reactions, the details of complex photochemical processes including organic compounds, the mechanisms of particle growth, etc.

The haze which can be seen over a forest or a mountain is called "blue haze".[8] Its blue color is the origin of the name "blue mountain", which is popular as a name of mountain all over the world. Blue haze is believed to have its origin from terpenes, volatile oils secreted from plants. Terpenes quickly react with ozone, where ozone is produced photochemically in the atmosphere. As a result, oxides of low vapor pressure are produced. The oxidized terpenes condense and form chemically stable aerosols. The size of produced particles are smaller than the wavelength of visible light, so that they strongly scatter

light in blue range, namely they look blue.[8,11,12]

There are photochemical aerosols produced artificially in laboratories.[18,23~29,46] "Laser snow" is one of the aerosols produced by laser-induced photochemical reactions. The aerosol is produced from the mixture of gaseous alkali and hydrogen under the exposure to the laser beam from a dye or an argon ion laser (for example, λ=488.0 nm for NaH laser snow). The product has been identified as alkali hydride crystalline particle.[18,23~25]

"Benzene aerosol" is produced from the vapor of benzene under the exposure to ultraviolet rays from a krypton fluoride excimer laser (KrF laser, λ=249 nm). The constituent of product has not been identified.[26~29]

Many experiments have been done to simulate photochemical smog. In many types of smog chambers, kinds of compounds have been tested under the irradiation of sun light as well as simulated light sources such as a mercury lamp.[9,14,15,30~37] Today, many kinds of organic and inorganic compounds are recognized as causes of photochemical smog, and the guides in controlling air pollution are established. However, many fundamental questions remain, the constituent of products, especially of organic products, details of photochemical processes, mechanisms of aerosol growth, etc.[14]

Recently we found that many kinds of organic compounds such as dichlorobenzene, pinene, etc. produce aerosols when exposed to ultraviolet radiation (UV) of wavelengths shorter than about 310 nm.[38,51] The effective wavelength is much shorter than that for photochemical smog. In the case of photochemical smog, light in the visible range is of important. The UV radiation with such short wavelength as in the case of our organic aerosol formation

cannot reach lower atmosphere, for the thick air and the ozone layer cut it at upper atmosphere. Therefore our organic aerosols have many new features which are different from those of photochemical smog. This thesis will be devoted to the study about these organic aerosols.

As mentioned above, various kinds of photochemical aerosols are known and studied. However, our knowledge about them are limited yet. There are many problems to be studied. This work aims to shed light on some subjects of aerosols through the aerosol produced from organic compounds by UV radiation. We hope this work will be an aid in aerosol researches.

1.3 Outline of Present Work

In this thesis, we present the photochemical aerosol formation from twenty kinds of organic compounds by UV radiation.

We first discovered the phenomena by chance when we were working over a hand-made argon ion laser(Ar^+ laser).[38] Hating that dusts in the air across the light pass of the Ar^+ laser, we covered the light pass from the Brewster window to the output mirror with a transparent glass tube. In a few minutes, a large amount of aerosol was produced in the tube (Fig. 1.3). The particles scattered the laser beam strongly. The photochemical aerosol formation was not induced by laser emission, for the aerosol was produced when the electric discharge occurred without laser emission. The aerosol was found to be produced by the UV radiation from the Ar discharge tube. The material origin was estimated to be a small amount of organic compound in the air of laboratory. Since the discovery, we have tested various organic compounds, mainly aromatics and terpenes, changing the UV radia-

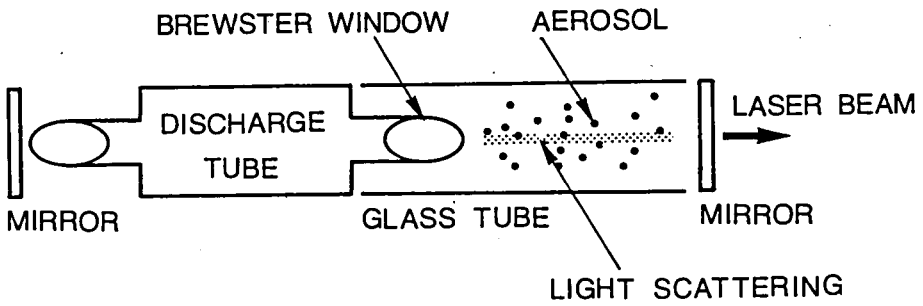

Fig. 1.3 Experimental setup for aerosol formation with a discharge tube of argon ion laser.

tion source from the Ar discharge tube to a deuterium lamp (D_2-lamp) or a KrF excimer laser.[51]

Let us illustrate the aerosol formation from p-dichlorobenzene by UV radiation from the D_2-lamp. We put a bit of p-dichlorobenzene, which is powder of white crystal at room temperature, at a bottom of 50 cc cylindrical glass cell, for example, a beaker (Fig. 1.4). Holding the mouth of the cell to the window of the D_2-lamp, which radiates the UV radiation of continuous spectrum from 180 to 400 nm in wavelengths, we turn the lamp on. In a few seconds, white smoke appears in the the cell. The aerosol formation from p-dichlorobenzene is observed in this way.

Chapter 2 is devoted to such aerosol formation experiments, where we use two kinds of UV radiation sources, the D_2-lamp and the KrF excimer laser. The former radiates the UV light with a continuous spectrum from about 180 to 400 nm. The latter radiates the monochromatic UV light with wavelength 249 nm. In

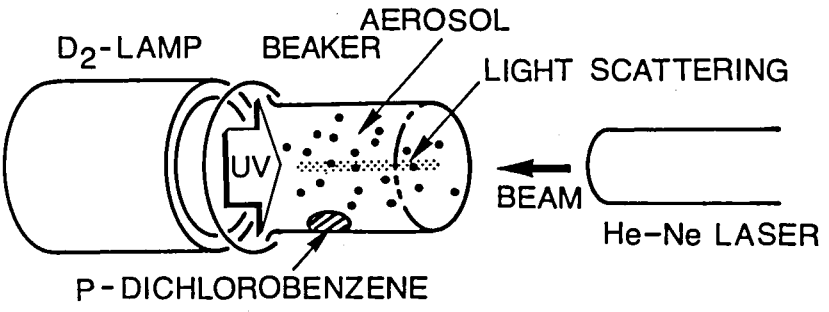

Fig. 1.4 Experimental setup for aerosol formation with a deuterium lamp (D_2-lamp).

this experiment, we test more than twenty kinds of organic compounds, such as p-dichlorobenzene and α-pinene. In addition, we study the aerosol producibility of organic compounds when they react with O_3 in the absence of UV radiation. We discuss possible chemical processes to produce aerosols in the different experimental situations described above.

In Chapters 3 and 4, we report on the measurements of size distribution of the aerosol produced from p-dichlorobenzene and its temporal change. Our measurement is based on the wavelength- and polarization-dependence of light scattering from the produced aerosol particles.[71)]

In Chapter 3, we describe at first on the principle of measurement and propose its application to the measurement of particle size distribution of aerosol produced from p-dichlorobenzene under the UV irradiation from the D_2-lamp. Based on the measured temporal change of size distribution, we discuss the processes of aerosol growth in detail. In Chapter 4, we

present the similar measurements of size distribution of aerosol produced by UV radiation from the KrF laser. We apply UV radiation pulses from the KrF laser only at the beginning, whereas in the case of D_2-lamp, the UV radiation is continuously applied. Difference between these cases are discussed. The raw material of aerosol is p-dichlorobenzene in both measurements.

In Chapter 5, we attempt several experiments to study various properties of the aerosol and its formation. Using an airtight cell, we try to produce aerosol in pure Ar gas, which is aiming to make clear the role of O_2 in the photochemical processes. We test both p-dichlorobenzene and α-pinene.

We also try to identify the constituents of product by gas-chromatograph-mass-spectroscopy and infrared-spectroscopy. In addition, the differences of aerosol formations from mono-, di-, tri-, tetra- and hexachlorobenzene are discussed.

Chapter 6 is devoted to the general conclusions. We will summarize the present work.

CHAPTER 2

PHOTOCHEMICAL AEROSOL FORMATION FROM ORGANIC GASES

2.1 Introduction

A large part of aerosols in the atmosphere is believed to take its origin from vegetation.[1] Organic compounds such as terpenes, which are the volatile oils secreted from plants, produce aerosols by reactions with ozone (O_3) in the air.[9~12,14,39] The haze over a forest or a mountain is believed to be produced in this way. On the other hand, the aerosols that take their origin from the petroleum industry are important from the view of environmental problem.[14,16] Organic compounds such as aromatics are believed to contribute largely to the outdoor photochemical smog. Contrary to the case of terpenes, aromatics are generally low reactive with ozone.[14,40,41]

In this way, the organic aerosol formation is known to play an important role in the outdoor photochemical smog. However there are sill many problems to be researched; constituents of products, physical and chemical, especially photochemical processes of aerosol formation and growth, influence on visibility and human health, etc.

In this chapter, we show that twenty kinds of organic gases such as p-dichlorobenzene (aromatic) or α-pinene (terpene) produce aerosol in the air under the exposure to the ultraviolet (UV) radiation.[51] The aerosol formation from such gases can easily be observed even in a very simple setup as mentioned in Sec. 1.3 (Fig. 1.4), which consists of a beaker and a deuterium

lamp (D_2-lamp) emitting the UV radiation with a continuous spectrum of wavelength from 180 to 400 nm. The raw material, for example a small amount of powder of p-dichlorobenzene, is put in the beaker, then it is sealed roughly with the window of the D_2-lamp. In a few seconds after the switch-on, one may find the appearance of white smoke in the beaker. When some visible laser beam such as a helium neon laser (He-Ne laser) is applied, the strong light scattering from produced particles is observed.

Though the effective wavelength to produce the aerosol is different a little for each compound, the compound which produce aerosol by the UV radiation with wavelengths longer than about 310 nm is not found so far. The UV radiation with wavelengths shorter than about 310 nm is essential to produce the aerosol. These wavelengths are much shorter than in the case of lower atmospheric photochemical aerosol.[5,20,21,42] The UV radiation of such short wavelengths in the solar radiation cannot reach the lower atmosphere near the ground level because of the absorption at upper atmosphere.

The D_2-lamp we used as a UV radiation source radiates continuous spectrum from 180 to 400 nm in wavelengths, which can excite and/or dissociate the organic molecules and also produce ozone from the air as well. Both of these processes can contribute to the aerosol formation. To separate these two effects, we used a krypton fluoride excimer pulse laser (KrF laser) operated at the wavelength 249 nm, which is too long to produce ozone, whereas it can excite organic molecules. We found sixteen kinds of organic compounds of the twenty produce aerosol by the KrF laser.

On the other hand, it is known that organic compounds such

as α-pinene produce aerosol by reaction with ozone.[8,9,14,35,39,43] To make clearer roles of ozone, we also studied the aerosol productions from organic gases by the reaction with ozone in the absence of UV light.

Two types of laser-induced aerosol formations have been reported so far; "Laser Snow" and "Benzene Aerosol". The Laser Snow is the particles produced when the alkali-metal atoms and molecules mixed with hydrogen gas are exited by a dye or an Argon ion laser. The product has been identified as alkali hydride crystalline particle.[18,23~25] Benzene Aerosol is produced from the vapor of benzene under the exposure to the UV radiation from a KrF excimer laser. The constituent of product has not been identified so far.[26~29] Benzene Aerosol may be largely concerned with our organic aerosol.

2.2 Aerosol Production Experiments with Ultraviolet Radiation and Ozone

2.2.1 Aerosol Formation with Ultraviolet Radiation

The organic compounds that we studied are listed in Table 1. They belong to aromatics, cycloalkanes or terpenes. The compounds marked with * in Table 1 are those known to be more or less concerned with the origin of the outdoor photochemical smog. The photochemical aerosol formations from the gases containing those compounds are observed so far in several smog chamber experiments.[9,13,14,35,40,41]

The experimental setup is shown in Fig. 2.1. We put a few bits of or a few droplets of the compound in the cell. The cell was $1\times2\times4.5$ cm^3 in dimension and made of quartz which was transparent to UV radiation of wavelengths longer than 180 nm. It

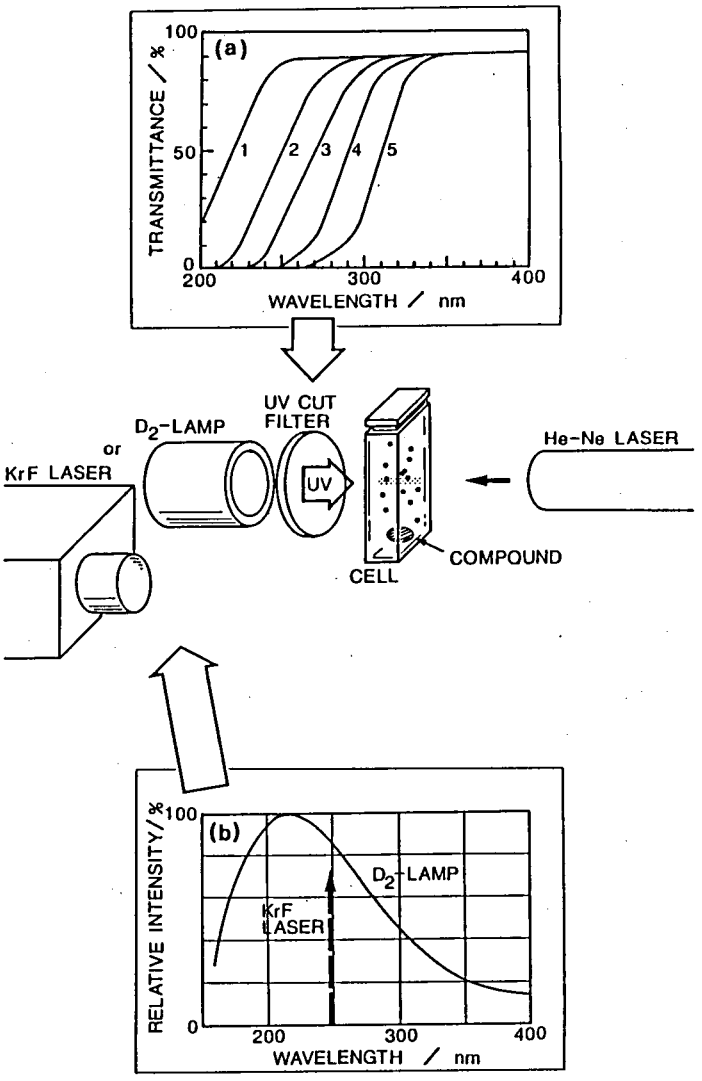

Fig. 2.1 Experimental setup for photochemical aerosol formation by ultraviolet (UV) radiation. (a) Transmittance characteristics of UV-cut filters (1~5) used to determine the threshold wavelength of UV light in photochemical aerosol formation, and (b) spectra of radiations of two UV light sources, the deuterium lamp (D_2-lamp) and the krypton fluoride excimer laser (KrF laser).

was filled with clean and particle-free air at 1 atm, at room temperature.

We used two UV radiation sources. One was a D_2-lamp with 5 cm in diameter, which radiates the UV light with a continuous spectrum from 180 to 400 nm in wavelength as shown in Fig. 2.1(b). The total power density was about 200 mW/cm^2 at the position of the cell. The other was a pulsed KrF laser which radiates monochromatic light with wavelength 249 nm as shown in Fig. 2.1(b). The power density was about 100 mJ/cm^2 per a pulse at the position of the cell.

The formation of aerosol was detected by monitoring the light scattering of a He-Ne laser. In the case of the D_2-lamp, we applied the UV light to the cell for a few minutes, and observed whether aerosol was produced or not. In the case of the KrF laser, we applied the several UV light pulses and observed.

Inserting UV-cut filters of different cutoffs between the D_2-lamp and the cell, we determined the longer limit of the UV radiation wavelengths effective in producing aerosol. The filters used here had their cutoff wavelengths at 220, 250, 270, 290 and 310 nm respectively as shown in Fig. 2.1(a).

2.2.2 Aerosol Formation with Ozone in the Absence of Ultraviolet Radiation

To study the reaction of each compound with ozone in the absence of UV light, we performed the additional experiments with a setup shown in Fig. 2.2. Ozone was produced by the electrical discharge in the flow of oxygen (O_2), then it was led into the cell which contains one of the compounds. The cell was carefully isolated from the UV radiation due to the discharge. Then we

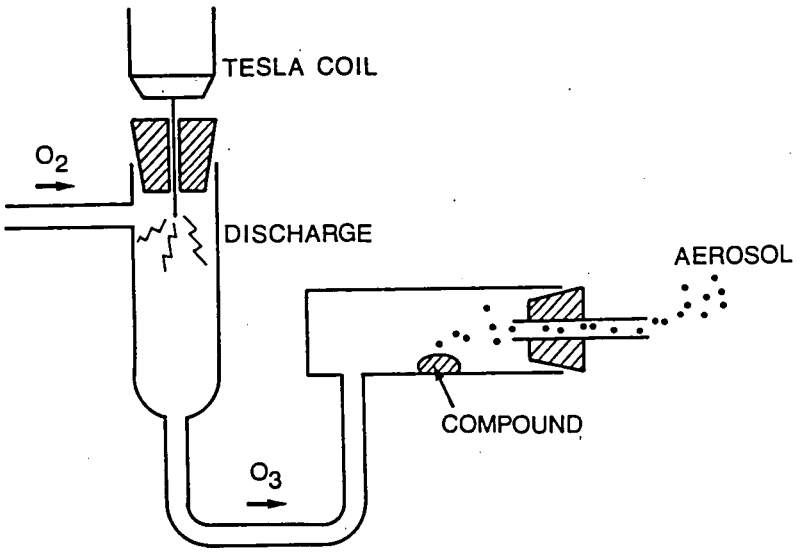

Fig. 2.2 Experimental setup to study the activity of each compound with ozone. Ozone is produced by gaseous discharge.

observed whether the aerosol was produced or not.

2.3 Experimental Results

The experimental results are shown in Table 2.1. In the case of the D_2-lamp, all of the tested compounds produce aerosol. Among these compounds, benzoic acid, diphenyl, cyclohexane, camphene and camphor do not produce aerosol in the case of the KrF laser. As to the experiments with ozone, aniline, phenol and styrene in aromatics and α- and β-pinene, isoprene and limonene in terpenes produce aerosol by reaction with ozone in the absence of UV light.

The value λ_{th} in Table 2.1 represents threshold wavelength, i.e. the radiation with wavelength longer than λ_{th} does not contribute to aerosol production. The cutoff characteristics of

		D_2-lamp	KrF-laser	ozone	λ_{th} (nm)
AROMATICS					
aniline	$C_6H_5NH_2$	○	○	○	310
phenol	C_6H_5OH	○	○	○	250
styrene*	$C_6H_5CH=CH_2$	○	○	○	310
benzene*	C_6H_6	○	○	×	310
chlorobenzene	C_6H_5Cl	○	○	×	290
o-dichlorobenzene	$C_6H_4Cl_2$	○	○	×	270
m-		○	○	×	310
p-		○	○	×	270
naphthalene	$C_{10}H_8$	○	○	×	220
toluene*	$C_6H_5CH_3$	○	○	×	250
xylene*	$C_6H_4(CH_3)_2$	○	○	×	250
benzoic acid	C_6H_5COOH	○	×	×	220
diphenyl	$C_6H_5-C_6H_5$	○	×	×	220
CYCLOALKANE					
cyclohexane	C_6H_{12}	○	×	×	220
TERPENES					
α-pinene*	$C_{10}H_{16}$	○	○	○	310
β-*		○	○	○	250
isoprene*	C_5H_8	○	○	○	250
limonene*	$C_{10}H_{16}$	○	○	○	250
camphene	$C_{10}H_{16}$	○	×	×	220
camphor	$C_{10}H_{16}O$	○	×	×	220

○ ..... aerosol observed

× ..... no aerosol observed

Table 2.1 Raw materials of organic aerosols. The compounds marked with * are believed to be more or less concerned with photochemical smog.[14)]

UV-cut filters used to determine the threshold wavelength λ_{th} are not sharp so that there remains the uncertainty of the threshold value λ_{th}. However we know that the radiation of wavelengths at least shorter than about 310 nm is indispensable for aerosol production and the value of λ_{th} is dependent on the compound.

2.4 Discussions and Conclusions

All the tested compounds produce aerosol under the exposure to the UV radiation from the D_2-lamp. Many other compounds are expected to produce aerosol under the similar conditions.

The spectrum of the UV radiation from the D_2-lamp spreads continuously from 180 to 400 nm in wavelength. Many of organic compounds have their absorption bands in this range, so they are expected to be excited or dissociated by the UV radiation from the D_2 lamp;

$$X + h\nu \text{ ---> } X^*, \qquad (2.1)$$

where X represents the organic molecule, and X^* represents its excited molecule. As a result of the reaction above, a certain condensable molecule X' is produced by the reaction with another molecule or by dissociation;

$$X^* \text{ ...> } X' . \qquad (2.2)$$

Then X' is condensed to be aerosol;

$$(X')_n \text{ ...> aerosol} . \qquad (2.3)$$

Let us call the process of this type "the process related to light absorption".

Under our experimental conditions, there are some possible UV absorbers in addition to organic compounds, e.g. oxygen (O_2),

nitrogen (N_2), water (H_2O) and carbon dioxide (CO_2) in the air. These molecules are known[21] to absorb the radiation with wavelength shorter than about 250 nm and dissociate;

$$O_2 + h\nu \longrightarrow O + O \qquad \lambda<242 \text{ nm}, \qquad (2.4)$$

$$H_2O + h\nu \longrightarrow O + OH \qquad \lambda<242 \text{ nm}, \qquad (2.5)$$

and

$$CO_2 + h\nu \longrightarrow CO + O \qquad \lambda<228 \text{ nm}. \qquad (2.6)$$

With respect to nitrogen (N_2), the wavelengths of the radiation from the D_2-lamp are too long to dissociate it.

The radicals produced in reactions (2.4)~(2.6) may react with organic molecules studied here and produce some condensable species. Especially we pay attention to the reaction (2.4), which leads to the production of ozone (O_3). Ozone may oxidize partially some of organic compounds studied here and produce condensable compounds;

$$O_2 + h\nu \cdots\rangle O_3, \qquad \lambda<242 \text{ nm} \qquad (2.7)$$

$$O_3 + X \cdots\rangle Y, \qquad (2.8)$$

and

$$(Y)_n \cdots\rangle \text{aerosol}, \qquad (2.9)$$

where Y is the oxide of compound X. Let us call this type of process "the process related to ozone", since the UV light does not play a direct role in aerosol formation.

The reactions of olefins, aromatics, terpenes, etc. with ozone and other radicals such as O or OH are studied so far, as a result, it is believed that the reactions of olefins and terpenes

with ozone contribute largely to outdoor photochemical smog, on the other hand, aromatics generally have low activity with ozone and reactions with OH radical are more important.[14,21,30,40,44,45,47~50] Of course, in the case of outdoor photochemical smog, ozone and other radicals are not produced through reactions (2.4)~(2.7). The wavelengths of the sunlight related to outdoor photochemical smog are too long to cause reactions (2.4)~(2.7) directly. Ozone and other radicals are believed to be produced as results of complicated photochemical reactions starting with the light absorption by nitrogen dioxide (NO_2), which is the only absorber of the sunlight of visible range.[21]

In our case, for the compounds that produce aerosol by the reaction with ozone in the absence of UV light, the process related to ozone must also be included in the photochemical aerosol formation. For example, α-pinene produces aerosol in both cases of the UV radiation from the D_2 lamp and ozone in the absence of UV light. Under the exposure to UV radiation, it is believed that ozone produced photochemically from the air reacts with α-pinene and produce aerosol.

Contrarily, the process related to light absorption may play major roles for the compounds that are low reactive with ozone. For example, p-dichlorobenzene produce aerosol in the only case of the UV light. Therefore photochemical process with p-dichlorobenzene is major. Though ozone may be produced under the exposure to UV radiation, it may not play major role in aerosol formation.

On the other hand, the spectrum of UV radiation from the KrF laser is monochromatic at 249 nm in wavelength. Then the process

related to light absorption may be possible, but the reactions with ozone (2.7)~(2.9) will be very slow, because it is known that ozone is not produced at this wavelength as seen the reaction (2.4). So we can neglect the process related to ozone in the case of aerosol production by the KrF laser. In this case, the initial reaction must be the UV absorption of organic molecule, i.e. the reaction (2.1). Similarly the processes related to reactions (2.5) and (2.6) must be also negligible.

Of course, complicated photochemical reactions including organic compounds may produce ozone or other active molecules as in the case of outdoor photochemical smog. However, it can be said that the photochemical production of such active species is not the initial reaction to produce aerosol. The initial reaction must be the UV absorption of organic compound, i.e. the reaction (2.1).

As mentioned already, all compounds listed in Table 2.1 produce aerosol under the presence of the UV radiation from the D_2-lamp, and some of them produce aerosol by the light from the KrF laser at 249 nm and/or by the reaction with ozone under no irradiation of UV light. So the compounds studied here can be classified into following four types.

Type 1: active to both of the the KrF laser light and ozone. Aniline, phenol, styrene, α- and β-pinene, isoprene and limonene belong to this type. Each of them has different λ_{th}, which suggests that not only the reaction with ozone but also the process related to light absorption are important to produce condensable molecules.

Type 2: active to the KrF laser light but inactive to ozone. Benzene, chlorobenzene, o- , m- and p-dichlorobenzene,

naphthalene, toluene and xylene belong to this type. They are aromatics. There is no compound of this type belonging to terpenes. As the compounds of this type have low reactivity with ozone, the process related to ozone is not dominant, and the process related to the light absorption must be essential.

Type 3: inactive to the KrF laser light but active to ozone. In this case, the light absorption by organic compounds is not essential, and only reaction with ozone is important in production of aerosol. However, as seen in Table 2.1, there is no compound belonging to this type as far as we tested.

Type 4: inactive to both the KrF laser light and ozone. Benzoic acid, diphenyl, cyclohexane, camphene and camphor belong to this type. All values of λ_{th} for this group are shorter than 220 nm, which is consistent with the inactivity to the KrF laser light at 249 nm in wavelength. Therefore the process related to the light absorption with wavelengths shorter than 249 nm or the process related to the photodissociation (2.5) or (2.6) must be essential.

As mentioned before, a hydroxyl radical OH is thought to be important in the outdoor photochemical smog related to aromatics.[14,21,50] In our cases, O, OH or CO may play the similar role. However, if the reaction (2.5) or (2.6) is dominant in all cases, the value λ_{th} must be determined as the threshold wavelength of reaction (2.5) or (2.6), which dose not explain experimentally obtained dependence of λ_{th} on the compounds.

Terpenes have been believed to react quickly with ozone and produce partially oxidized compound with low saturation pressure, which results in the production of aerosol.[8,9,14] We have,

however, found exceptions such as camphene and camphor. In addition, even terpenes, which are highly reactive with ozone, do not belong to the type 3 but to the type 1, that is, there is an additional process to produce aerosols, which is free from ozone and is related directly to the light absorption of terpenes.

In the present work, we have found twenty kinds of organic compounds that produce aerosol by the UV radiation with wavelengths shorter than about 310 nm. The roles of the UV light which can be considered are (1) to produce ozone which oxidize the compounds and (2) to excite compounds to electronically excited states and partly vibrational states in the ground state, which leads to the reaction with other molecules to produce condensable molecules. We have found that in addition to (1), (2) and the simultaneous process (1) and (2) are also important in production of aerosol, the processes depending strongly on the kind of organic compounds.

CHAPTER 3

SIZE DISTRIBUTION OF AEROSOL PRODUCED FROM P-DICHLOROBENZENE BY CONTINUOUS EXPOSURE TO ULTRAVIOLET RADIATION

3.1 Introduction

In general aerosol consists of many particles with different size. The distribution of particle size is given by a particle size distribution function. The typical definition of a particle size distribution is

$$dN = f(a)\cdot da, \tag{3.1}$$

where dN represents the number density of particles with radius between a and a+da.[3,4]

The particle size distribution changes every moment as particles grow. The mechanism to change particle size distribution is, for example, coalescence. Coalescence is the process in which two particles coalesce each other and produce one larger particle as shown in Fig. 3.1(a). The number of small particles decreases and that of larger particles increases, whereas, the total volume of particles does not change. Another typical process is condensation. Condensable molecules, which is too small to be called a particle, are condensed into particles as shown in Fig. 3.1(b). Both the number and the volume increase. There is a process called deposition. In this process, condensable molecules deposit onto a surface of larger particle, where the volume increases but the number of particles is conservative (Fig. 3.1(c)). One may say that there is no clear

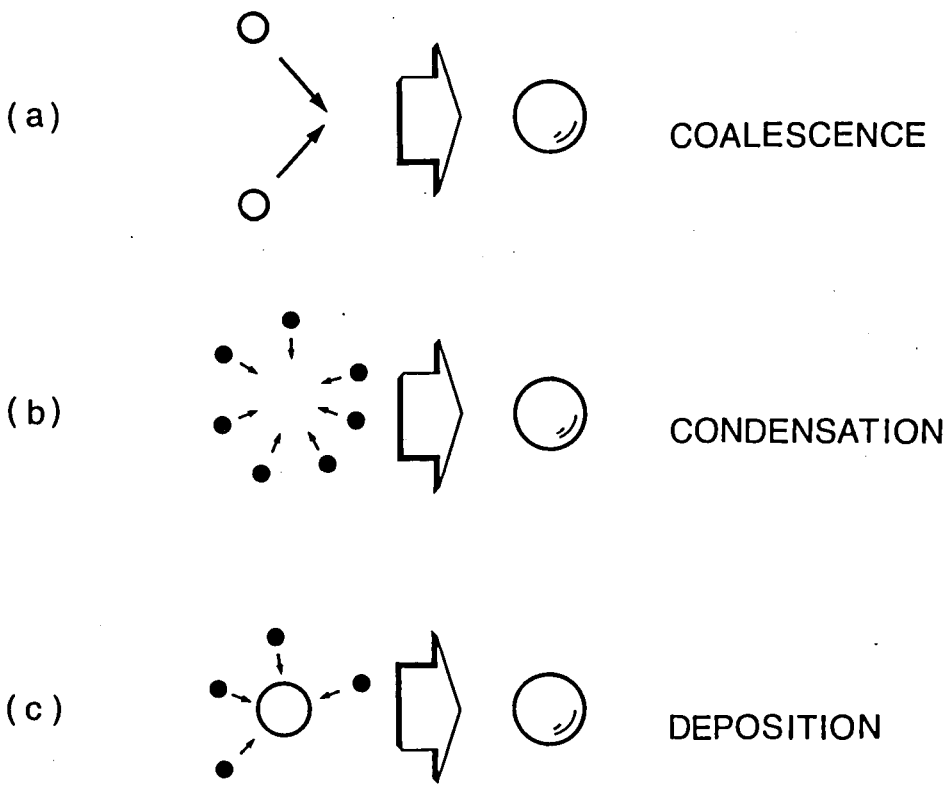

Fig. 3.1 Basic mechanisms of aerosol growth, where ● - condensable molecule and ○ - particle.

boundary between a condensable molecule and a very small particle, therefore it is nonsense to distinguish condensation from coalescence. However there is, in general, a clear gap between a molecule and a small particle. A particle which consists of a number of has a certain minimum radius. Even if the vapor of condensable molecule becomes supersaturated, the particle of radius smaller than the minimum cannot grow and will evaporate soon. If a particle of radius larger than the limit is produced by chance, it can grow.[5] Therefore we can usually dis-

tinguish a molecule and a small particle. We do not count molecules as particles. Then we call the coalescence between molecules "condensation", the coalescence between particles "coalescence" and the coalescence between molecules and particles "deposition" without confusion. In addition to this classification, the process in which molecules deposit on a particle is also called "heterogeneous nucleation", whereas, the process in which molecules condense each other without nuclei is called "homogeneous nucleation". This is the classification based on whether the nucleus as a center of deposition exists previously or not.

The temporal change of particle size distribution give us much information about these aerosol formation and growth processes. If we obtain the particle size distribution, we also know the total number (N_{total}), radius (R_{total}), surface (S_{total}) and volume (V_{total}) of particles by calculation. They are defined respectively as follows:

$$N_{total}=\int_0^\infty f(a)da \ , \tag{3.2}$$

$$R_{total}=\int_0^\infty a\cdot f(a)da \ , \tag{3.3}$$

$$S_{total}=\int_0^\infty 4\pi a^2\cdot f(a)da \ , \tag{3.4}$$

and

$$V_{total}=\int_0^\infty \frac{4}{3}\pi a^3\cdot f(a)da \ , \tag{3.5}$$

where we suppose that the produced particle is spherical. Let us consider the case that the temporal change of N_{total}, S_{total} and

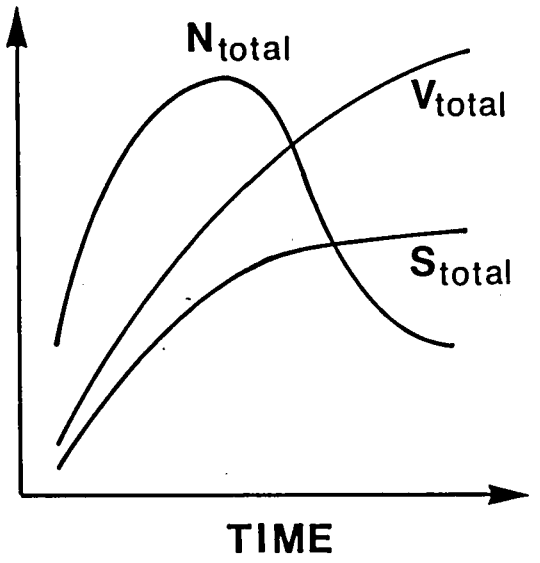

Fig. 3.2 Example of temporal changes of total number (N_{total}), surface (S_{total}) and volume (V_{total}) of aerosol particles. From this, much information is obtained about aerosol growth.

V_{total} are given as shown in Fig. 3.2. At the beginning, there is no nucleus, then supersaturated molecules condense each other, and produce many but small particles. N_{total} and V_{total} rapidly increase. Once a large number of particles are accumulated in the air, coalescence between particles occurs, as a result, N_{total} decreases. If the process of this stage is due to purely coalescence, V_{total} must be conservative. As V_{total} is increasing, we know that deposition of molecules onto a surface of large particle exists. As described above, we can know much about the aerosol growth from the changes of N_{total}, R_{total}, S_{total} and V_{total}.

The measurements of the temporal change of particle size distribution of aerosol are, however, not so many, and they mainly consider the coalescence of homogeneous oil droplets or

smoke particles.[52~54,61] As to the aerosol production by photochemical process, where homogeneous nucleation and heterogeneous one complicatedly combine together, the growth of aerosol, especially the temporal change of the size distribution has not been studied in detail so far, except for several studies.

Husar et al.[32] prepared 90 m^3 polyethylene balloon containing the environmental air, and observed the aerosol formation which occurs when the balloon is exposed to the solar radiation. They measured the size distribution of the aerosol and its temporal change with Whitby Aerosol Analyzer, and compared the results with the real Los Angeles photochemical smog. The raw material was not, however, identified.

Sato et al.[18] studied in detail the temporal change of the particle size distribution of Laser Snow. They produced aerosol from the mixture of cesium vapor and gaseous hydrogen by exposure to laser beam from an Ar^+ laser, and measured the particle size by the method based on the light scattering from particles.

As described in Chapter 2, we found that twenty kinds of organic compounds produce aerosol when the vapors are exposed to ultraviolet (UV) radiation with wavelengths shorter than about 310 nm. The raw materials mainly belong to aromatics such as p-dichlorobenzene, and terpenes such as α-pinene.[51] In this chapter, we report on the optical measurements of the temporal change of the size distribution of aerosol produced from p-dichlorobenzene ($C_6H_4Cl_2$) by UV radiation. Though p-dichlorobenzene produces much larger amount of aerosol than other materials tested in Chapter 2, it has not been drawn attention in the researches for photochemical smog.[14]

Let us here refer to the conventional measurements of particle size distributions which are based on the light scattering. The method which is based on the polarization ratio has been applied to some quasi static aerosol systems.[55~61] The outline of the method is as follows. When the incident light is nonpolarized, the polarization ratio is defined as the ratio of two components of the scattered light, the one polarized parallel and the other polarized perpendicularly to the plane of observation defined as the plane which contains the direction of propagation of incident light and the direction of observation as

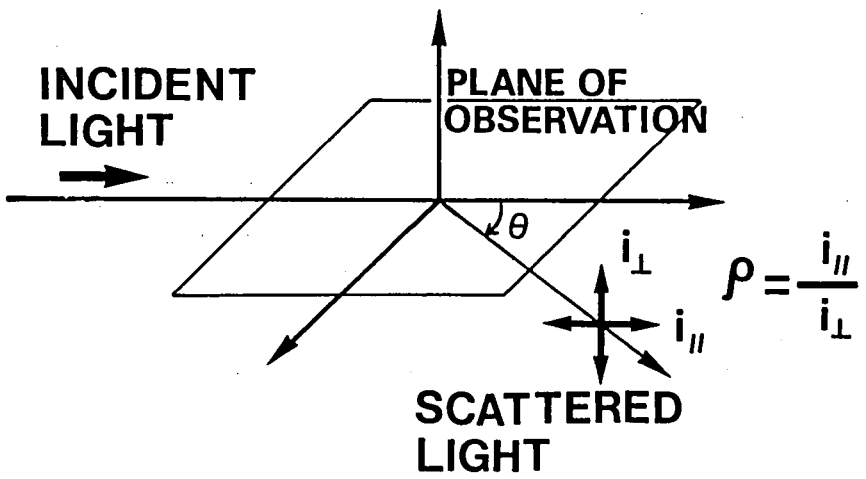

Fig. 3.3 Definition of polarization ratio ρ, where incident light is not polarized.

Fig. 3.3. The polarization ratio is very sensitive to the particle size and the angle of observation, which is defined as the angle θ between the direction of propagation of incident light and the direction of observation (Fig. 3.3). In the method

of polarization ratio, the dependence of the ratio on the angle are measured. For an assumed particle size distribution function, the dependence are theoretically calculated by the Mie formula. Comparing the theoretically calculated dependence with the measured dependence, one can determine whether the assumed function is fit or not. This is the outline of the method of the polarization ratio. Kerker et al.[61] applied this method to the colloidal sulfur and reported the temporal change of its particle size distribution. They assumed the log normal distribution function which will be mentioned later as Eq. (3.24). Assuming the Stevenson distribution function (Eq. (3.26) mentioned later), Heller et al.[56] applied the method to the measurement of particles of polystyrene.

Using the polarization ratio method, one can determine only the relative frequency of distribution because he measure only the ratio of the components of the scattered light. In our present work, we do not use the dependence of the polarization ratio on the angle of observation but the dependence of the scattered light intensities on the polarization and wavelength. We measure the absolute intensity of scattered light, which enables us to determine the absolute value of size distribution. In addition, we simultaneously assume several different distribution functions, in which the log normal and the Stevenson are also included, and compare their advantages and disadvantages.

We first produce aerosol from the vapor of p-dichlorobenzene by continuous irradiation of UV radiation. Then we apply two laser beams with different wavelengths into aerosol as probes, and measure the dependence of the scattered light intensity on the polarization and wavelength at the angle of

observation θ=90°. The measured dependence are compared with the theoretically calculated dependence. The theoretical dependence are calculated by assuming the size distribution function which has three adjustable parameters. These parameters are adjusted so that the calculated and the measured dependence give good agreement.

The necessity to assume previously the size distribution function seems to be a disadvantage. However, once we know the approximate size distribution, we can improve it. The principle of our measurement is not based on sampling of aerosol but on measurement of the light scattering from particles, so it never disturbs the aerosol formation as long as we use the probe beams of off-resonant wavelengths for the compounds concerned. In addition, we have only to measure a few dependence for combinations of wavelength and polarization enough to determine three adjustable parameters, we can keep up with the rapid temporal change.

3.2 Principle of Measurement

3.2.1 Mie Theory

First we recall the Mie theory[19] which our measurement bases on. Let us use the coordinates shown in Fig. 3.4. At the origin, there is a spherical and homogeneous particle with radius a, and with complex refractive index n relative to the surrounding medium. The particle is irradiated by a plane monochromatic light with wavelength λ, with the direction of propagation in the z-direction and with the electric vector $E^{(i)}$ in the x-direction. The Mie theory shows the scattered light electric vectors $E_\theta^{(s)}$ and $E_\phi^{(s)}$ satisfy the following relations:

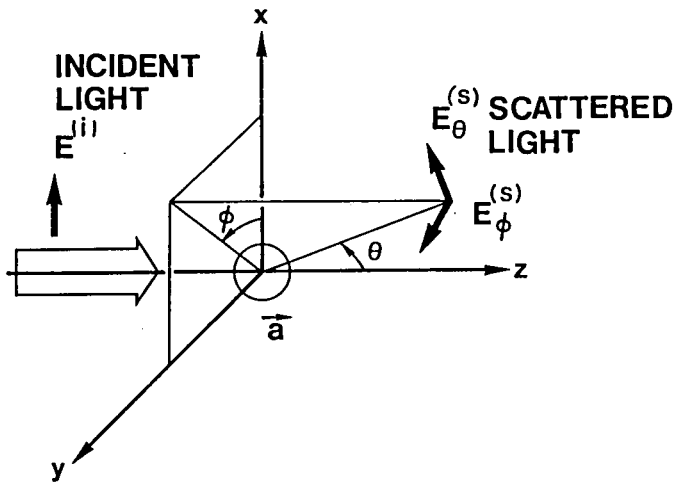

Fig. 3.4 Coordinates with the origin at the center of a particle, the z-direction in the direction of incident light propagation and the x-direction in the direction of electric vector of incident light.

$$|E_\theta^{(s)}|^2 = |E^{(i)}|^2 \cdot i_{\parallel}(\lambda,a;\theta)\cdot\cos^2\phi \ , \tag{3.6}$$

$$|E_\phi^{(s)}|^2 = |E^{(i)}|^2 \cdot i_{\perp}(\lambda,a;\theta)\cdot\sin^2\phi \ , \tag{3.7}$$

where

$$i_{\parallel}(\lambda,a;\theta) = \frac{\lambda^2}{4\pi^2 r^2} \times \left| \sum_{k=1}^{\infty} (-i)^k \left[{}^{e}B_k P_k^{(1)\prime}(\cos\theta)\sin\theta - {}^{m}B_k \frac{P_k^{(1)}(\cos\theta)}{\sin\theta} \right] \right|^2 , \tag{3.8}$$

$$i_{\perp}(\lambda,a;\theta) = \frac{\lambda^2}{4\pi^2 r^2} \times \left| \sum_{k=1}^{\infty} (-i)^k \left[{}^{e}B_k \frac{P_k^{(1)}(\cos\theta)}{\sin\theta} - {}^{m}B_k P_k^{(1)\prime}(\cos\theta)\sin\theta \right] \right|^2 . \tag{3.9}$$

The functions used above are as follows:

$$e_{B_k}=i^{k+1}\frac{2k+1}{k(k+1)}\cdot\frac{n\psi_k'(q)\psi_k(nq)-\psi_k(q)\psi_k'(nq)}{n\zeta_k^{(1)\prime}(q)\psi_k(nq)-\zeta_k^{(1)}(q)\psi_k'(nq)}\ , \qquad (3.10)$$

$$m_{B_k}=i^{k+1}\frac{2k+1}{k(k+1)}\cdot\frac{n\psi_k(q)\psi_k'(nq)-\psi_k'(q)\psi_k(nq)}{n\zeta_k^{(1)}(q)\psi_k'(nq)-\zeta_k^{(1)\prime}(q)\psi_k(nq)}\ , \qquad (3.11)$$

$$q = \frac{\lambda}{2\pi a}\ , \qquad (3.12)$$

$$\psi_k(x) = \left(\frac{\pi x}{2}\right)^{1/2}J_{k+1/2}(x)\ , \qquad (3.13)$$

$$\zeta_k(x) = \psi_k(x)-i\kappa_k(x)\ , \qquad (3.14)$$

$$\kappa_k(x) =-\left(\frac{\pi x}{2}\right)^{1/2}N_{k+1/2}(x)\ , \qquad (3.15)$$

where $J_{k+1/2}(x)$ is the Bessel function, $N_{k+1/2}(x)$ is the Neumann function and $P_k^{(1)}(\cos\theta)$ is the associated Legendre's polynomials. The prime on ψ_k , $\zeta_k^{(1)}$ and $P_k^{(1)}$ represents the differentiation with respect to their arguments. The numerical calculation of Eqs. (3.8) and (3.9) are presented in some references.[62~66)]

We will consider the cases that the scattered light is observed from the x-direction ($\theta \sim 90°$, $\phi \sim 0°$) and from the y-direction ($\theta \sim 90°$, $\phi \sim 90°$) with a small solid angle $\Delta\phi \times \Delta\theta$. In both cases, the ϕ-dependence of Eqs. (3.6) and (3.7) can be ignored as follows. In the case of $\phi \sim 0°$, $\cos^2\phi \simeq 1$ and $\sin^2\phi \simeq 0$, then Eqs. (3.6) and (3.7) become $|E_\theta^{(s)}|^2 \simeq |E^{(i)}|^2\cdot i_{\parallel}\cdot 1$, and $|E_\phi^{(s)}|^2 \simeq |E^{(i)}|^2\cdot i_{\perp}\cdot 0$ (=0). For simplicity we rewrite these equations by $s_{\parallel}^{(s)}=s_{\parallel}^{(i)}\cdot i_{\parallel}\cdot 1$ and $s_{\perp}^{(s)}=s_{\parallel}^{(i)}\cdot i_{\parallel}\cdot 0$ (=0), where the square of electric vector is denoted by s, which is proportional the power density. The su-

perscript (i) and (s) represent that the components are the incident and scattered light respectively. The subscript $\parallel$ ($\perp$) represents that the corresponding electric vector is parallel (perpendicular) to the plane of observation defined as the plane which contains the direction of propagation of incident light and the direction of observation (θ, ϕ). In this case, the plane is the x-z plane.

On the other hand, in the case of $\phi \sim 90°$, $|E_\theta^{(s)}|^2 \simeq |E^{(i)}|^2 \cdot i_\parallel \cdot 0$ (=0) and $|E_\phi^{(s)}|^2 \simeq |E^{(i)}|^2 \cdot i_\perp \cdot 1$, then the plane of observation is the y-z plane, and $s_\parallel^{(s)} = s_\perp^{(i)} \cdot i_\parallel \cdot 0$ (=0) and $s_\perp^{(s)} = s_\perp^{(i)} \cdot i_\perp \cdot 1$. Combined together, these equations are written as

$$s_\mu^{(s)} = s_\nu^{(i)} \cdot i_\mu(\lambda, a; \theta) \cdot \delta_{\mu,\nu} \quad , \quad (\mu, \nu = \parallel, \perp), \tag{3.16}$$

where $\delta_{\mu,\nu}$ is Kronecker's delta. Hereafter the subscript μ represents the direction of polarization $\parallel$ or $\perp$. It should be noted that there is no scattered light $s_\parallel^{(s)}$ ($s_\perp^{(s)}$) corresponding to the incident light $s_\perp^{(i)}$ ($s_\parallel^{(i)}$). Therefore we will hereafter consider only non-zero equations, $s_\parallel^{(s)} = s_\parallel^{(i)} \cdot i_\parallel$ and $s_\perp^{(s)} = s_\perp^{(i)} \cdot i_\perp$, which correspond respectively the case that both the polarizations of incident light and the scattered light are parallel along the plane of observation, and the case that both are perpendicular against the plane. Although the ϕ-dependence can be ignored as described above, the θ-dependence of i_μ, which is given by Eqs. (3.8) and (3.9), is relatively large even for small change of θ. Then we will average i_μ over θ as described later.

In the case of $a \ll \lambda$, it is known that Eq. (3.16) is reduced to $s_\perp^{(s)} \propto a^6$ and $s_\parallel^{(s)} \sim 0$. This case is called the Rayleigh scattering. On the other hand, in the case of $a \gg \lambda$, the light scat-

tering becomes like a mirror reflection, then $s_{\perp}^{(s)} \sim s_{\parallel}^{(s)} \propto a^2$. In the midway between these two limiting cases, that is, in the case of $a \sim \lambda$, $s_{\mu}^{(s)}$ changes complicatedly as particle radius changes. The light scattering in this range is called the Mie scattering. As described here, $s_{\mu}^{(s)}$ contains the information about particle radius, so we will use it to know the particle size distribution.

3.2.2 Application of Mie Formula to Practical Light Scattering Problem

To measure $s_{\parallel}^{(s)}$ and $s_{\perp}^{(s)}$, we must place two detectors on the x- and the y-axes. This arrangement is inconvenient in the practical case because we must take account of the differences between the sensitivities of two detectors and of the losses in two optical passes which are caused by the walls of the cell containing aerosol and the lenses to focus the scattered lights. So it is better to use one detector to avoid the above complications which cause some error. By switching the polarization of the incident light in the x-direction and in the y-direction alternately (Fig. 3.5), we can measure both $s_{\parallel}^{(s)}$ and $s_{\perp}^{(s)}$ by a single detector placed on the y-axis. In this case, the plane of observation is the y-z plane. When the incident light is polarized in the x- (y-) direction, which is represented as $s_{\perp}^{(i)}$ ($s_{\parallel}^{(i)}$) in Fig. 3.5, the observed scattered light corresponds to $s_{\perp}^{(s)}$ ($s_{\parallel}^{(s)}$).

Let us consider the light scattering by the ensemble of particles with different radii. Here, we will deal with the case that the number density of particles is so high that the disposition of particles can be treated statistically, but not so

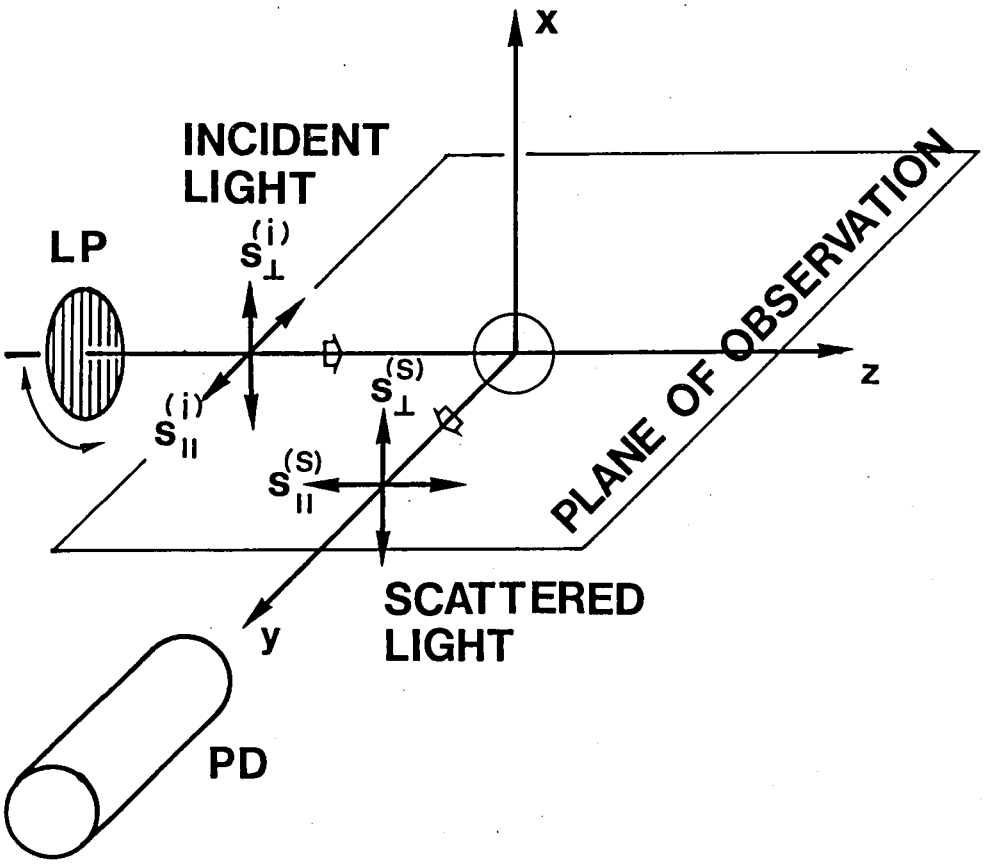

Fig. 3.5 Definition of scattered light intensities $s_{\parallel}^{(s)}$ and $s_{\perp}^{(s)}$. By switching the polarization of the incident light in the x-direction and in the y-direction alternately (LP -linear polarizer), $s_{\parallel}^{(s)}$ and $s_{\perp}^{(s)}$ can be measured by a single photodetector (PD) placed on the y-axis. When the incident light is polarized in the x-(y-) direction, which is represented as $s_{\perp}^{(i)}$ ($s_{\parallel}^{(i)}$), the observed scattered light corresponds to $s_{\perp}^{(s)}$ ($s_{\parallel}^{(s)}$).

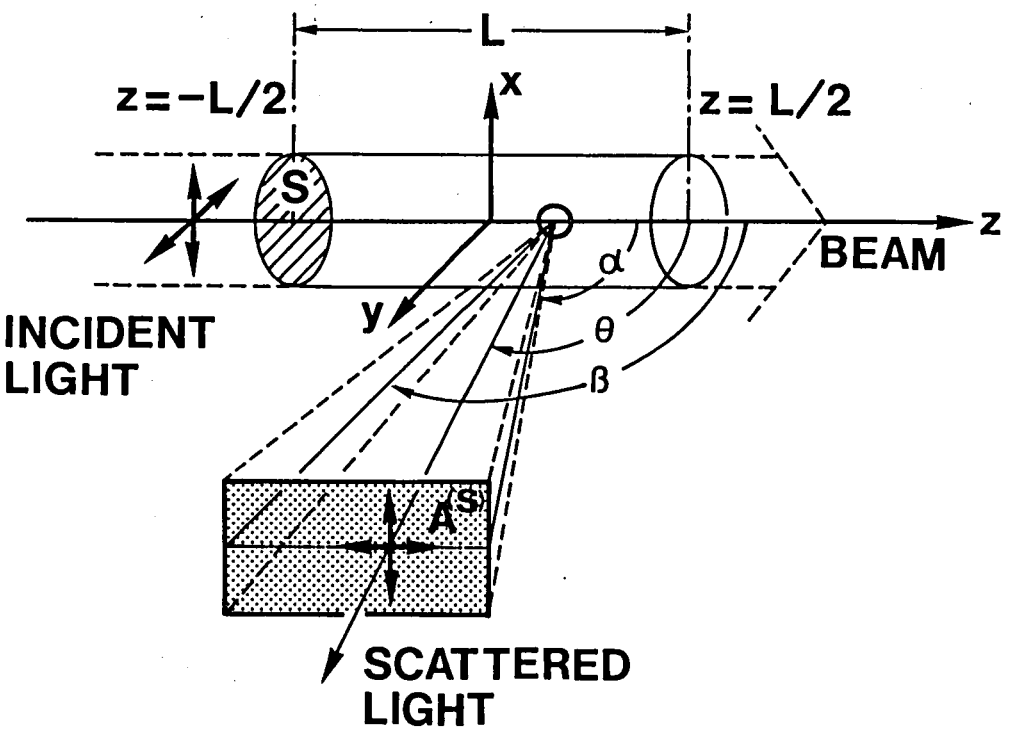

Fig. 3.6 Averaging of the scattered light intensity over scattering angle θ. S -cross section of incident light beam, L -length of the volume to be observed, and $A^{(s)}$ - area of window of photodetector.

high that the effect of multi-scattering cannot be negligible.

If the latter assumption fails, we cannot regard there is no scattered light $s_{\parallel}^{(s)}$ ($s_{\perp}^{(s)}$) corresponding to the incident light $s_{\perp}^{(i)}$ ($s_{\parallel}^{(i)}$) (see Eq. (3.16)). Since a large number of particles spread spatially at random, the interference among the scattered light waves are smeared out. Then, the total scattered light intensity is simply given by the sum of the scattered light intensity from each particle. See Fig. 3.6. When S is the cross section of incident light beam, and L is the length of the volume to be observed, which lies along the z-axis, the total scattered light intensity $I_{\mu,\lambda}^{(s)}$ is written as

$$I_{\mu,\lambda}^{(s)} = A^{(s)} \cdot \int_0^{\infty} \{S \cdot L \cdot f(a) \cdot s_{\mu}^{(s)}\} \, da, \qquad (3.17)$$

where the quantity S·L represents the observed volume, $A^{(s)}$ is the area of the window of the detector, and f(a) is the size distribution function of particles.

Putting Eq. (3.16) into above Eq. (3.17), and considering that $S \cdot s_{\mu}^{(i)}$ represents the total intensity of incident light, which we rewrite as $I_{\mu,\lambda}^{(i)}$, we will define the normalized scattered light intensity $I_{\mu,\lambda}$ as

$$I_{\mu,\lambda} = I_{\mu,\lambda}^{(s)} / I_{\mu,\lambda}^{(i)} = A^{(s)} \cdot L \cdot \int_0^{\infty} f(a) \cdot i_{\mu}(\lambda, a; \theta) \, da \quad . (3.18)$$

The expression by Eq. (3.18) are accurate when the area of the detector and the observed volume are infinitesimal so that the θ dependence of i_{μ}, which is given by Eqs. (3.8) and (3.9), is negligible. In practical cases, both have certain finite dimensions, so we must consider the ambiguity of θ on i_{μ}. In such a case, we have only to use $\bar{i}_{\mu}$ for i_{μ}, where $\bar{i}_{\mu}$ is an averaged quantity given below. See Fig. 3.6. First, let us consider

the area of the detector. There is a particle at the position z on the z-axis. The mean value of i_μ at the position of the detector is given by averaging i_μ over θ from $\alpha(z)$ to $\beta(z)$, where $\alpha(z)$ and $\beta(z)$ are the angles from the z-direction to both sides of the window of the detector. Next, considering the finiteness of the observed volume, we averaged it again over z from z = -L/2 to L/2, where the positions of z = -L/2 and L/2 correspond to the both sides of the observed volume. Then we get $\bar{i}_\mu$ as

$$\bar{I}_\mu(\lambda,a)= \frac{1}{L}\int_{-L/2}^{L/2}\left[\frac{1}{\beta(z)-\alpha(z)}\int_{\alpha(z)}^{\beta(z)} i_\mu(\lambda,a;\theta)d\theta\right] dz \quad . \quad (3.19)$$

However there is no necessity for averaging it over the x- and the y-direction when the diameter of probe beam is much smaller than the length of observed volume L and the distance r from the beam to the detector.

3.2.3 Determination of Particle Size Distribution Function

We have obtained the expression (3.18) to calculate the scattered light intensity from a given particle size distribution function. We have to, however, solve the 'reverse' problem. Namely in practical case, we obtain the intensities of the scattered light, and from them we have to determine the size distribution. Hereafter $I^{(i)}_{\mu,\lambda}$ and $I^{(s)}_{\mu,\lambda}$ respectively represent the incident and scattered light intensities observed in experiment. From these observed values, we can get the normalized intensity of the scattered light $I^{Obs}_{\mu,\lambda}$ defined as

$$I^{Obs}_{\mu,\lambda}= I^{(s)}_{\mu,\lambda}/ I^{(i)}_{\mu,\lambda} \quad . \quad (3.20)$$

Then, comparing this with Eq. (3.18), the problem is reduced to solving the integral equation:

$$I^{Obs}_{\mu,\lambda} = A^{(s)} \cdot L \cdot \int_0^\infty f(a) \cdot \bar{i}_\mu(\lambda,a)\, da \ , \qquad (3.21)$$

with respect to f(a). If we could measure a broad spectrum of $I^{Obs}_{\mu,\lambda}$ over all λ from 0 to infinity, f(a) were strictly determined at least in principle. Even then it is not easy to solve Eq. (3.21) directly. It is impossible of course to measure the complete spectrum of $I^{Obs}_{\mu,\lambda}$ over all λ. Let us grope for the way how to use the separate $I^{Obs}_{\mu,\lambda}$ as to the combinations of polarizations (μ = ∥, ⊥) and some certain wavelengths ($\lambda = \lambda'$, λ'', ···). The more combinations give the more accurate results. The number of combinations, however, cannot be large in practical case. Another limitation is that we can utilize only narrow wavelength range of visible light as probes. The ultraviolet range disturbs the aerosol formation by producing particles. Considering available light sources for the probes and the simplicity of instrumental arrangement, it is advisable to use two laser beams with different wavelengths λ' and λ'' as probes. Then we can utilize four $I^{Obs}_{\mu,\lambda}$: $I^{Obs}_{\parallel,\lambda'}$, $I^{Obs}_{\perp,\lambda'}$, $I^{Obs}_{\parallel,\lambda''}$ and $I^{Obs}_{\perp,\lambda''}$. We will previously assume the shape of f(a) permitting several ambiguities. Putting the assumed f(a) into Eq. (3.18), we can theoretically calculate the intensity of the scattered light, which we write as

$$I^{Cal}_{\mu,\lambda} = A^{(s)} \cdot L \cdot \int_0^\infty f(a) \cdot i_\mu(\lambda,a)\, da \ . \qquad (3.22)$$

Then we will determine f(a) so that the deviation of $I^{Cal}_{\mu,\lambda}$ from $I^{Obs}_{\mu,\lambda}$ becomes smallest. When the number of $I^{Obs}_{\mu,\lambda}$ is four, we can introduce at most four adjustable parameters into f(a). Let us assume f(a), permitting the ambiguities of the normalization

coefficient A and two adjustable parameters α and β, which characterize the shape of distribution functions. We will call these functions the assumed functions.

In this work, we have used the following functions. The Gauss distribution;

$$f(a)= A\cdot\exp\{-\frac{(a-\alpha)^2}{2\cdot\beta^2}\} , \tag{3.23}$$

the Log-normal distribution;

$$f(a)= \frac{A}{a}\cdot\exp\{-\frac{(\ln a-\ln \alpha)^2}{2\cdot\ln^2\beta}\} , \tag{3.24}$$

the Junge distribution;

$$\begin{aligned} f(a)&= 0 && (a<\alpha) ,\\ &= A\cdot a^{-\beta} && (a>\alpha) , \end{aligned} \tag{3.25}$$

the Stevenson distribution;

$$\begin{aligned} f(a)&= 0 && (a<\alpha) ,\\ &= A\cdot(a-\alpha)\cdot\exp\{-(\frac{a-\alpha}{\beta})^3\} && (a>\alpha) , \end{aligned} \tag{3.26}$$

and the Modified exponential distribution;

$$f(a)= A\cdot\exp\{-(\frac{a}{\alpha})^{\beta}\} . \tag{3.27}$$

Each distribution has been used to approximate a size distribution of specific aerosol. The Gauss distribution is known to give the approximate size distribution of rain-droplets.[67] The Log-normal distribution is known to be widely applicable to the size distribution of many kinds of aerosol or powder produced through smashing.[4,54,58~61] The Junge distribution has been often applied to the size distribution of stratospheric aerosol since Junge et al. first proposed.[68] Here we have introduced

cut-off radius α to remove the singularity at a=0. In the original work of Junge et al. such a limit was not considered. However it is natural to assume the existence of the minimum or maximum radius in the Junge distribution, for it is impossible that the density becomes infinite for small a, or finite for infinitesimally large a. As the maximum radius is naturally introduced by the nature that the Junge distribution function converges to zero for large a, we here introduce the minimum radius α. The Stevenson distribution was used as an approximate size distribution of emulsions etc.[69] Recently Kurosu et al. applied the Modified exponential distribution to approximate particle size distribution of Laser Snow and assured its usefulness (unpublished).

Each of these distribution functions has three adjustable parameters A, α and β. Since we are able to use four $I^{Obs}_{\mu,\lambda}$, one is excess. We will use this excess freedom in order to determine which assumed function gives the best fitting.

Each of these distribution functions has three unknown parameters A, α and β. Since we are able to use four $I^{Obs}_{\mu,\lambda}$, one is excess. We will use this excess freedom in order to determine which assumed function gives the best fitting.

Here we mention how to determine A, α and β. Putting the assumed functions introduced above into Eq. (3.22), we can calculate $I^{Cal}_{\mu,\lambda}$, which are now the function of A, α and β. From the experiments, we get $I^{Obs}_{\mu,\lambda}$. We define the deviation E by

$$E = \sum_{\mu,\lambda} \left(\frac{I^{Obs}_{\mu,\lambda} - I^{Cal}_{\mu,\lambda}}{I^{Obs}_{\mu,\lambda}} \right)^2 , \qquad (3.28)$$

and determine A, α and β so that the deviation E becomes smal-

lest. The way is the following. We separate the simple coefficient A from the assumed function f(a), that is, $f(a) = A \cdot f'(a;\alpha,\beta)$. From Eq. (3.22),

$$I^{Cal}_{\mu,\lambda} = A^{(s)} \cdot L \cdot A \cdot \int_0^\infty f'(a;\alpha,\beta) \cdot i_\mu(\lambda,a) da \ . \qquad (3.29)$$

Then the deviation E is reduced to

$$E = Q \cdot (A - P/Q)^2 + M - P^2/Q \ , \qquad (3.30)$$

where

$$P = \sum_{\mu,\lambda} x_{\mu,\lambda} \ , \qquad Q = \sum_{\mu,\lambda} x^2_{\mu,\lambda} \ , \qquad (3.31)$$

$$x_{\mu,\lambda} = [\ A^{(s)} \cdot L \cdot \int_0^\infty f'(a;\alpha,\beta) \cdot i_\mu(\lambda,a) da\ ] \ / \ I^{Obs}_{\mu,\lambda} \qquad (3.32)$$

and

$$M = \sum_{\mu,\lambda} 1 = 4 \ : \text{ the number of } I^{Obs}_{\mu,\lambda} \ ; \text{ constant.} \qquad (3.33)$$

To minimize the deviation E smallest, we have only to survey the α-β plane and determine them so that P^2/Q becomes maximum, then $A = P/Q$.

In this way, from the four values of $I^{Obs}_{\mu,\lambda}$ which are measured simultaneously at a given time T after the beginning of aerosol production, we can determine the distribution function f(a) at T. We will call these four values of $I^{Obs}_{\mu,\lambda}$ 'a set of $I^{Obs}_{\mu,\lambda}$'. Repeating this procedure for the different assumed functions, we can choose the best assumed function which gave the smallest E, i.e. the best fit at T. Repeating this for different T, we obtained the temporal change of distribution function.

3.2.4 Total Number, Radius, Surface and Volume of Distribution Function

Once we determine the distribution function, we can evaluate the various quantities, for examples,

$$N(a_{th})=\int_0^{a_{th}} f(a)da \ , \tag{3.34}$$

$$R(a_{th})=\int_0^{a_{th}} a\cdot f(a)da \ , \tag{3.35}$$

$$S(a_{th})=\int_0^{a_{th}} 4\pi a^2\cdot f(a)da \tag{3.36}$$

and

$$V(a_{th})=\int_0^{a_{th}} \frac{4}{3}\pi a^3\cdot f(a)da \ . \tag{3.37}$$

They represent physically number, radius, surface and volume respectively. We will hereafter call them 'moments' of distribution function. $N(a_{th})$ represents the number density of particles whose radii are between 0 and a_{th}. The total number density N_{total} (Eq. (3.2)) is defined as the limit of $N(a_{th})$ with $a_{th}\rightarrow\infty$. Other total moments R_{total}, S_{total} and V_{total} are defined similarly (Eqs. (3.3)~(3.5)).

The temporal changes of moments give us much information about the mechanism of aerosol formation and growth. As described in the beginning of this chapter, for instance, the velocity of increase of volume shows the velocity of gas to particle conversion, or if the volume is conservative while the number decreases, then particles are grown by coalescence.

3.2.5 Comparison with Conventional Methods

It is significant to point out advantages and disadvantages of the method. Compared with other conventional methods, this measurement is purely optical, we need not worry about the disturbance within the aerosol growth as long as we use the off-resonant probes for compounds concerned. This point is very important for our purpose, to study not the static size distribution but the temporal change. We cannot utilize a particle counter which disturbs the aerosol formation by sampling. In addition to this disadvantage, a particle counter of sampling type takes time to scan a range of radii or to count particles, and therefore it is not suitable for the survey of temporal change even if they are commercially available. Our method can sufficiently keep up with the rapid temporal change because we have only to observe four $I^{Obs}_{\mu,\lambda}$ at a given T. In addition, the sensitivity is very high in principle because there is no background noise, and when using sufficiently fine beam as probes, our method may obtain high spatial resolution.

There is another advantage. As we measure a set of $I^{Obs}_{\mu,\lambda}$ simultaneously, we can study a single event of aerosol formation without assuming any experimental reproducibility. In the study of Laser Snow, Sato et al.[18] measured the temporal change of one component of $I^{Obs}_{\mu,\lambda}$ in one procedure. Until repeating this procedure for the different components, i.e. the combinations of polarization and wavelength, they could not obtain the temporal change of the set of $I^{Obs}_{\mu,\lambda}$. As a result, they had to assume the reproducibility of aerosol. This time, the improvement of experimental setup described in Sec. 3.3 makes it possible to

measure the temporal change of a set of $I^{Obs}_{\mu,\lambda}$ in one procedure. Then we can discuss the aerosol formation without assuming any reproducibility.

On the other hand, when the real size distribution of aerosol is far from our assumed functions, for instance, when the distribution has plural peaks, our method may fail. If we know the broad range spectrum of scattered light, we may be able to deal with even such a case. Simizu et al.[70] tried to determine the size distribution of bacteria without using the assumed function. They measured the spectrum of scattered light over all angle of observation, and solved that inversion scattering problem by a Fourier transformation technique. If using such a method, we, indeed, need not to assume the distribution function. But it takes longer time to measure the broad range spectrum, which makes it difficult to study the rapid temporal change.

In the case of the polarization ratio method,[54,58~60] as one must measure the angular dependence of polarization ratio, he needs to worry about the angular dependence of the transmittance in light passes even if he uses a cylindrical cell containing aerosol. Since we do not use the angular dependence, we can ignore the difference of light passes. In addition to this, as we measure the absolute intensities of the scattered light instead of the polarization ratio, we can evaluate in principle the absolute number density as well as the relative frequency.

3.3 Experimental Setup

The experimental setup is shown in Fig. 3.7. The probe beams from the Ar^+ laser (λ=457.9 nm) and the He-Ne laser

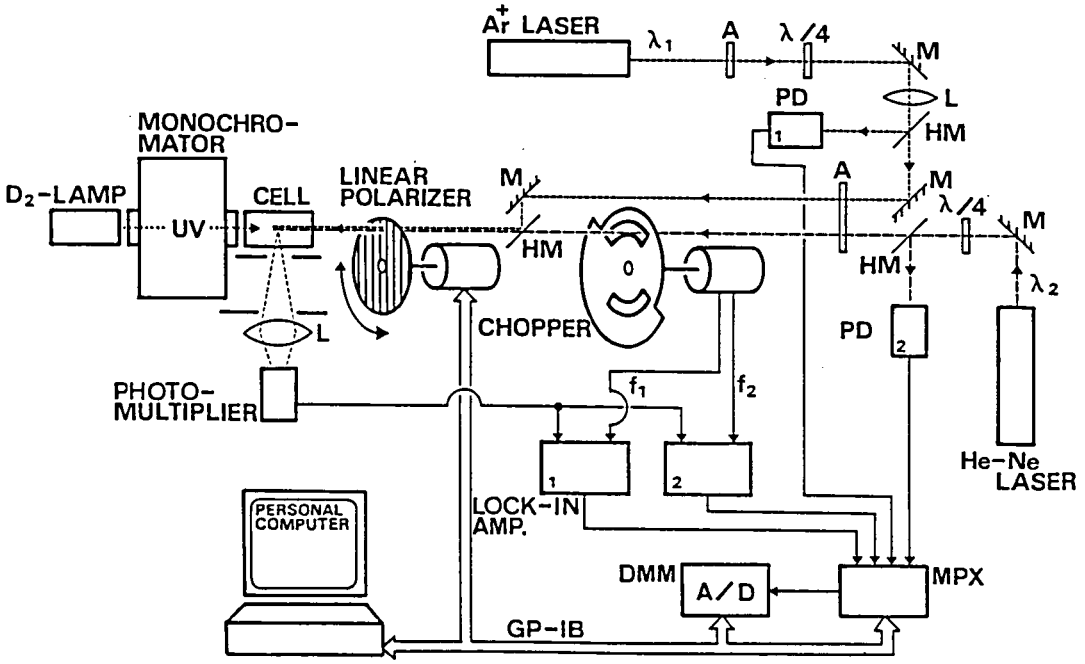

Fig. 3.7 Experimental setup for the measurement of temporal change in scattered light intensity. Symbols have the following significance: L -lens, PD -photodetector, A -attenuator, $\lambda/4$ -$\lambda/4$ plate, M -mirror, HM -half mirror, DMM -digital multimeter, GP-IB -control bus for computer, and MPX -signal multiplexer.

(λ=632.8 nm) are circularly polarized by $\lambda/4$ plates. The beams reflected by half mirrors are applied to the photo-detectors (solar cells) to monitor the intensities of incident beams. While, the transmitted beams are modulated by double beam mechanical chopper at different frequencies for the lock-in detection described later. The beams are made coaxial by another half mirror, and they are transmitted through a linear polarizer. The linear polarizer is rotative and switches alternatively the direction of polarization between the direction $\parallel$ and $\perp$. Since the laser beams are originally circularly polarized, there is no significant difference between the intensities of the beams polarized in the direction $\parallel$ and $\perp$. It is not necessary to make the intensities of the $\parallel$ and $\perp$ components strictly equal because we normalize the scattered light intensity by the incident beam intensity as described later. Linearly polarized beams are applied to the cell.

The cell is rectangular, 1x2x4.5 cm^3 in dimension, and it is made of quartz transparent to UV radiation of wavelengths longer than 180 nm. In the bottom of the cell, we placed a small amount of p-dichlorobenzene as a raw material of aerosol. The saturated vapor pressure of p-dichlorobenzene is about 1.5 mmHg at 20°C. As the surrounding gas, we use three kinds of gases in order to study the effects of surrounding gas on the aerosol formation and growth. we choose particle free clean air, N_2 and O_2, each of which is filled at 1 atm at room temperature.

The source of UV radiation is a deuterium lamp (D_2 lamp). The light from the D_2-lamp is filtered by monochromator to select the wavelength of UV radiation to be applied to the cell. In the present experiment, we set the wavelength at 220 nm with the

bandwidth about 8 nm, then the power of the UV radiation applied into the cell was roughly estimated about 1 mW/cm^2, which is enough to produce a large number of particles in the cell. There is an additional reason why we here use the monochromator. When no filtered UV radiation is applied directly to the cell, the gas in the cell is rapidly heated up by the radiation, which causes the convection and fluctuate the scattered light. As the monochromator cut most of power from the D_2-lamp, especially the infrared components, heating is reduced. However, most power of UV radiation effective to produce aerosol are filtered and the aerosol production rate becomes much slower.

The laser light scattered by produced particles passes through a 2×2 cm^2 slit placed at 4.2 cm apart from the probe beam, and then it is focused by a lens and detected by a

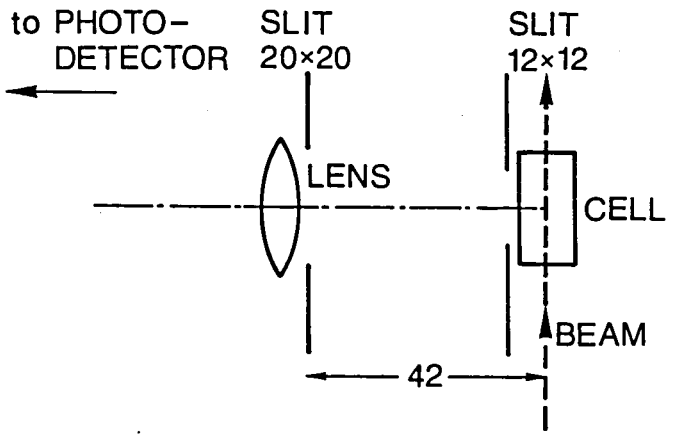

Fig. 3.8 Dimension of the optical system in Fig. 3.7.

photomultiplier (Fig. 3.8).

To determine the size distribution at a given time T, it is necessary to measure the scattered light intensities

$I^{(s)}_{\parallel,\lambda=457.9\ nm}$, $I^{(s)}_{\perp,\lambda=457.9\ nm}$, $I^{(s)}_{\parallel,\lambda=632.8\ nm}$ and $I^{(s)}_{\perp,\lambda=632.8\ nm}$ simultaneously. First the linear polarizer is set in the direction $\parallel$, and the intensities $I^{(s)}_{\parallel,\lambda=457.9\ nm}$ and $I^{(s)}_{\parallel,\lambda=632.8\ nm}$ are separately measured by two lock-in amplifiers tuned at different frequencies of the chopper described before. The time constants of both lock-in amplifiers are 100 msec. The outputs are alternatively converted from analogue to digital and stored in memory of the desk-top computer. Then the linear polarizer is switched to the direction $\perp$, and $I^{(s)}_{\perp,457.9\ nm}$ and $I^{(s)}_{\perp,632.8\ nm}$ are similarly measured. A set of $I^{(s)}_{\mu,\lambda}$ is measured within two seconds, which is much shorter than the changes of the scattered light intensities in the present experiment. We can fully regard them as measured at the same time. We repeat the same procedure many times after the beginning of UV light irradiation.

The desk-top computer does not only store the data but also controls the switching of the directions of linear polarizer, the selecting of the outputs of lock-in amplifiers and the sampling of the A/D converter. In addition, it normalizes the scattered light intensities $I^{(s)}_{\mu,\lambda}$ by the incident beam intensities $I^{(i)}_{\mu,\lambda}$ at each moment.

The incident beam intensities are always monitored as described before. To relate the outputs of monitors to the real intensities of incident beams $I^{(i)}_{\mu,\lambda}$, we used the following method. We put a small mirror in the particle free cell and guide the reflected beams into the photomultiplier. Weakening the laser beam with ND-filters, we measure the reflected beam intensities in the same procedure described above, i.e. the procedure to measure the intensities of the lights scattered by particles. Once we measure the attenuation factors of the ND-

filters and the reflection factors of the mirror for a given combination of wavelength (λ=457.9 or 632.8 nm) and polarization (μ=$\parallel$ or $\perp$). we can relate the outputs of monitors to the real intensities of incident beams $I^{(i)}_{\mu,\lambda}$. Then, converting the outputs of monitors to $I^{(i)}_{\mu,\lambda}$, we obtain the accurately normalized scattered light intensities $I^{Obs}_{\mu,\lambda}$ by $I^{(s)}_{\mu,\lambda}$ / $I^{(i)}_{\mu,\lambda}$.

3.4 Experimental Results and Discussions

3.4.1 Temporal Change in Scattered Light Intensity

Using the experimental setup described in Sec. 3.3, we measured the temporal changes of $I^{Obs}_{\mu,\lambda}$, the normalized intensities of the light scattered by aerosol particles. Those particles were produced by UV radiation with the wavelength 220 nm and with the power density about 1 mW/cm^2. The raw material of the aerosol was the vapor of p-dichlorobenzene with the pressure about 1.5mmHg. The surrounding gas was the particle free clean air, N_2 and O_2 at 1 atm, at room temperature.

Typical changes of $I^{Obs}_{\mu,\lambda}$ are shown in Fig. 3.9, where (a) is the case that the surrounding gas is air, (b) N_2 and (c) O_2.

From Fig. 3.9(a), we can see that the intensity of the shorter wavelength (λ=457.9 nm) rises faster than that of the longer wavelength (λ=632.8 nm), and that, for each wavelength, the intensity of polarization $\perp$ rises faster than that of polarization $\parallel$. At T~10 min, $I^{Obs}_{\mu,\lambda}$ show maxima, and for T>10 min, they slightly decrease and approach steady state values. This behavior of $I^{Obs}_{\mu,\lambda}$ shows that as particles grow larger, the light scattering transits from the Rayleigh like scattering to the Mie scattering.

In the cases of N_2 (Fig. 3.9(b)) and O_2 (Fig. 3.9(c)), the

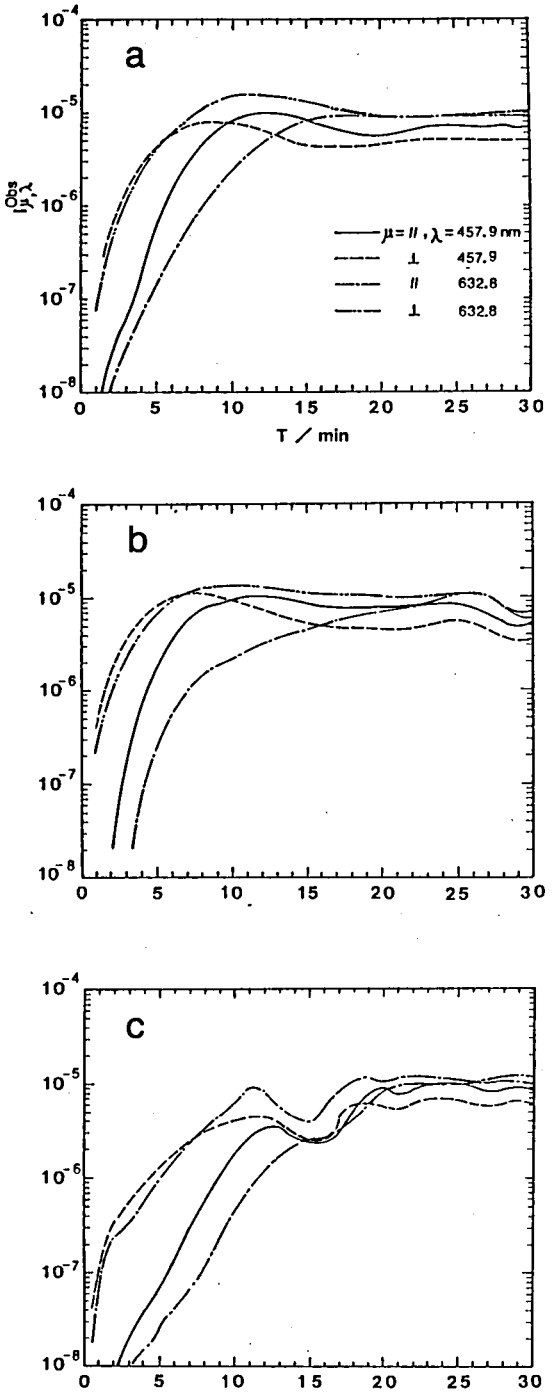

Fig. 3.9 Temporal change in scattered light intensities $I^{Obs}_{\mu,\lambda}$. In the case of (a), the surrounding gas is air; in (b), N_2; and in (c), O_2.

temporal change of $I^{Obs}_{\mu,\lambda}$ are qualitatively similar. In the former case, the rising of $I^{Obs}_{\mu,\lambda}$ is faster than in the case of air, and in the latter case, it is slower than in the case of air. There is a surrounding gas dependence of aerosol formation velocity.

As shown in Fig. 3.9, the changes of $I^{Obs}_{\mu,\lambda}$ is very smooth, which shows the convection of the air in the cell is sufficiently slow. In addition, there is no significant changes of $I^{Obs}_{\mu,\lambda}$ within the time required to sample a set of $I^{Obs}_{\mu,\lambda}$ (about 2 seconds) as described in Sec. 3.3. So the set of $I^{Obs}_{\mu,\lambda}$ can be considered as measured simultaneously at the given T.

3.4.2 Temporal Change in Size Distribution

In order to calculate $I^{Cal}_{\mu,\lambda}$ theoretically by using Eq. (3.22), we have to know the refractive index n of products, but the constituents of products have not been identified yet. So we have approximated the refractive index of products by that of the raw material p-dichlorobenzene, i.e. about 1.5 at the wavelength of 580 nm, and we have assumed that it is constant over the range of wavelength concerned. Using Eq. (3.22), we have calculated $I^{Cal}_{\mu,\lambda}$ assuming the five assumed functions (Eqs. (3.23)~(3.27)), each of which has three adjustable parameters. Then we have determined the best fit function and its parameters by comparing $I^{Cal}_{\mu,\lambda}$ and $I^{Obs}_{\mu,\lambda}$ by Eq. (3.28).

The temporal changes of the functions determined in this way are shown in Fig. 3.10, where the horizontal axis represents the radius of particles, and the vertical axis represents the number density of particles in terms of dN/d(log a) particles/cm^3. Figure 3.10(a), (b) and (c) are respectively in the cases of air N_2 and O_2. In the same figure, we also show which assumed func-

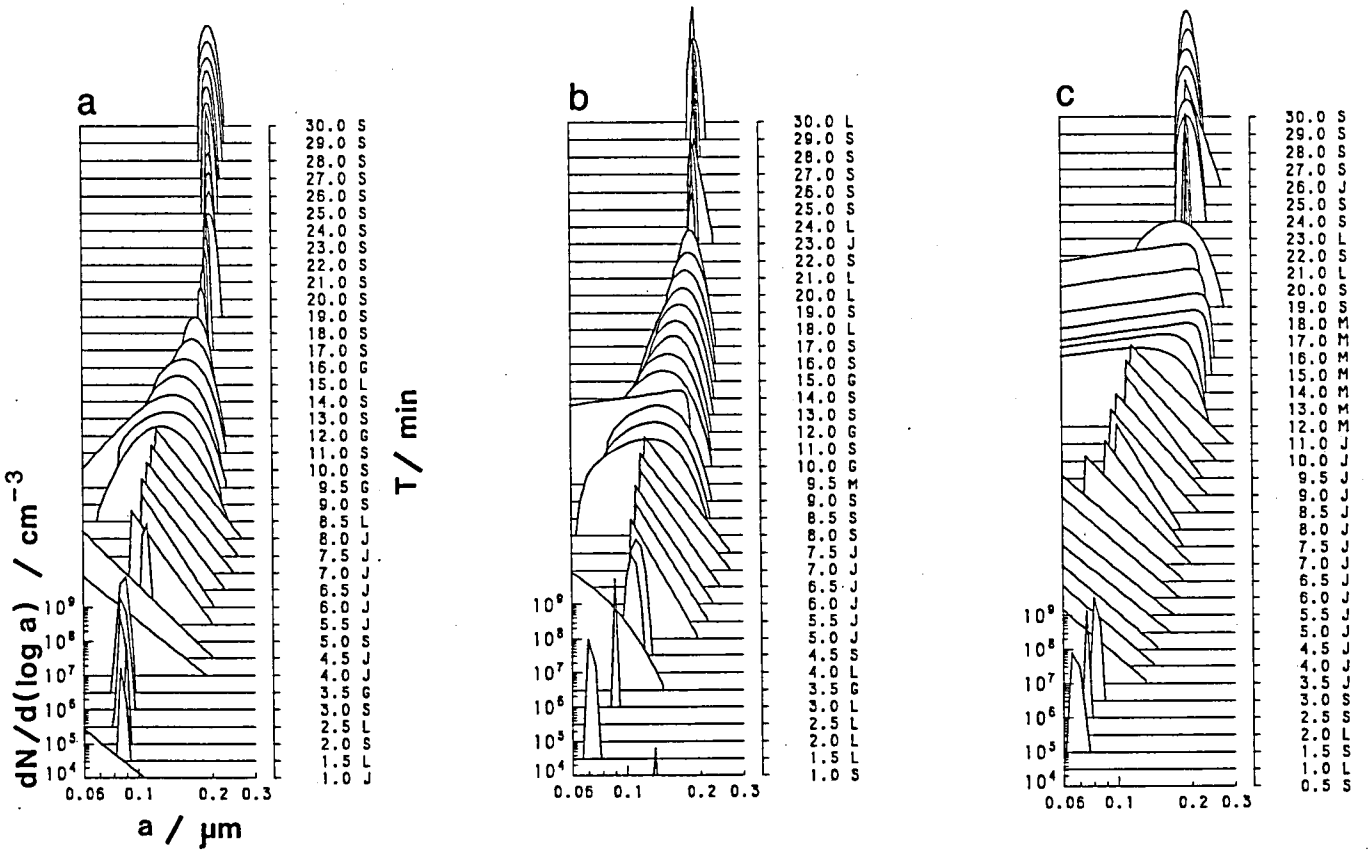

Fig. 3.10 Temporal change in particle size distribution. In the case of (a), the surrounding gas is air; in (b), N_2; and in (c), O_2. Symbols "G", "L", "J", "S" and "M" respectively represent that the Gauss, the Log-normal, the Junge, the Stevenson and the Modified exponential distribution give the best fitting at the time T.

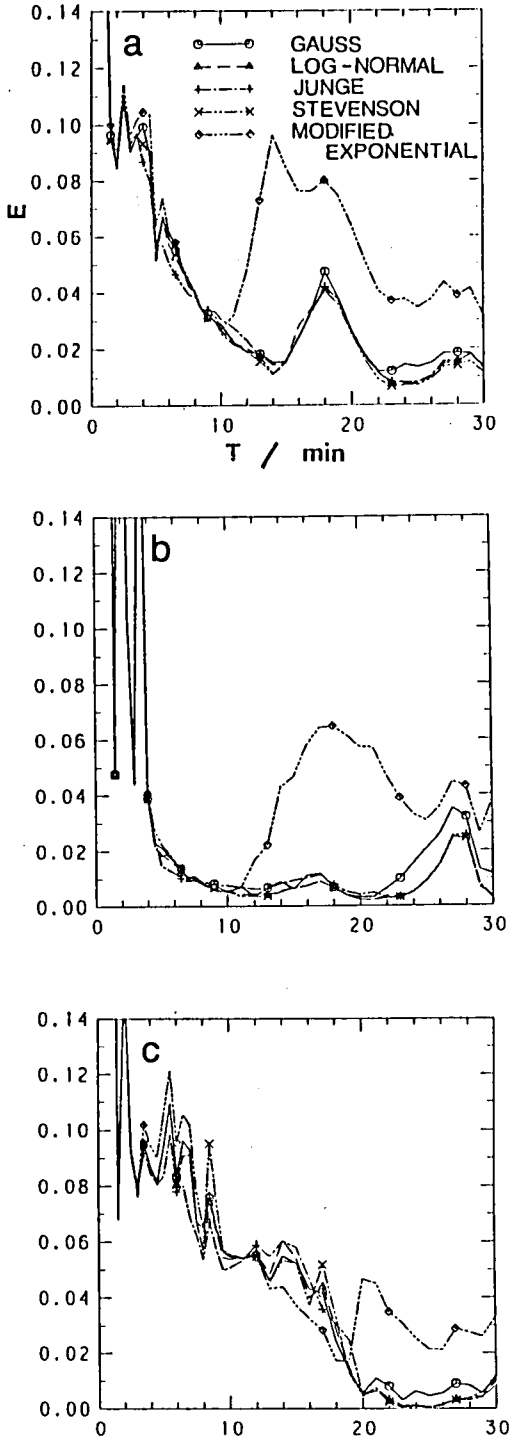

Fig. 3.11 Temporal change in mean square deviation E for each distribution function. In the case of (a), the surrounding gas is air; in (b), N_2; and in (c), O_2.

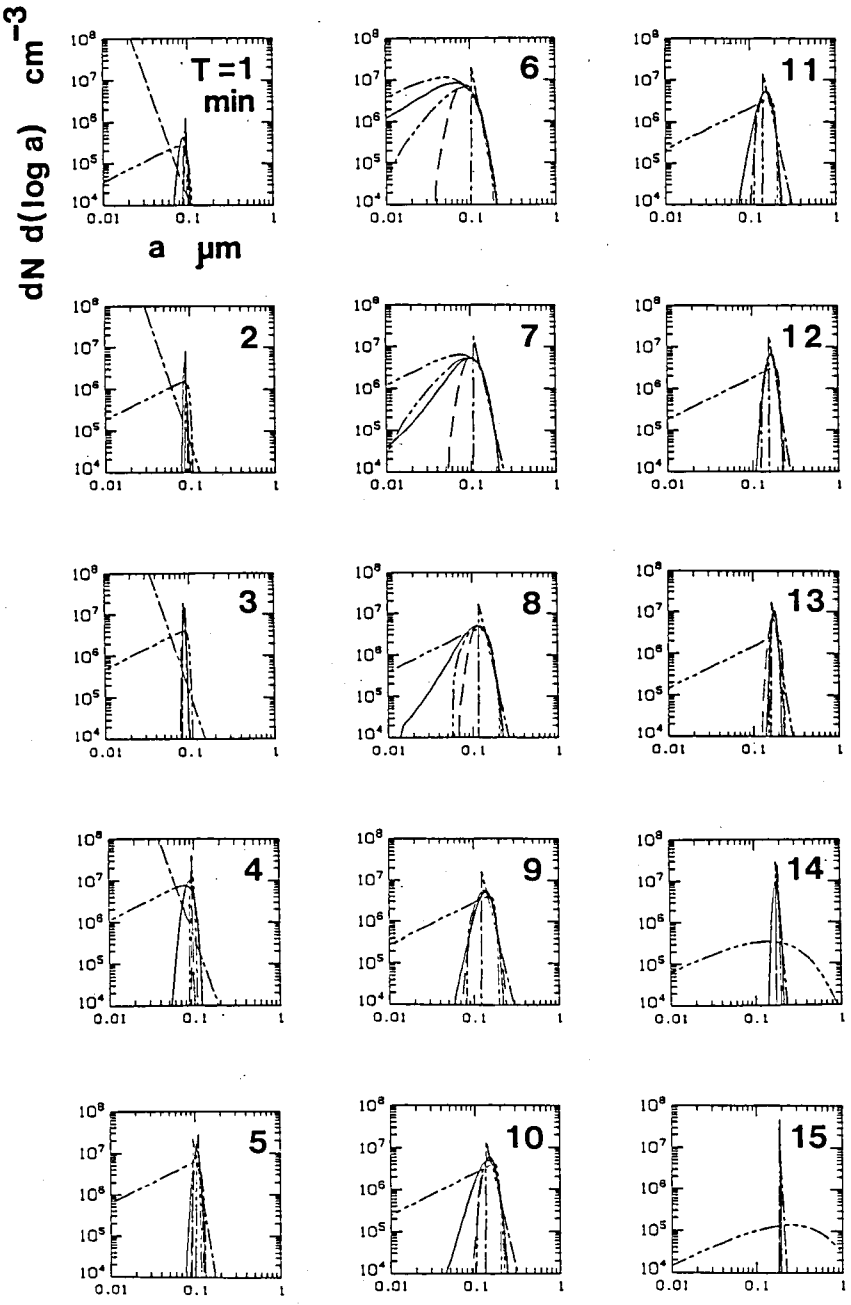

Fig. 3.12 Plots of the Gauss (————), the Log-normal (--------), the Junge (——·——), the Stevenson (——··——) and the Modified exponential

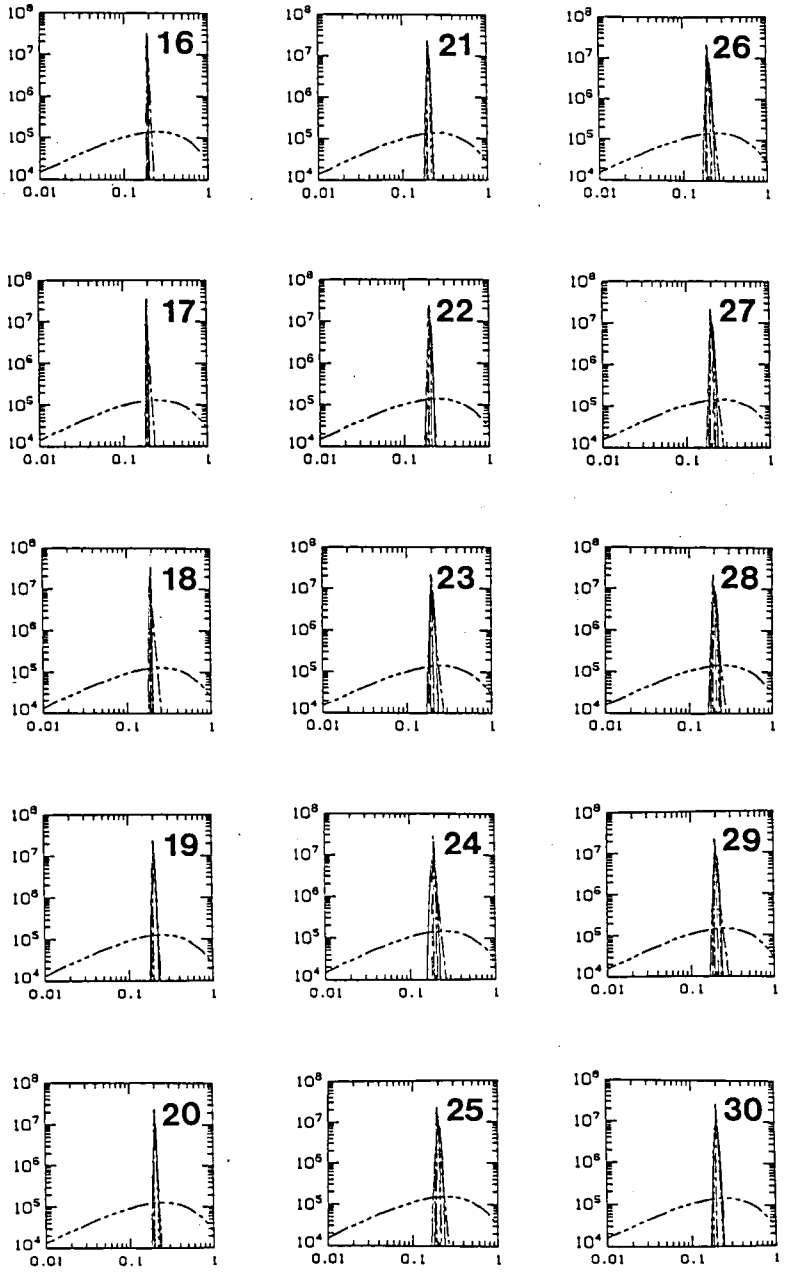

(—···—) distribution at every one minute after the beginning of ultraviolet light irradiation, where the surrounding gas is air.

tion gives the best fit at each T. The characters "G", "L", "J", "S" and "M" represent that the Gauss, the Log-normal, the Junge, the Stevenson and the Modified exponential function (Eqs. (3.23)~(3.27)) respectively give the smallest E among them at the time. Figure 3.11 shows the changes of the values E for each assumed function, where (a), (b) and (c) are respectively in the cases of air N_2 and O_2. Figure 3.12 shows the temporal change of the plots of five assumed functions at every 1 minute in the case of air. For other cases, the results are qualitatively similar.

Hereafter let us discuss mainly the case that the surrounding gas is air. Using Figs. 3.10(a), 3.11(a) and 3.12, we will discuss the changes of the distributions dividing them into three time ranges.

a) For about T<4 min : Figure 3.12 shows the following. The Gauss, the Log-normal and the Stevenson give almost the same plot. The distribution of the function is very narrow, and the position of the peak of the number density is smaller than 0.1 μm or so. However the plots from the Junge and the Modified exponential are quite different. The latter two suggests that the distribution spreads toward smaller radius. In addition to such a disagreement in the shape of the distribution function, as Fig. 3.10(a) shows, the best fit function changes frequently for the different T. We also know from Fig. 3.11(a) that the values of E for any assumed function are generally large, and moreover, there is no significant difference between them. Therefore, at the beginning of aerosol formation i.e. in the case that particles have not been larger than 0.1 μm yet, we cannot declare which assumed function is the best. It may be due to our using

the light of visible range as probes. When particles are much smaller than the wavelengths of probes, in other words, when particle size is nearly in the range of the Rayleigh scattering, the dependence of $I^{Obs}_{\mu,\lambda}$ on the particle size becomes monotonous. Even if the scattered light is intense, one cannot predict whether the intensity is due to the size of a particle or the number of particles. Under such a circumstance, the difference in the shape of distribution function cannot be reflected in the difference of $I^{Obs}_{\mu,\lambda}$. Both the high but narrow distribution function and the low but broad one may give the same $I^{Obs}_{\mu,\lambda}$. Therefore any assumed function seems to be more or less fit as long as we know from the value E.

Large E may be due to the experimental error. As the intensities of the scattered light in this time range are very weak, even small experimental error, for instance, the error due to the slight difference between the transmittances of the optical paths for different polarizations and wavelengths, makes the large false dependence of $I^{Obs}_{\mu,\lambda}$. Our analysis interprets the false as the real dependence, as a result, $I^{Cal}_{\mu,\lambda}$ and $I^{Obs}_{\mu,\lambda}$ never agree, so the value E becomes large. In addition, in the range of the Rayleigh like scattering, $I^{Obs}_{\perp,\lambda} >> I^{Obs}_{\parallel,\lambda}$. We measure $I^{Obs}_{\perp,\lambda}$ and $I^{Obs}_{\parallel,\lambda}$ in the same range of lock-in amplifier, so the signal to noise ratio of $I^{Obs}_{\parallel,\lambda}$ much worse than that of $I^{Obs}_{\perp,\lambda}$. That may be one of the reason why the value E is large for small T.

b) For about 5<T<13 min : As shown in Fig. 3.12 at T=7 min typically, five assumed functions give almost the same plot even quantitatively for the range of radii $0.1<a<0.2$ μm. The number density decreases monotonous, from a=0.1 to 0.2 μm. On the other hand, for $a<0.1$ μm, each assumed function gives a separate

distribution. There is, however, the common tendency that the number density for much smaller particles rather decreases and there is a peak of the density at about a~0.1 μm. As to the deviation E shown in Fig. 3.11(a), there is no significant difference between the values E among five assumed functions. They become smaller as time elapses.

From above discussions, the estimated distribution at least in the range of 0.1<a<0.2 μm may be accurate. The particles of this range may be dominant in the analysis, and hide the influence from particles out of the range. Any assumed function more or less gives good fitting. However we cannot clearly declare about the distribution in the range of smaller radius. The reason may be the same as in the case for T<5 min.

c) For about T > 14 min : From Fig. 3.12, we know that the Gauss, the Log-normal, the Junge and the Stevenson give the same plot qualitatively. The size distribution is near monodisperse, and the peak of the density is at about a~0.2 μm. The plot of the Modified exponential is, however, entirely different from others. In addition, as Fig. 3.11(a) shows, the deviation E for the Modified exponential is very large in spite of small E of others. Therefore we conclude that the real distribution is near monodisperse in this time range, and any assumed function gives good approximation except for the Modified exponential. The Modified exponential cannot originally express such a distribution as has a peak and decreases rapidly for smaller radius, so the Modified exponential must lead large E. The fact that the Modified exponential cannot give good approximation for large T is also one of the evidences that there are few small particles for large T.

The Junge distribution may have some disadvantage, although it gives as small E as the Gauss, the Log-normal and the Stevenson do. In the case fo the Junge for large T, there is a tendency that the larger the parameter β is, the smaller the deviation E is. The larger β means that the distribution is sharper and nearer to monodisperse distribution. In addition, the cut-off radius α of the Junge almost corresponds to the position of the peak of the Gauss, the Log-normal and the Stevenson. These give the additional evidences to the conclusion that the real distribution is near monodisperse. There remains a question about the fitness of the Junge.

3.4.3 Temporal Change in Number, Radius, Surface and Volume

Using the distributions obtained above, we calculated the moments defined by Eqs. (3.34)~(3.37). The results are shown in Fig. 3.13, where (a), (b) and (c) are respectively in the cases of air, N_2 and O_2. Here we adopted the Stevenson distribution throughout T. The reason why we here chose the Stevenson is the following. When the temporal changes of moments are calculated from the chain of functions selected as the best at each different T, they sometimes show unnatural discontinuities at the time when the type of the best function switches, for example, at T=5 min in Fig. 3.10(a), where the best function switches from the Junge to the Stevenson. So it may be advisable to use one type of the assumed functions throughout T at least in order to evaluate moments. As shown in Fig. 3.10 the Stevenson frequently gives the best fit for T>9 min. Figure 3.11 shows the value E of the Stevenson is not so inferior in comparison with others even

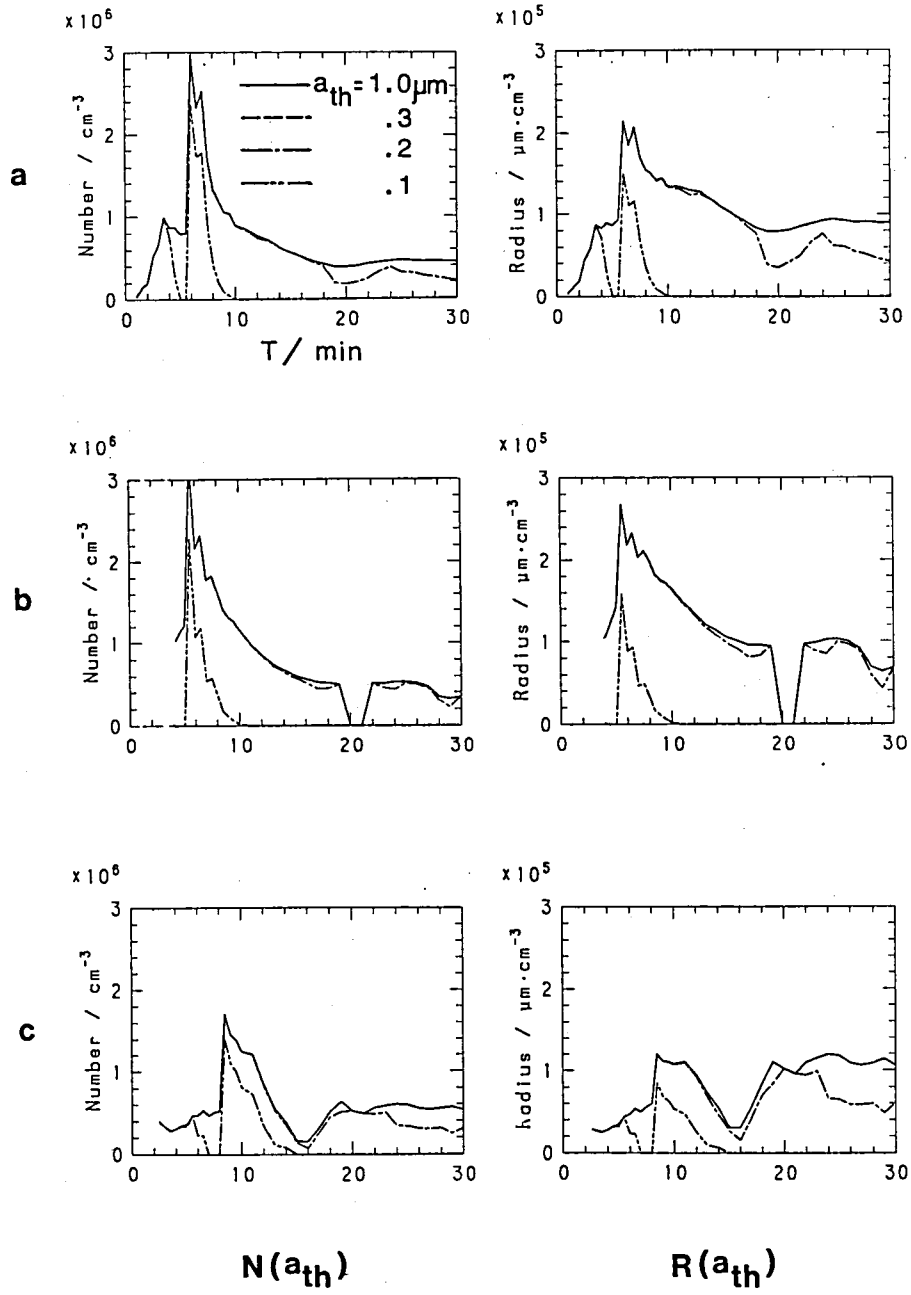

Fig. 3.13 Temporal changes of number $N(a_{th})$, radius $R(a_{th})$, surface $S(a_{th})$ and volume $V(a_{th})$.

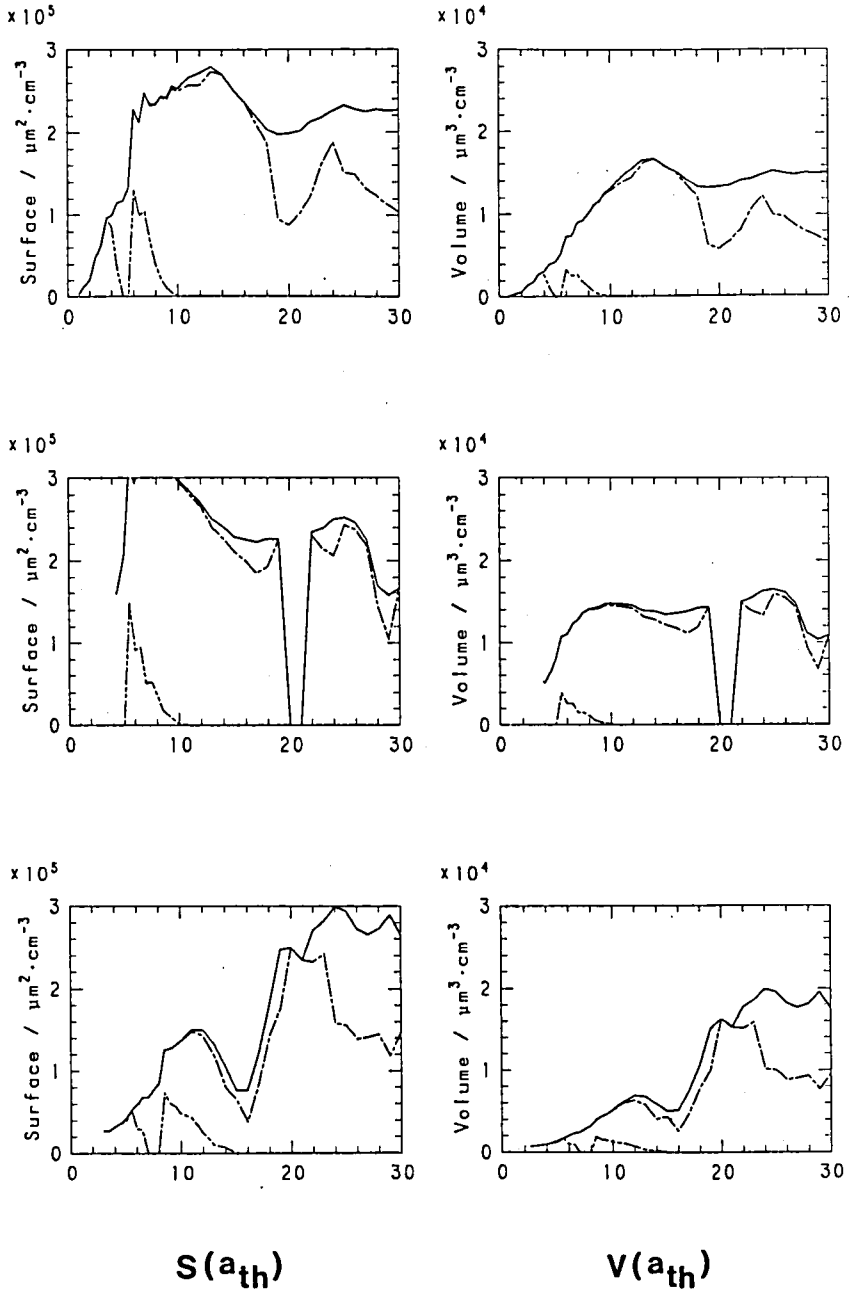

In the case of (a), the surrounding gas is air; in (b), N_2; and in (c), O_2.

in the case of smaller T. When applied throughout T, the Stevenson gives rather smooth temporal changes of moments. In addition, the moments calculated from the Gauss and the Log-normal give almost the same moments as the Stevenson does. Figure 3.14 shows this situation. Figures 3.14(a), (b), (c), (d) and (e) correspond to the changes of $V(a_{th})$ in the cases that the Gauss, the Log-normal, the Junge, the Stevenson and the Modified exponential are respectively applied throughout T in the case of air. Comparing Figs. 3.14(a) (for the Gauss), (b) (for the Log-normal) and (d) (for the Stevenson), the differences between them are less than a few percent. Therefore, to apply the Stevenson for small T must make no significant error for estimating moments.

To the contrary, the Junge and the Modified exponential distributions seem to be unsuitable for estimating moments. As described in Sec. 3.4.2, there is a doubt about the accuracy of the Modified exponential for large T (Fig. 3.14(e)). On the other hand, when used throughout T, the Junge sometimes shows unnatural discontinuities (Fig. 3.14(c)).

The changes of $N(a_{th})$, $R(a_{th})$, $S(a_{th})$ and $V(a_{th})$ are shown in Fig. 3.13, which mean physically the accumulated number, radius, surface and volume of particles respectively, and Figs. 3.13 (a), (b) and (c) are respectively in the cases of air, N_2 and O_2. In Fig. 3.13, we have calculated moments for a_{th}= 0.1, 0.2, 0.3 and 1.0 μm. These graphs show which size of particles contribute to each moment. In this figure, the line of $N(a_{th}$=0.3 μm) falls just on the line of $N(a_{th}$=1.0 μm), which implies that we can regard $N(a_{th}$=0.3 μm) as the total number density N_{total}. In other words, there are few particles with

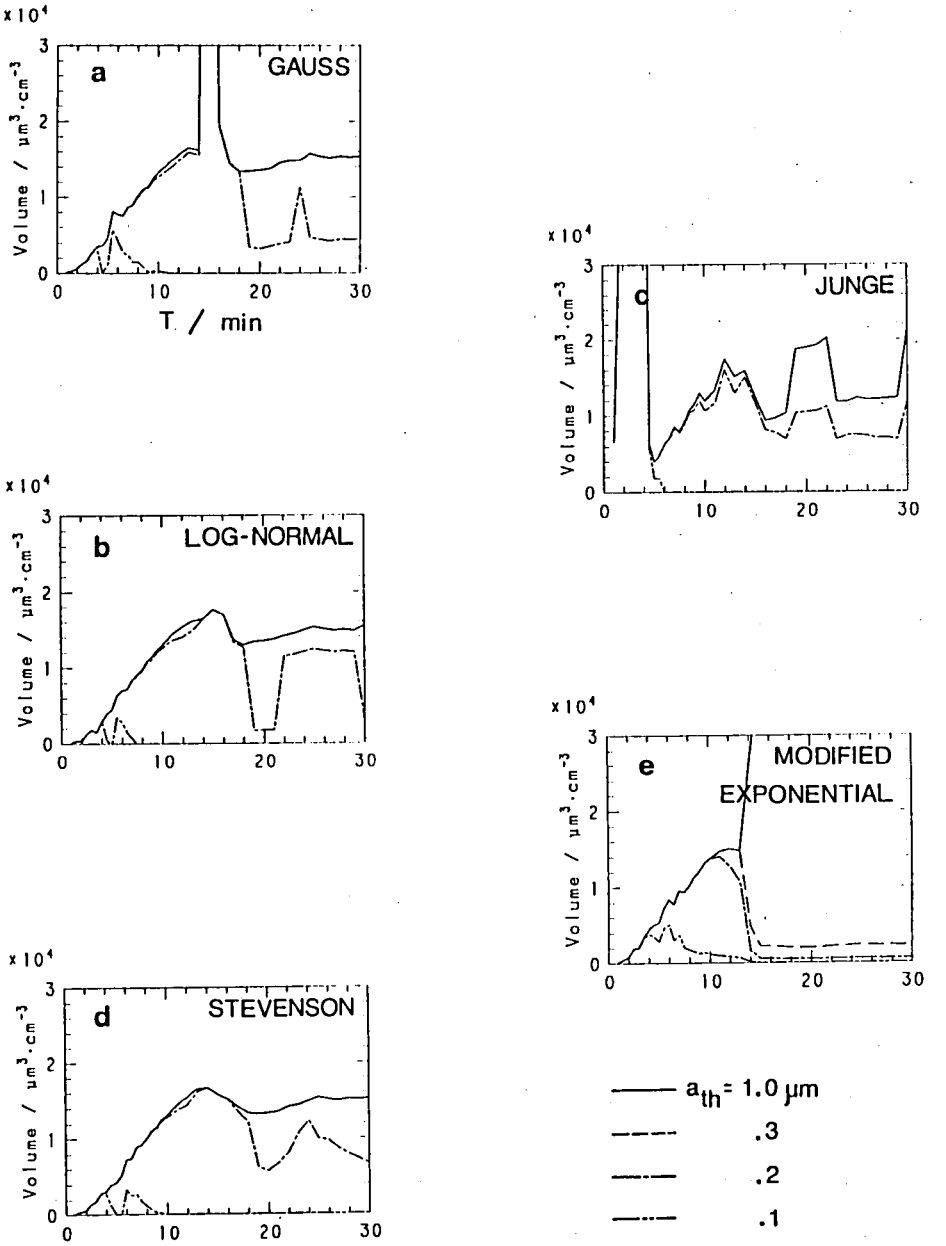

Fig. 3.14 Temporal change of volume $V(a_{th})$, where (a), (b), (c), (d) and (e) are respectively in the cases that the Gauss, the Log-normal, the Junge, the Stevenson and the Modified exponential distribution are applied to calculate the volume. Here the surrounding gas is air.

radii larger than 0.3 μm. This circumstance is similar in the cases of R_{total}, S_{total} and V_{total}.

It is remarkable that the moments from the Gauss, the Log-normal and the Stevenson agree very well as shown in Fig. 3.14 though these assumed functions are different in their shapes especially for their wings. It may be because, we in truth measure not the size distribution but the moments. For particles much smaller than the wavelengths of probes, i.e. for the light scattering of the Rayleigh like, we at last measure the moment of sixth order, for the intensity of the scattered light is proportional to the sixth power of radius there (see Sec. 3.2.1). On the other hand, for particles much larger than wavelengths, we measure the geometrical cross section of particles, i.e. the moment of the second order. Between these two limiting cases, we may measure a moment of a certain order. Therefore our analysis may give the first priority to the estimation of moments, and the estimation of distribution function may be secondary. Therefore it is also not a wonder that the moments from the Gauss, the Log-normal and the Stevenson agree very well.

3.4.4 Process of Aerosol Growth

Using Figs. 3.10 and 3.13, in other words, basing on the temporal changes of the distributions and the moments, we can imagine the mechanism of aerosol growth. The discussion below can be qualitatively applied for any case of air, N_2 or O_2. To study quantitatively, we hereafter pay attention to the case that the surrounding gas is air.

First the photochemical reaction produces many condensable molecules, though the products and the chemical process have not

been clear yet. As these molecules are much smaller than the wavelengths of probes, our measurement may not have enough sensitivity to them. When the density of such molecules becomes high enough, i.e. are super saturated, homogeneous nucleation starts. The molecules condense each other to be small but many particles. Since there is no nucleus first, the nucleation at this stage must be homogeneous.

The total number of small particles rapidly rises up, and the size becomes larger enough to scatter the visible light effectively. This process goes at $T<6$ min, and most of number density consists of particles of $a<0.1$ μm. The total number of such small particles continues to increase until it reaches over 3×10^6 particles/cm^3. Once the number density of such small particles becomes high enough, coalescence begins. The conditions of this turning point is that $a\sim0.1$ μm and $N_{total}>3\times10^6$ particles/cm^3, and it is realized at $T\sim6$ min.

For $T>6$ min, particles coalesce each other, and the number of particles rapidly decreases, while the total volume continues to increase. If the aerosol growth at this stage is purely due to coalescence, the volume must be conservative. Therefore condensable molecules are being produced photochemically and they are deposited on the surface of large particles without experiencing small particles. The rapid growth of surface makes it possible.

For $6<T<10$ min, the size distribution becomes gentle in its shape, it becomes to have a peak, and the position of the peak moves gradually from 0.1 to 0.2 μm. As time elapses, particles of $a<0.1$ μm decrease and those of $0.1<a<0.2$ μm becomes dominant. The breadth of distribution function becomes larger until

T~10 min, then it becomes smaller for T>10 min. At T~10 min, the decrease of number density becomes gentle, which shows the coalescence becomes ineffective to make particles larger. On the other hand, the volume continues to increase until T~13 min, which shows deposition on the surface makes volume larger.

For T>10 min, since a plenty of accumulated surface has already grown up, most of condensable molecules and very small particles on their way to be grown up directly deposit on the surface of large particles. Small particles cannot grow, then the number of particles of a<0.2 μm decreases by deposition. On the other hand, gravitational settling effectively removes particles larger than 0.2 μm as we will check numerically in Sec. 3.4.5. As a result, for T>10 min, the distribution becomes narrower and narrower. The increase of volume is saturated at T~13 min. Coalescence is no longer effective, for the number density is almost conservative. Both the total number and volume stay at almost the stable value, the equilibrium seems to be established. At this stage N_{total}~7×10^5 particles/cm^3 and V_{total}~1.7×10^4 μm^3/cm^3, most of which consists of particles of 0.1<a<0.2 μm. The breadth of distribution continues to decrease. At T~17 min, the breadth becomes smallest, where the size distribution is almost monodisperse. After that, the breadth becomes a little larger, but the distribution no longer becomes widely spread.

For 17<T<20 min, there is a symptom that particles of a>0.2 μm increase and those of a<0.2 μm decrease. It may be due to deposition. However particles larger than 0.2 μm soon disappear by gravitational settling, which causes the decrease of number and surface of such large particles. The decrease of

surface reduces the deposition and urges the growth of smaller particles, which causes the increase of number of particles smaller than 0.2 μm at 20<T<24 min. For T>24 min, there is a symptom that this cycle repeats. For T>24 min, the breadth seems to be a little large, but the radius stays at 0.2 μm and no longer becomes larger.

3.4.5 Mechanism of Change in Particle Size Distribution

It is remarkable that the size distribution function, which has once become broader, becomes narrower again as time elapses. For T>14 min, the distribution is near monodisperse and the most frequent radius is 0.2 μm (Figs. 3.10 and 3.13). When the radius of particle is 0.2 μm and the density is about 1, the Stokes terminal settling velocity is about 10^{-3} cm/sec. Since the probe beams are about a few millimeters in diameter, it takes a few minutes for the particles to come out of the beam. Let us consider the case that most of particles are with radii 0.1 μm and with density 5×10^{5} particles/cm^3 as shown in Fig. 3.13(a) for T>20 min. If they are removed from the view in 5 minutes, the velocity to remove volume is 5×10^{-11} cm^3/cm^3·sec. On the other hand, as shown in Fig. 3.13(a), the total volume is increasing proportionally to time from zero to 1.7×10^{4} μm^3/cm^3 in 13 min at the beginning of aerosol formation. The velocity to produce volume is 2×10^{-11} cm^3/cm^3·sec. This production must be kept for T>20 min. Considering that we here ignore the fall from upper space, we know that the loss by gravitational settling and the gain by production of particles almost balance.

The large limit of radius is explained above, but why is there no small particle for large T? Once the large total

surface of particles is accumulated, condensable molecules and very small particles on their way to be grown up are directly deposited on the surface, therefore small particles cannot grow.

3.4.6 Vapor Pressure of Product

Though the products and the chemical process have not been clear yet, we will roughly estimate the vapor pressure of molecules produced photochemically. As discussed before, the growth of particles at T>10 min is mainly due to the deposition of condensable molecules onto the surface of large particles. The flux Φ by diffusion of small particles of radius R_s onto a large particle of radius R_l is given by $4\pi R_l D N_s$, where D is diffusion coefficient of small particle and N_s is the density of small particles. The velocity of deposition per unit volume is given by $(4\pi R_s^3/3)\cdot\Phi\cdot N_l$, where N_l is the density of large particles. We will consider the case that the velocity of deposition balances with the velocity of producing volume of particles. The latter is about 2×10^{-11} $cm^3/cm^3\cdot sec$ as estimated before (Sec. 3.4.5). Then we obtain a equation,

$$\frac{4}{3}\pi R_s^3 \cdot 4\pi R_l D N_s \cdot N_l \sim 2\times10^{-11}. \qquad (3.37)$$

Let us consider the case that $R_l \sim 0.2$ μm, $N_l \sim 5\times10^5$ particles/cm^3 as shown in Fig. 3.13(a) for large T. Since D is the function of R_s, R_s and N_s are unknown. We will assume the case that the small particle is the condensable molecule which is produced photochemically from p-dichlorobenzene, but is like a molecule of p-dichlorobenzene, whose molecular weight is 147 and density is 1.25. Then $R_s \sim 4\times10^{-8}$ cm and $D \sim 1\times10^{-1}$ cm^2/sec for air at 20 °C. We at last obtain $N_s \sim 9\times10^9$ particles/cm^3. It is 3×10^{-7} mmHg, and

is much smaller than the vapor pressure of p-dichlorobenzene 1.5 mmHg. If the vapor pressure of condensable species is so low, condensation and deposition described above are probable.

3.4.7 Quantum Efficiency of Photochemical Reaction

We will roughly evaluate the efficiency of photochemical reaction, and show that if the condensable monomer like dichlorobenzene is produced photochemically, its photochemical reaction may be not a chain process. However we do not know what photochemical reaction occurs or what the product is, yet. So we assume the following process. A molecule of p-dichlorobenzene absorbs a photon and becomes a monomer which is not so different from a molecule of dichlorobenzene and is condensable to be particles. As estimated before, the velocity to produce volume is 2×10^{-11} $cm^3/cm^3\cdot sec$. Though we do not know the constituent of products, let us suppose its density is 1.25 and molecular weight is 147 (these values are of p-dichlorobenzene itself). Then the velocity of molecule to particle conversion is 1×10^{11} $molecules/cm^3\cdot sec$. The number of photons which are absorbed by p-dichlorobenzene and cause photochemical reaction must be the same. On the other hand, The molar absorption coefficient of p-dichlorobenzene is 174 (though its value is at wavelength 258 nm). This means the intensity of UV radiation decreases by about three percent during passing through 1 cm in the cell, where we consider the vapor pressure of p-dichlorobenzene is 1.5 mmHg at room temperature. The intensity of the incident UV radiation is about 1 mW/cm^2. Then the photon flux at wavelength 220 nm is 1×10^{15} $photons/cm^2\cdot sec$. A three percent of them, which are absorbed by p-dichlorobenzene, is

3×10^{13} photons/cm^3·sec. Therefore the quantum efficiency is about 0.003. If the basic photochemical process is chain like, it becomes larger than 1.

3.4.8 Influence of Surrounding Gas on Aerosol Formation

Comparing Figs. 3.13(a) (for the case of air), (b) (N_2) and (c) (O_2), we can know the influence of the surrounding gases on the formation of aerosol. It is as N_2, air, O_2 in order of aerosol formation velocity. It is shown that the presence of O_2 in the surrounding gas suppress or delay the aerosol formation. The influence of O_2 on aerosol formation will be discussed in Sec. 4.1 in detail.

3.4.9 Validity of Present Measurement

We will check the validity of previous assumptions. One of the significant assumptions is that the produced particle is homogeneous and spherical. In the observation with a microscope, we can see that a spherical and relatively large particle on the wall of the cell catches smaller particles floating in the air and becomes larger and spherical particle. This behavior suggests that the products are liquid like and particles floating in the air may be spherical. But the homogeneity is not necessarily clear. It is possible that the particle in the air has some core in it.

Another assumption is the refractive index n. The value of n of product is, however, unknown so far. We had to previously give n as that of the raw material, p-dichlorobenzene (n=1.5285 for Na D line). Let us assume that n is one of the parameters to be estimated in this experiment. Figure 3.15 shows the change of

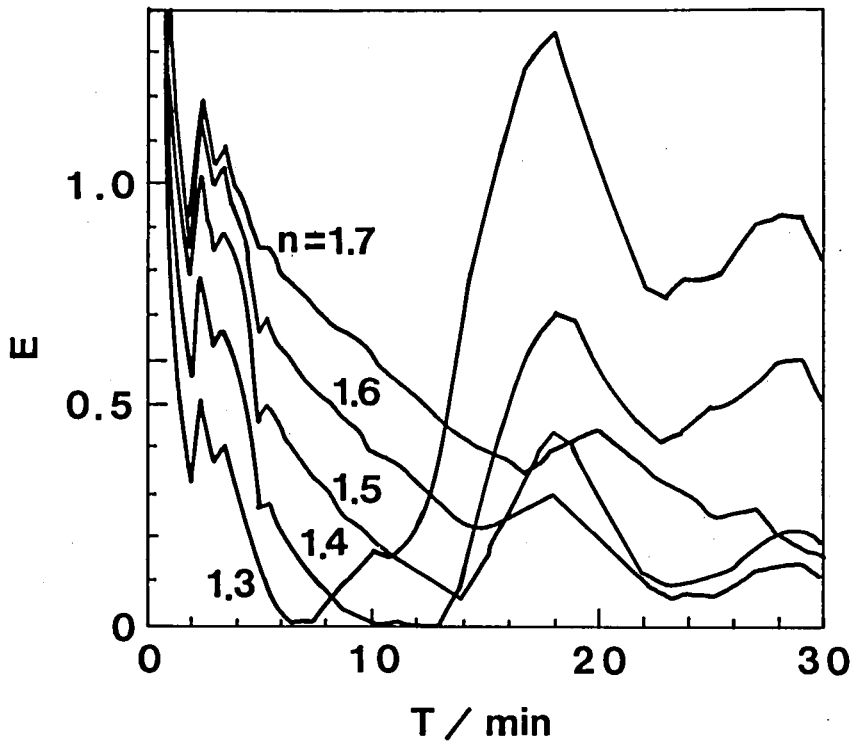

Fig. 3.15 Temporal change in mean square deviation E when the determination of the size distribution is performed changing the assumed refractive index n of particle from 1.3 to 1.7.

the deviation E when we did the determination of the size distribution corresponding to the $I^{Obs}_{\mu,\lambda}$ in Fig. 3.9(a) (in the case of air) changing the assumed value of n from 1.3 to 1.7. If we regard the value of n which gives the smallest E as most probable, Fig. 3.15 shows that as time elapses n becomes larger and larger. It is unlikely that the constituents of products alter. Therefore, Fig. 3.15 may reflect the following situation. Each aerosol particle is not homogeneous and has a core and a shell surrounding the core. As the shell grows, the ap-

parent n changes. Or such a complicated change of n as shown in Fig. 3.15 may vanish when the imaginary part of n is accurately taken into account. Any way, as Fig. 3.15 shows, our assumption that the refractive index of product is the asme as that of raw material, p-dichlorobenzene my be appropriate as the first approximation.

How about the effect of multiscattering? The mean free path of the photon of probe beams can be roughly estimated as $1/\sigma N_{total}$, where σ is the geometrical cross section of particle and N_{total} is its number density. Let us consider the particles of radius 0.2 μm. Then $\sigma \sim 10^{-8}$ cm^3 and $N_{total} \sim 10^6$ particles/cm^3. The mean free path is about 10^2 cm, which is much larger than the dimension of the cell. So the effect of multi-scattering is surely negligible.

3.5 Conclusions

In this chapter, we have reported the optical measurements for the particle size distribution of the aerosol produced from p-dichlorobenzene by UV radiation with wavelength 220 nm, with power density about 1 mW/cm^2. The method is based on the measurement of the wavelength- and polarization-dependence of the light scattered by particles.

Generally the assumed function such as the Gauss, the Log-normal and the Stevenson seems to be superior for estimating the particle size distribution and the moments. The Junge and the Modified exponential are also useful partly.

For T<6 min, the aerosol formation is homogeneous. The number of particles rapidly rises up until it reaches the peak at T~6 min. At the peak, the number of particles, most of which

consists of particles of $a<0.1\ \mu m$, is more than about 3×10^6 particles/cm^3. For $T>6$ min, particles grow mainly by coalescence. While the number of particles decreases, the total volume of particles increase until T~13 min. It is due to the deposition of products on particle's surface, that is, the growth of particles is partly heterogeneous. The distribution function becomes broader until T~10 min, then it becomes narrower again. For T~13 min, the increase of total volume is saturated at $1.7\times10^4\ \mu m^3/cm^3$, where $a\sim0.2\ \mu m$ and $N_{total} \sim 7\times10^5$ particles/cm^3. The breadth of distribution becomes narrower and narrower. For large T, the distribution is near monodisperse, where mean radius is 0.2 μm, $N_{total} \sim 5\times10^5$ particles/cm^3 and $V_{total} \sim 1.5\times10^4\ \mu m^3/cm^3$. The large limit of radius seems to be restricted by gravitational settling. At this stage, the loss by gravitational settling and the gain by photochemical production of particles almost balance.

From the rough estimation of the efficiency of photochemical reaction, the basic photochemical process may be not a chain reaction.

This time, we have first got the quantitative information as to the aerosol formation from p-dichlorobenzene by UV radiation. In the future, some numerical model may be able to explain the results. We couldn't measure aerosol from other material than p-dichlorobenzene, because available monochromatic UV-source was very weak. If using strong and monochromatic UV-source like excimer laser, it may be possible to measure aerosol from other raw materials.

CHAPTER 4

SIZE DISTRIBUTION OF AEROSOL PRODUCED FROM P-DICHLOROBENZENE BY BRIEF EXPOSURE TO ULTRAVIOLET RADIATION

4.1 Introduction

The laser may be one of the most important invention in this century. The laser provides us with many powerful methods to induce some photochemical reactions with good selectivity or to investigate complicated reactions with fine spectroscopic resolution.

In spite of recent many triumphs in laser chemistry, there are few reports that study photochemical aerosol formations induced by the radiation from a laser. As far as we know, "Laser Snow" and "Benzene Aerosol Formation by a KrF Laser" are the only instances. Laser Snow is one of the aerosols produced by laser-induced photochemical reactions. The aerosol is produced from the mixture of vapor of alkali metal and gaseous hydrogen under the exposure to the laser beam from a dye or an argon ion laser (for example, λ=488.0 nm for NaH Laser Snow). The product has been identified as alkali hydride crystalline particle.[18,23~25] Benzene Aerosol is produced from the vapor of benzene under the exposure to ultraviolet (UV) radiation from a KrF excimer laser (λ=249 nm). The constituent of product has not been identified.[26~29]

In Chapter 2, we reported on the aerosol formation from many kinds of organic gases by a KrF excimer laser.[51] For examples

aniline, benzene, dichlorobenzene, α- and β-pinene etc. produce aerosol when exposed to UV radiation from the KrF laser. This is probably the first report on such many kinds of laser induced organic aerosol formations.

In Chapter 3, we also reported on the measurements of the temporal change of particle size distribution of aerosol produced from p-dichlorobenzene.[71] In the experiments, we used a D_2-lamp as a source of UV radiation. As the UV radiation from the D_2-lamp was continuously applied, the production of condensable species continued during the measurements. Therefore, the production of condensable species coexists with the processes of aerosol growth such as condensation, coalescence, deposit, etc. Though such a coexistence is universal in usual aerosol formations, many concurrent processes complicate the problems.

If we produce condensable species in the brief time of the beginning, then observe the aerosol growth without any more production of condensable species, it may be expected that the process of aerosol growth becomes simpler and easier for our analysis. Under such experimental conditions, a monodispersed particle size distribution is initially formed, then it is developed into a heterodispersed distribution. Such processes have been studied theoretically[72~77] and inspected by several experiments.[3,4,52~54,78,79] Keith and Derrick tested tobacco smoke.[52] Huser used the aerosol produced by combustion of propane.[3] Those experiments show that the theory and experiments agree well as far as the condensation due to Brownian motion is concerned, and the developed distribution function is like the Log-normal (Eq. (3.24)).[3] However, the experiment with photochemical aerosol production as the method to prepare initial

aerosol has not been attempted as far as we know.

The experiment with photochemical aerosol production has some advantages compared with those using smoke or other dusts. The former can produce condensable species instantaneously in time and homogeneously in space. The homogeneity of the size of initial species (maybe molecules) is good. In addition, the initial particles are directly produced in the field to be observed. For the latter, on the other hand, one must introduce the initial particles from a certain aerosol generator into the vessel to be observed. The homogeneity of the size of initial particles is not necessary assured and the handling to introduce particles into the vessel may modify the initial distribution.

Using a pulse laser as a UV radiation source for photochemical aerosol formation, it may become possible to produce condensable species instantaneously in time and homogeneously in space. As the photochemical reaction to produce some condensable species is much faster than the process of aerosol formation, the initial particle size distribution is expected to be well monodispersed. In addition to these advantages, the power of the laser is concentrated in narrow wavelength range, then the convection caused by the heating up of the wall of the cell or that of the air in the cell is effectively suppressed compared with the case that the radiation from the UV lamp with broad spectrum is applied directly without filtering.

In this chapter, we report on the optical measurement of the temporal change of the particle size distribution of aerosol from p-dichlorobenzene. Unlike the measurement described in Chapter 3, the aerosol is produced by exposure to the UV radiation from a KrF excimer pulse laser (λ=249 nm). We first produce

the condensable species by applying several the UV radiation pulses from the KrF laser in a brief time, then observe the temporal change of the particle size distribution without applying any more UV radiation pulses. The method of measurement is the same as described in Chapter 3, which is based on the light scattering from produced particles.

4.2 Experiments

The principle of measurement and experimental setup are the same as described in Chapter 3 (Secs. 3.2 and 3.3). The different points are as follows (see Fig. 4.1).

The UV radiation source is not a D_2-lamp but a KrF excimer laser, which radiates monochromatic UV radiation with wavelength 249 nm and with power density P about 1.8 $mJ/cm^2 \cdot$pulse at the position of the cell. Unlike the UV radiation source used in Chapter 3, the UV light from the KrF laser is directly applied into the cell without filtering by a monochromator, because the

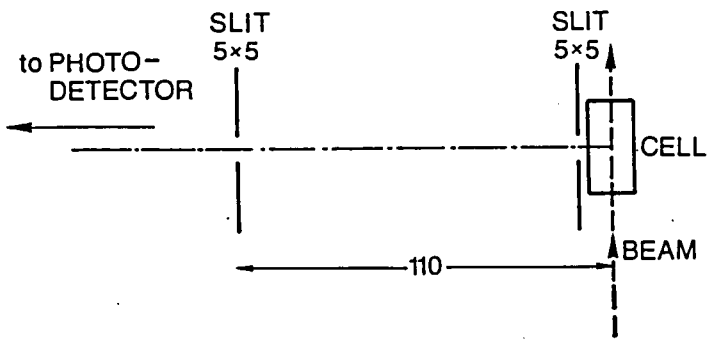

Fig. 4.1 Dimension of optical system.

radiation from the KrF laser is fully monochromatic. To measure the power dependence of aerosol formation, we change P by in-

serting a quartz glass plate as a ND filter between the excimer laser and the cell. Then P becomes 1.8 mJ/cm^2·pulse (without the plate) and 1.3 mJ/cm^2·pulse (with the plate). The beam size of the KrF laser at the cell is about 1×1 cm^2.

The cell, which contains bits of p-dichlorobenzene, is filled with air at 1 atm, at room temperature.

After applying 40 pulses from the excimer laser into the cell at the rate of about 5 Hz, we record the changes of $I^{Obs}_{\mu,\lambda}$ (μ=∥,⊥ and λ=457.9, 632.8 nm), the intensity of the scattered light normalized by the intensity of the incident light as defined by Eq. (3.20). About 5~40 pulses is necessary to produce particles enough to be detected by this experimental setup. A few pulses is not enough. In order to protect the photomultiplier, the power supply to photomultiplier is off during UV irradiation.

We also make the scattering solid angle ($\Delta\theta\times\Delta\phi$ in Figs. 3.4~3.6) small, by using the small 0.5×0.5 cm^2 slit placed at 11.0 cm apart from the probe beam as shown in Fig. 4.1 (compare with Fig. 3.8 for the previous experiments in Chapter 3). If $\Delta\theta$ is small, it is expected that the information about the θ dependence of $I^{Obs}_{\mu,\lambda}$ will be less lost by averaging over θ as in Eq. (3.19). However the decrease of the solid angle causes the diminution of the scattered light intensity to be detected, then signal to noise ratio gets worse.

Unlike the optical setup in Chapter 3 (Fig. 3.8), the scattered light is restricted through the slit described above, then applied directly into the window of the photomultiplier (Fig. 4.1). The lens to correlation the scattered light is not used. Then there is no loss by lens. In addition the dimension

of observed field (L in Fig. 3.6) is clearly recognized, for the image near boundary of observed field is blurred when lens is used.

In order to determine the size distribution at a given time T according to the method described in Chapter 3, we must measure the four values of $I^{Obs}_{\mu,\lambda}$ corresponding to the different combinations of wavelengths (λ=457.9, 632.8 nm) and polarizations (μ=∥,⊥) at the time T. In Chapter 3, we did not measure this set of $I^{Obs}_{\mu,\lambda}$ strictly at the same time but at the series of different times. In that case, the velocity of aerosol formation was much slower compared with the time which was required to measure a set of $I^{Obs}_{\mu,\lambda}$, then we could regard them as measured at the same time. This time, in order to study the rapid change of particle size distribution just after applying of UV radiation pulses, we get the values of $I^{Obs}_{\mu,\lambda}$ strictly at the same time by interpolation. The analysis of $I^{Obs}_{\mu,\lambda}$ has be done as described in Chapter 3.

4.3 Experimental Results and Discussions

4.3.1 Temporal Change in Scattered Light Intensity

Figure 4.2 shows the change of $I^{Obs}_{\mu,\lambda}$, where (a) and (b) correspond to the case of P=1.8 mJ/cm^2·pulse and (c) and (d) P=1.3 mJ/cm^2·pulse, and T represents the time after applying UV radiation pulses. We take T=0 as the time when the first pulse is applied. Compared with the case of the continuous exposure to UV radiation in Chapter 3 (Fig. 3.9), the oscillation of $I^{Obs}_{\mu,\lambda}$ is very peculiar. There may be two possible interpretations. a) The oscillation is due to the convection, and b) it stands for the aerosol growth. When the convection exists, the cloud of aerosol gradually goes away from the probe beams, and in a

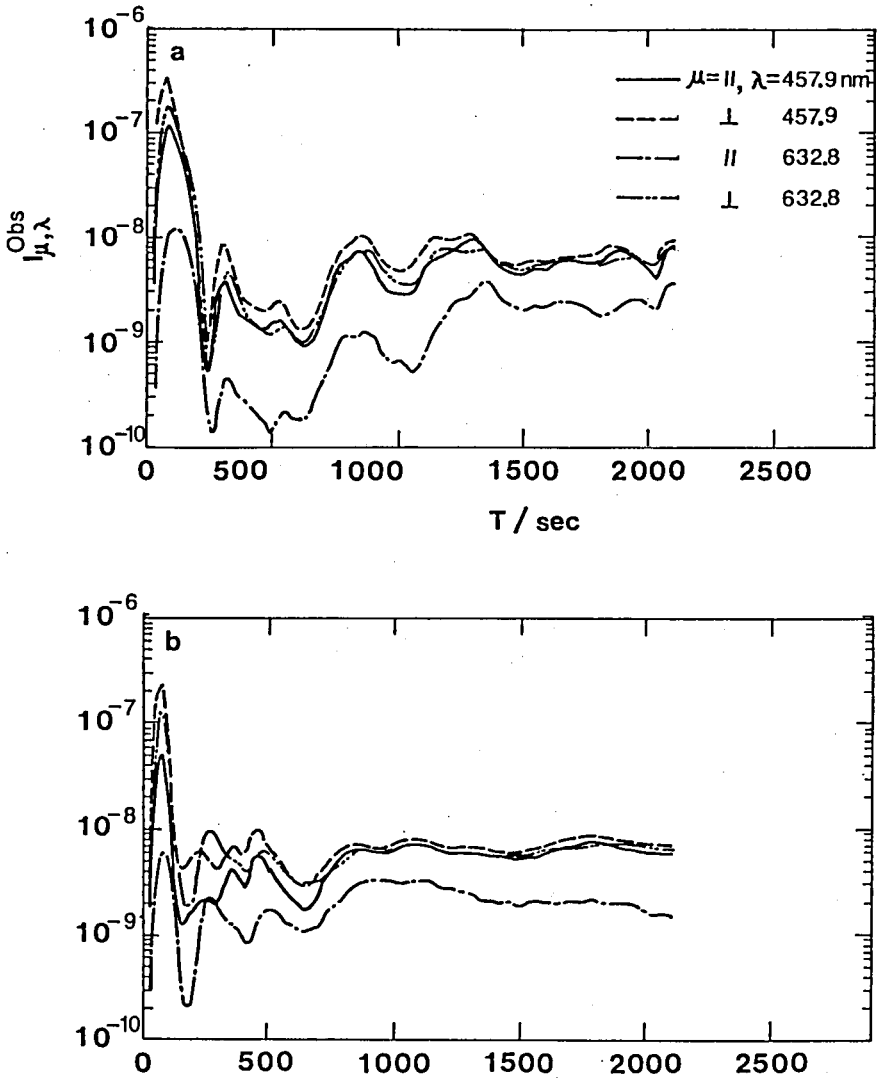

Fig. 4.2 Temporal change in scattered light intensities $I^{Obs}_{\mu,\lambda}$. In the cases of (a) and (b), P=1.8 mJ/cm^2·pulse; and in (c) and (d), P=1.3 mJ/cm^2·pulse.

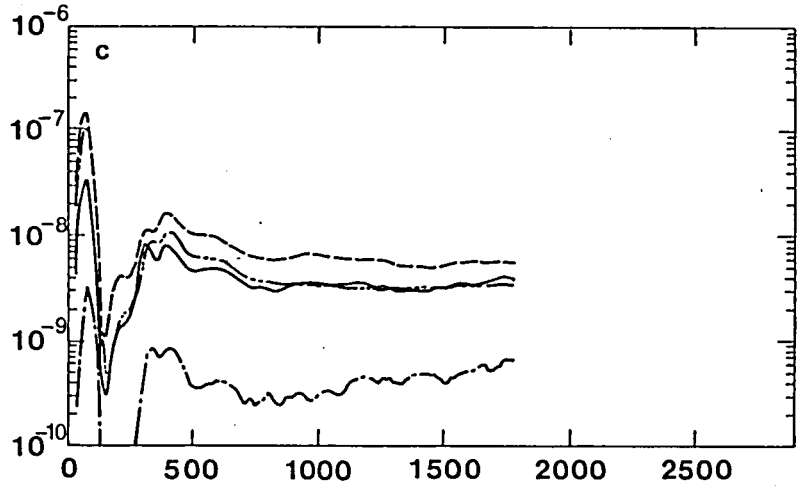
c
10^{-6}
10^{-7}
10^{-8}
10^{-9}
10^{-10}
0
500
1000
1500
2000
2500

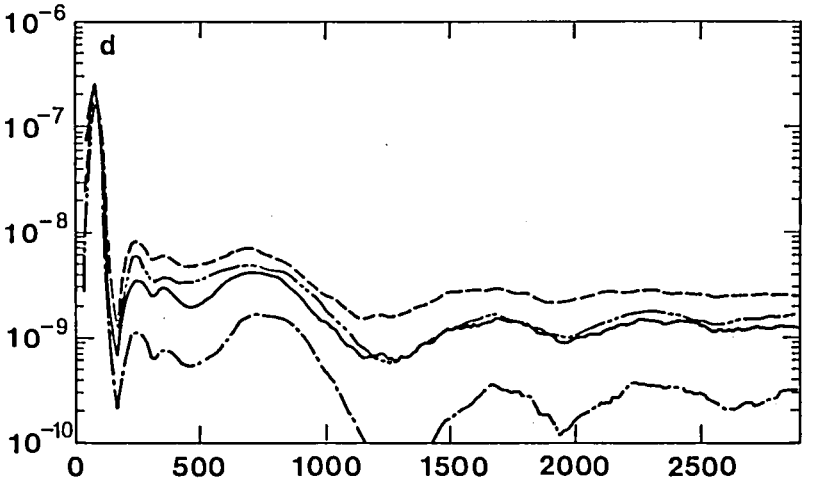
d
10^{-6}
10^{-7}
10^{-8}
10^{-9}
10^{-10}
0
500
1000
1500
2000
2500

moment, comes back into the beam, then $I^{Obs}_{\mu,\lambda}$ oscillates. As far as we observe by our eyes, we could not find the movement of aerosol cloud. There must be no heavy convection. The oscillation with long period of about 10 minutes in Fig. 4.2 may be due to the convection. As discussed in Chapter 2, the air in the cell is almost transparent to the UV radiation from the KrF laser (λ=249 nm), the heat source of convection may be the heating up of the wall of the cell by UV radiation absorption.

As mentioned in Sec. 3.2.1 the wavelengths of light scattered by particles of a certain radius depends on the radius of the particle. As particle grows larger, the light of longer wavelengths becomes to be scattered effectively. Looking at Fig. 4.2 carefully, one can notice that the phase of the oscillation differs a little for each $I^{Obs}_{\mu,\lambda}$. If the oscillation is completely due to convection, any component of $I^{Obs}_{\mu,\lambda}$ changes in phase. Therefore the oscillation partially stands for the aerosol growth, and the difference between the phases in temporal change of $I^{Obs}_{\mu,\lambda}$ reflects size distribution and its temporal change.

Each $I^{Obs}_{\mu,\lambda}$ reaches its maximum within a few minutes after the end of applying the UV radiation pulses, i.e. after the beginning of the measurement, then decreases rapidly. This processes are very quick compared with the results obtained in Chapter 3.

We have carefully set the experimental conditions as same as we can except for P, power density of incident UV radiation. Though both Figs. 4.2(a) and (b) are in the cases of P=1.8 mJ/cm^2·pulse, the reproducibility is not necessarily good. As to Figs. 4.2(c) and (d) (in the case of P=1.3 mJ/cm^2·pulse), the situation is the same. However, comparing Figs. 4.2(a), (b)

and (c), (d), especially paying attention to the $I^{Obs}_{\mu,\lambda=632.8\ nm}$ for each case, the dependence of $I^{Obs}_{\mu,\lambda}$ on P is apparent. The larger P is, the larger the amount of aerosol production is.

4.3.2 Temporal Change in Size Distribution

From $I^{Obs}_{\mu,\lambda}$ shown in Fig. 4.2, we determined the particle size distribution at each T according to the method described in Chapter 3. This time, we did not use the Modified exponential distribution (Eq. (3.27)). We tested the Gauss (Eq. (3.23)), the Log-normal (Eq. (3.24)), the Junge (Eq. (3.25)) and the Stevenson distribution (Eq. (3.26)). The results are shown in Fig. 4.3, where (a), (b), (c) and (d) respectively correspond to the results from Figs. 4.2(a), (b), (c) and (d). In any case, during our measurement, there seems to be no dramatic change of distribution function except for the gradual decreasing of the height of distribution function.

At the beginning of T, particles are already grown up, the size distribution is broadly heterodispersed and its wing had spread to 0.2~0.3 μm. Just after the end of applying UV radiation pulses, there must be a large amount of condensable species produced by photochemical reactions. However, in Fig. 4.3, we cannot find the process that such small species condense and grow to be larger particles. We turn the power supply to the photomultiplier on after the end of applying UV radiation pulses in order to protect the photomultiplier. It takes about 10 seconds to apply all 40 pulses. We take T=0 as the time when the first pulse is applied. Therefore, there is a blind period of about 10 seconds at the beginning of measurement. Since the initial process to produce aerosol is very quick and is completed

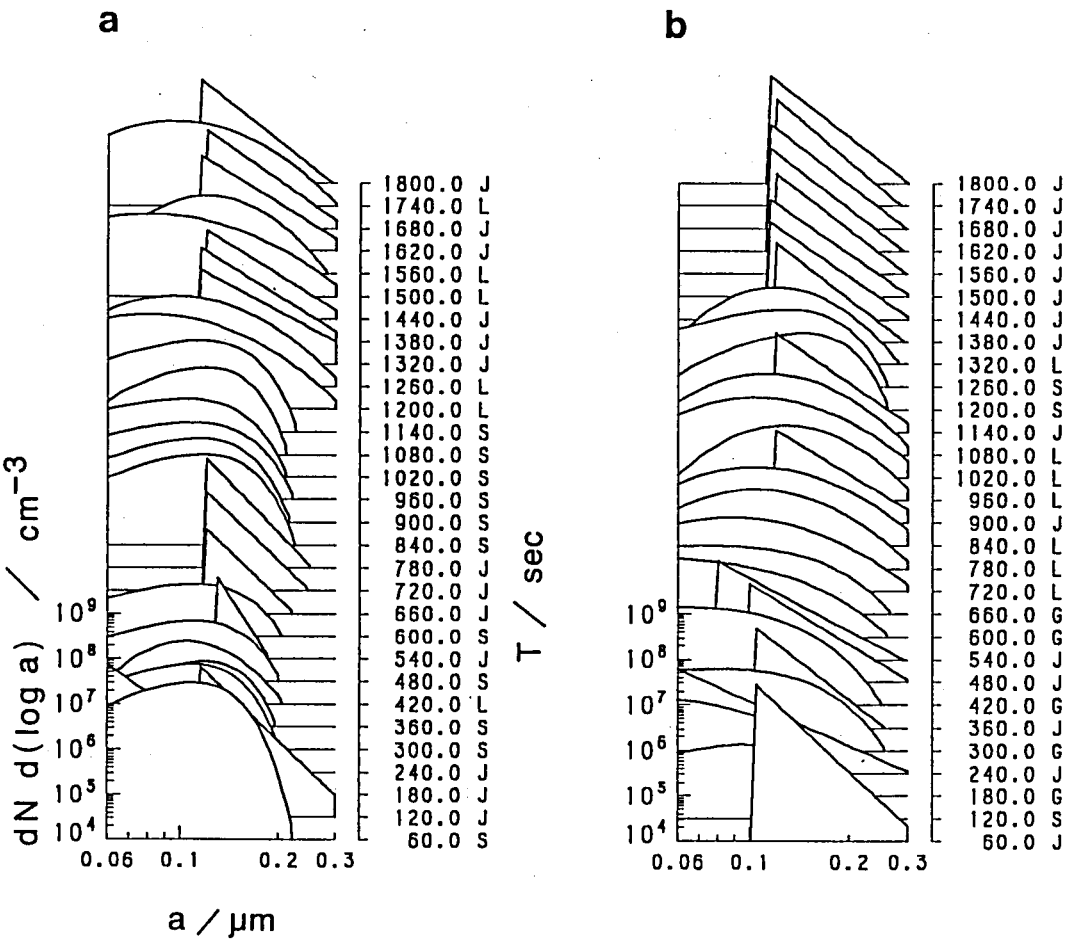

Fig. 4.3 Temporal change in particle size distribution. In the cases of (a) and (b), P=1.8 mJ/cm^2·pulse; and in (c) and (d), P=1.3 mJ/cm^2·pulse. Symbols "G", "L", "J" and "S" respectively represent that the Gauss, the Log-normal, the

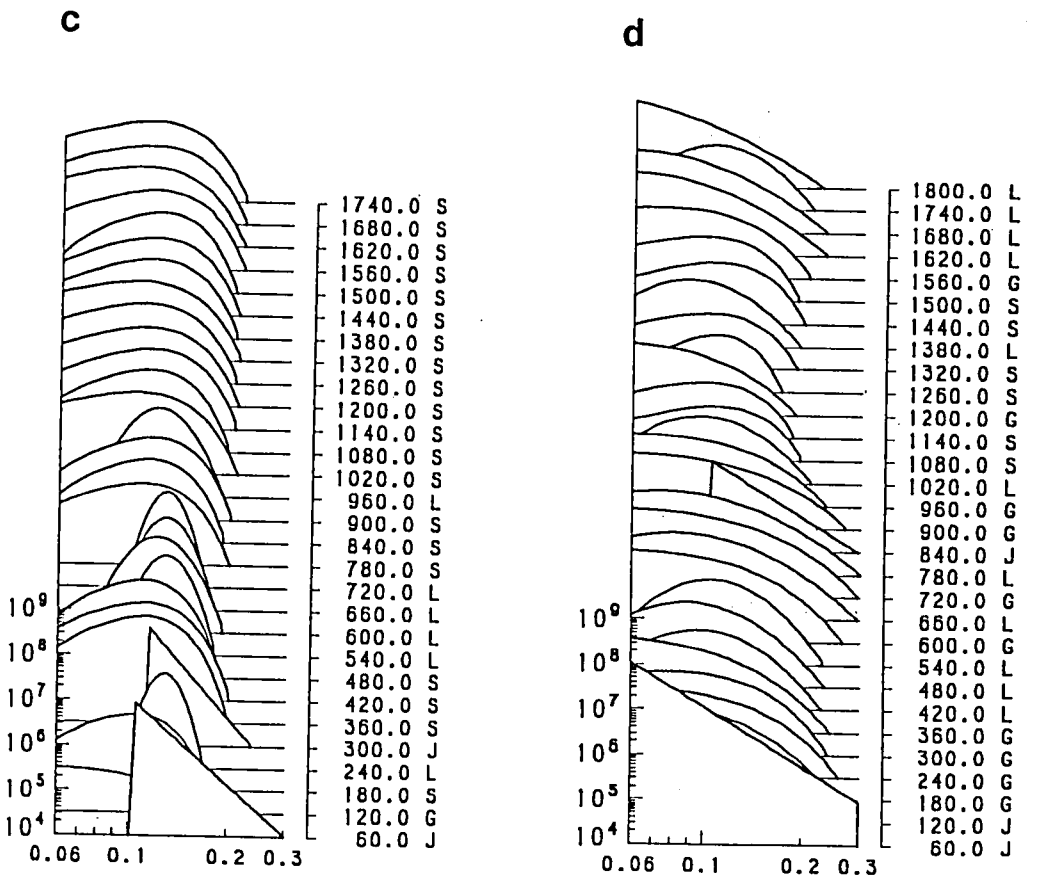

Junge and the Stevenson distribution give the best fitting at the given time T after the irradiation of ultraviolet light pulses.

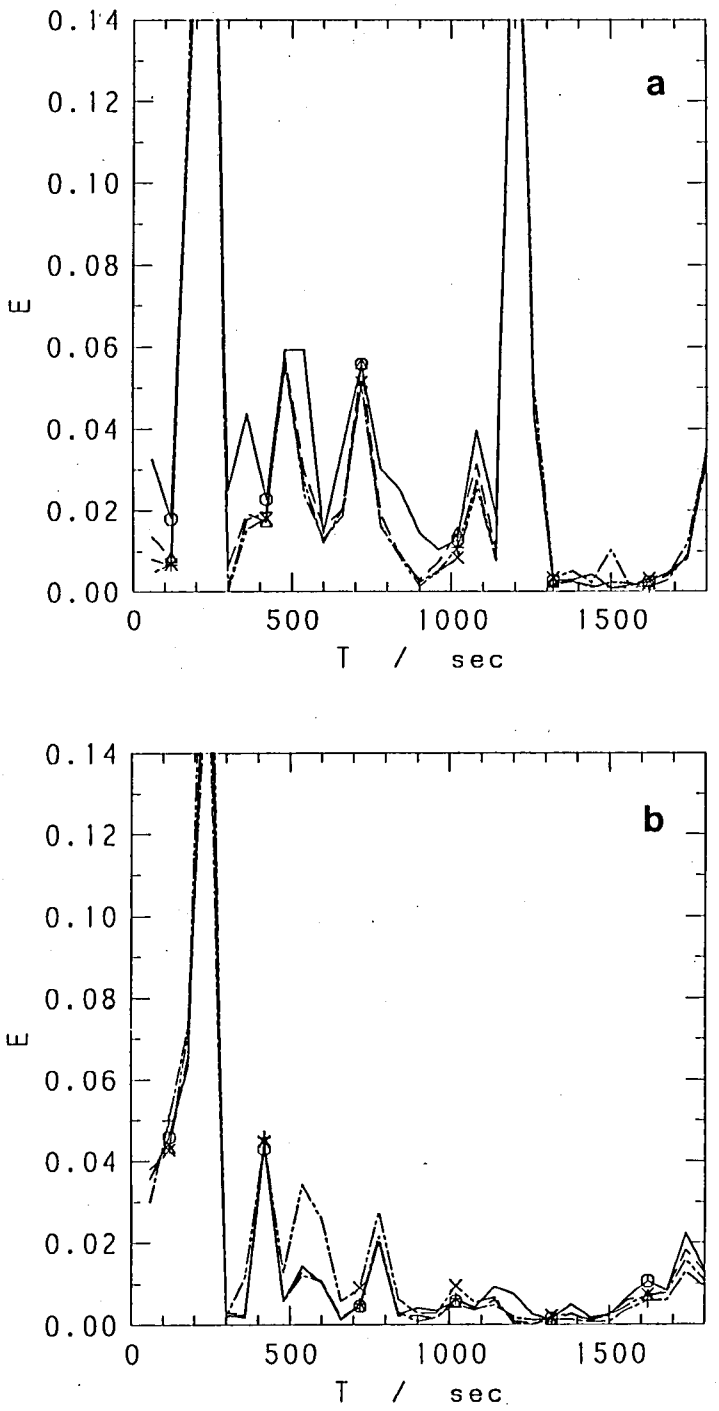

Fig. 4.4 Temporal change in mean square deviation E. In the cases of (a) and (b), P=1.8 mJ/cm^2·pulse; and in (c) and (d), P=1.3 mJ/cm^2·pulse.

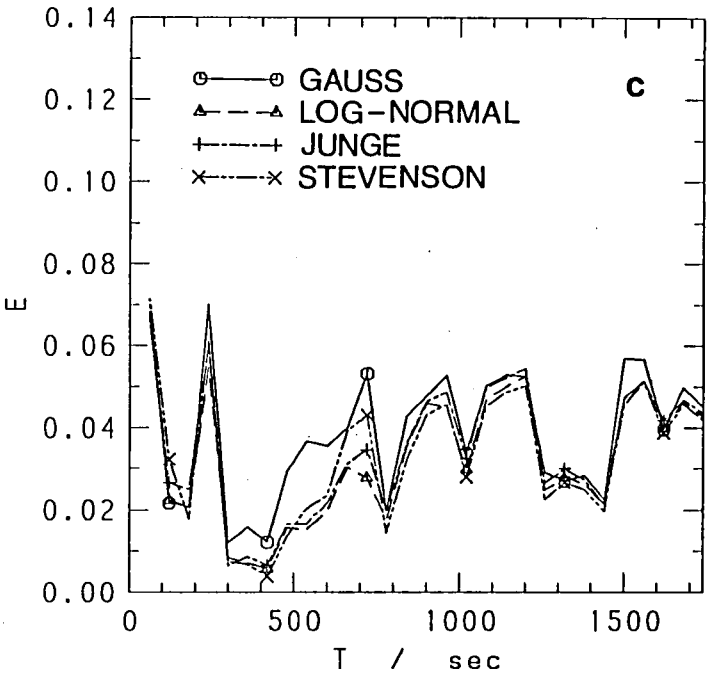
GAUSS
LOG-NORMAL
JUNGE
STEVENSON
c
E
0.14
0.12
0.10
0.08
0.06
0.04
0.02
0.00
0
500
1000
1500
T / sec

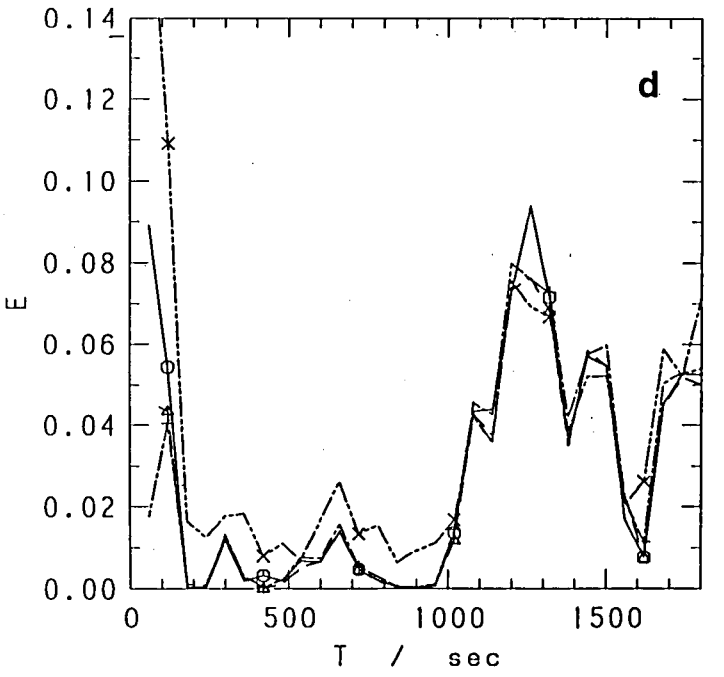
d
E
0.14
0.12
0.10
0.08
0.06
0.04
0.02
0.00
0
500
1000
1500
T / sec

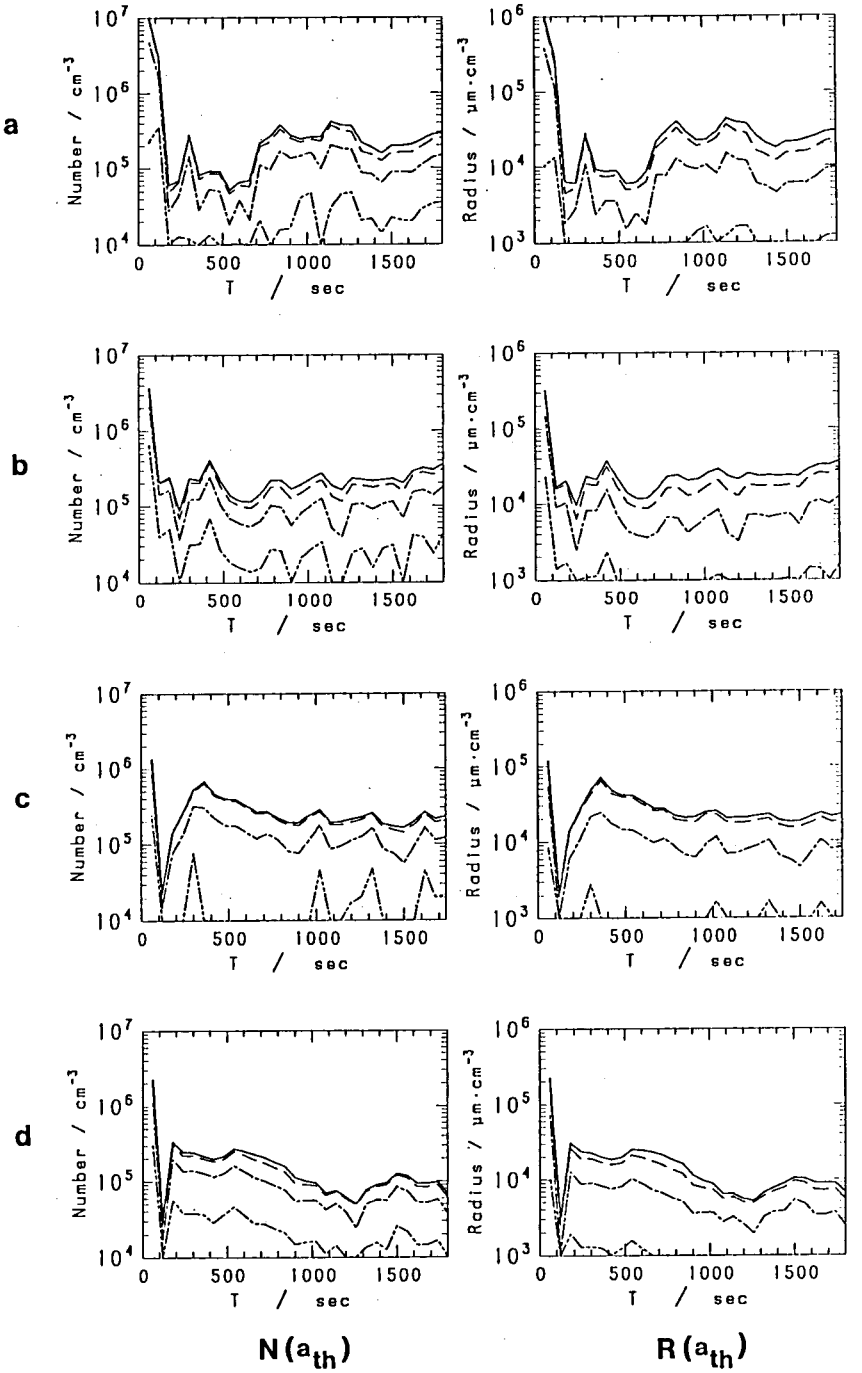

Fig. 4.5 Temporal changes of number $N(a_{th})$, radius $R(a_{th})$, surface $S(a_{th})$ and volume $V(a_{th})$ of particles. In the cases of (a) and (b), P=1.8 mJ/cm^2·pulse; and in (c) and (d), P=1.3 mJ/cm^2·pulse.

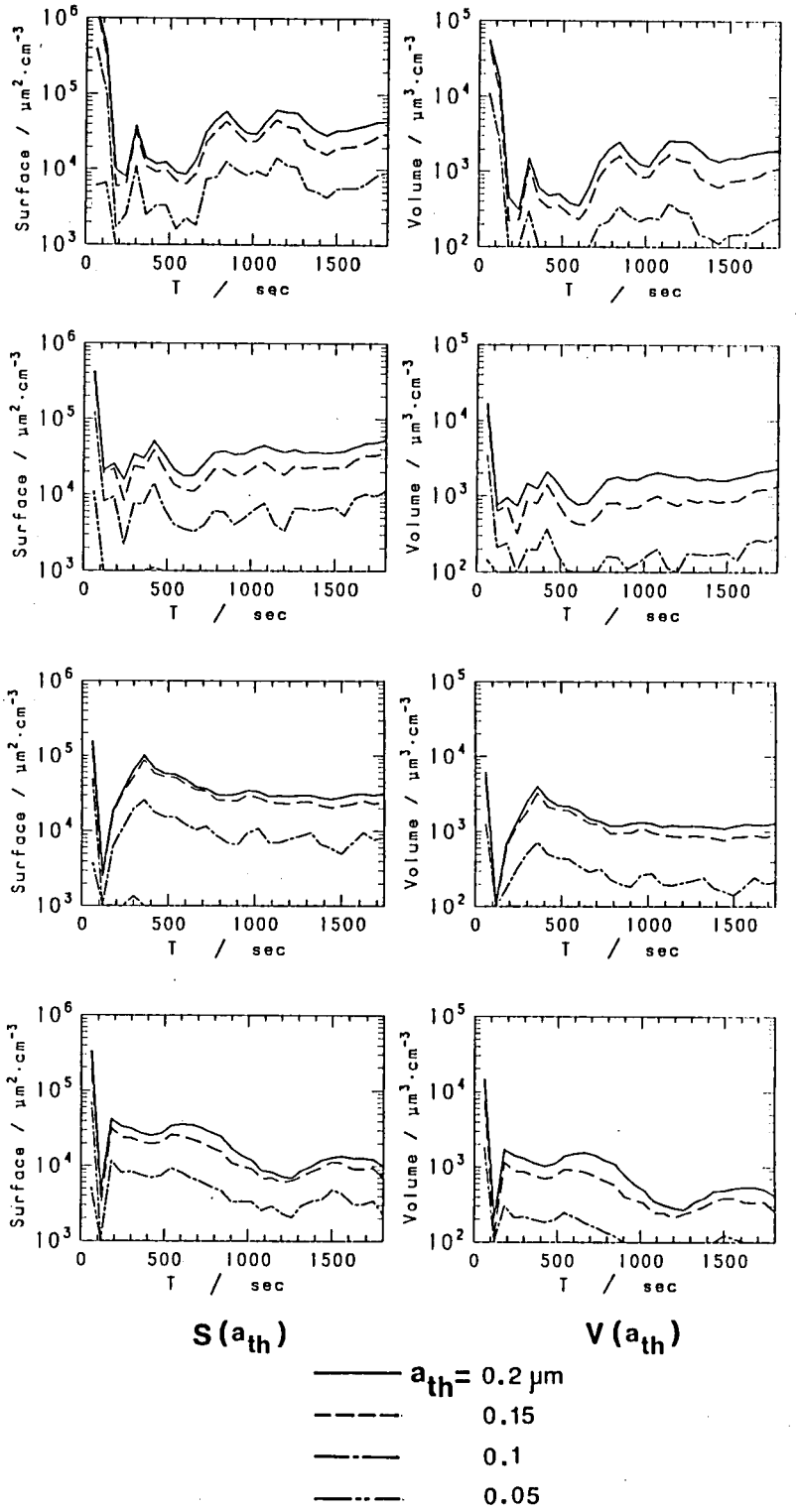
Surface / µm².cm⁻³
Volume / µm³.cm⁻³
T / sec
S(a_th)
V(a_th)
a_th= 0.2 µm
0.15
0.1
0.05

during the blind period.

In Fig. 4.3, the character "G", "L", "J" and "S" respectively represents that the Gauss, the Log-normal, the Junge and the Stevenson distribution give the best fitting at each T. There is no superiority among these four assumed functions. The best function is not fixed. It frequently changes for different T. From Fig. 4.4, which shows the change of E, the mean square deviation defined by Eq. (3.28), it is clear that there is no significant difference between the values of E of four assumed functions. As discussed in Sec. 3.4.2, the particles of radii larger than 0.1 μm are dominant in our analysis. Any assumed function which spreads broadly in this radius range gives more or less good fitting. The particles already grow up and spread broadly in this radius range, then there is no superiority among four assumed functions. We are confident of the results in this radius range. To the contrary, we cannot mention clearly to the distribution of radii smaller than 0.1 μm.

As mentioned in Sec. 4.1, the realized distribution function is believed to be like the Log-normal according to the theory of condensation by Brownian motion.[3] However, the Log-normal is no more than the approximate solution obtained from the numerical calculation. The validity of the Log-normal distribution at least in the visible light scattering region is not necessarily assured. From our results, the superiority of the Log-normal seems to be not clear.

In the case that the UV radiation from the D_2-lamp is continuously applied during the measurement as in Chapter 3, the shape of distribution function becomes narrow and near monodisperse for large T (Fig. 3.10). Unlike that case, such a

sharpening of distribution function for large T is not found this time (Fig. 4.3). The difference is due to whether the continuous supply of condensable species is present or not. Such a sharpened and nearly monodispersed distribution is not formed without the supply of new products.

4.3.3 Temporal Change in Number, Radius, Surface and Volume

Figure 4.5 shows the changes of moments of distribution function, i.e. number $N(a_{th})$, radius $R(a_{th})$, surface $S(a_{th})$ and volume $V(a_{th})$ calculated from Eqs. (3.34)~(3.37). Here we also adopted the Stevenson distribution throughout T as we done in Sec. 3.4.3. We calculated these moments for a_{th}=0.05, 0.1, 0.15 and 0.2 μm. Compared with the results from the case that the UV radiation from the D_2-lamp is continuously applied during the measurement as in Chapter 3 (Fig. 3.13), it is remarkable that all moments of $N(a_{th})$, $R(a_{th})$, $S(a_{th})$ and $V(a_{th})$ change similarly in phase. Under the ideal conditions, the volume must be conservative, for we do not produce any more condensable species after the end of applying UV radiation pulses. Therefore the similar change of $N(a_{th})$ and $V(a_{th})$ suggests the following. The process such as coalescence or condensation is not effective in changing these moments. The changes of moments are mainly due to the spatial fluctuation of particle distribution, for instance, convection.

However, the evidence of aerosol growth is also found. Let us pay attention to the change of volume, especially to Fig. 4.5(c). The ratio of the partial volume of particles with radii 0.15~0.2 μm to that with radii 0.1~0.15 μm is gradually

increasing, which shows the aerosol growth. Since the increase of number of particles with radii 0.15~0.2 μm, is not clearly found, the process of growth is due to deposition of small particles ($a<0.05$ μm) onto the surface of large particles.

Comparing Figs. 4.5 (a), (b) (for P=1.8 mJ/cm^2·pulse) and (c), (d) (for P=1.3 mJ/cm^2·pulse), the volume of the former cases is increasing little by little for large T. On the other hand, the volume of the latter cases is decreasing. Since the quantitative reproducibility is not necessarily good as remarked before, it is not clear whether the difference is correctly due to the P dependence of aerosol formation or not.

4.3.4 Aerosol Formation at the Beginning

For T=150~200 sec in Fig. 4.5, all moments of number, radius, surface and volume once decrease rapidly, then they again increase. Such a rapid decrease is also shown in the temporal change of $I^{Obs}_{\mu,\lambda}$ (Fig. 4.2). What is the cause of this rapid decrease?

To survey this, we studied the changes of distribution function and moments with finer time resolution for T<300 sec. The results are shown in Figs. 4.6 and 4.7, where (a) and (c) respectively correspond to the cases of (a) and (c) in Figs. 4.2, 4.3 and 4.5. From Figs. 4.6 and 4.7, it is found that both distribution function and moments dramatically change at the beginning.

In Fig. 4.6, the distribution is already developed at T=20 sec. It is peculiar compared with the case that the UV radiation from the D_2-lamp is continuously applied during the measurement as in Chapter 3. Let us pay attention to

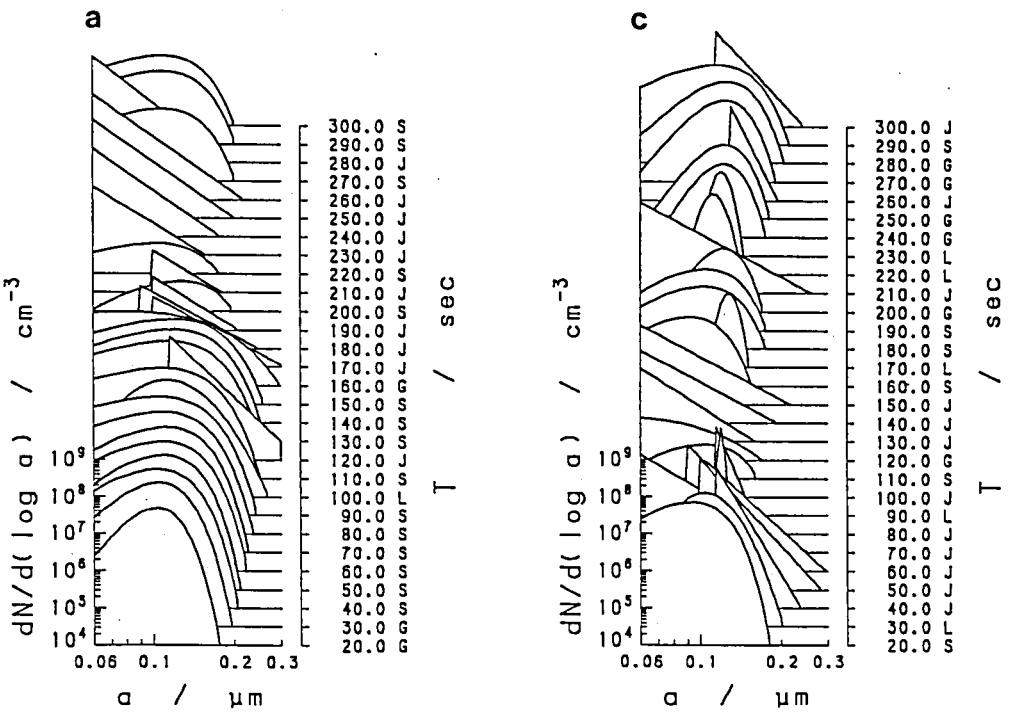

Fig. 4.6 Temporal change in particle size distribution at the beginning. In the case of (a), P=1.8 mJ/cm^2·pulse; and in (c), P=1.3 mJ/cm^2·pulse. Symbols "G", "L", "J" and "S" respectively represent that the Gauss, the Log-normal, the Junge and the Stevenson distribution give the best fitting at the time T after the irradiation of ultraviolet light pulses.

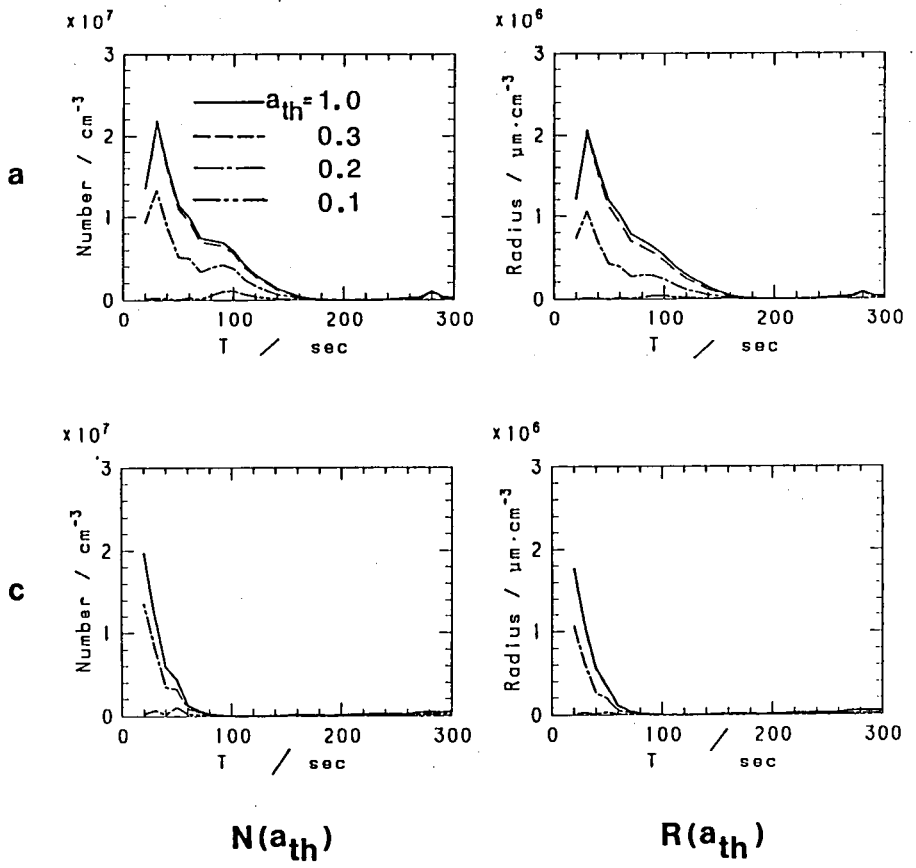

Fig. 4.7 Temporal changes of number $N(a_{th})$, radius $R(a_{th})$, surface $S(a_{th})$ and volume $V(a_{th})$ at the beginning. In the case of (a), P=1.8 mJ/cm^2·pulse; and in (c), P=1.3 mJ/cm^2·pulse.

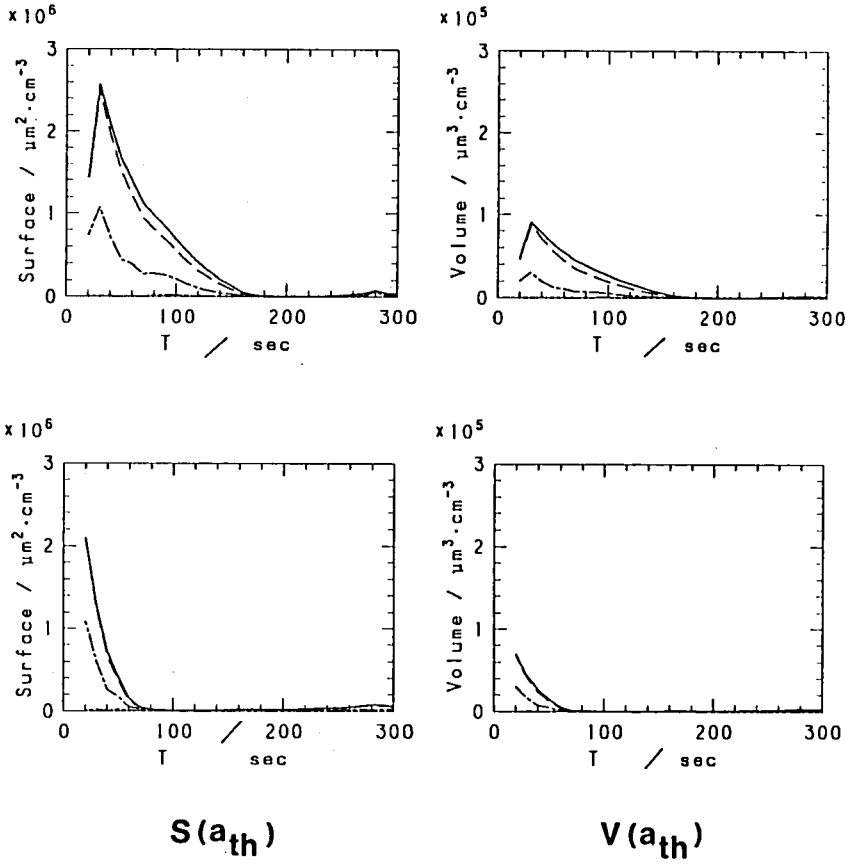
x10^6
Surface / μm^2·cm^-3
T / sec
x10^5
Volume / μm^3·cm^-3
T / sec
x10^6
Surface / μm^2·cm^-3
T / sec
x10^5
Volume / μm^3·cm^-3
T / sec

$S(a_{th})$ $V(a_{th})$

Figs. 4.5(a) and 4.6(a) (both are for P=1.8 mJ/cm^2·pulse). As time elapses, the wing of distribution function spreads to larger radii and the height of it decreases rapidly. As the distribution changes, the moment reaches its maximum at T=30 sec, then decreases rapidly, which shows the growth of aerosol is at its peak for T~30 sec, then it decreases.

As the terminal settling velocity of a particle with radius 0.1 μm is about 10^{-4}cm/sec.[4] The thickness of aerosol cloud is about 1 cm (the beam size of the KrF laser at the cell is about 1×1 cm^2) and we probe the center of it by the probe beam with diameter about 1 mm, then it takes about 1 hour for the settling to sweep particles away completely. Such a quick disappearance of particles cannot be explained by the gravitational settling.

From Fig. 4.7, the number of particles of radii 0.2~0.3 μm and that of radii smaller than 0.2μm fluctuate together in phase. The rapid disappearance of particles seems to be due to the convection. The convection carries particles away from the probe beam. As the particles group in the small volume in the air at the beginning of T, even small motion causes the rapid disappearance of particles from the view. As time elapses, particles diffuse in space, then such a rapid change is no longer observed when the cloud of particles is carried into the probe beam again by convection.

It is difficult to discuss the P dependence of moments quantitatively because of this convection. However, comparing Figs. 4.7(a) and (c), the existence of P dependence is clear. The higher P is, the larger the amount of produced aerosol is.

Comparing Figs. 4.7(a) and (c), we find the following. In the case of P=1.8 mJ/cm^2·pulse (for Fig. 4.7(a)), the peaks of

moments are observed. On the other hand, in the case of P=1.3 mJ/cm^2·pulse (for Fig. 4.7(c)), peaks are not observed. Large P seems to cause the delay of aerosol growth. However, we do not know the mechanism so far.

4.4 Conclusions

In this chapter, we reported on the aerosol formation from p-dichlorobenzene induced by a KrF excimer laser (λ=249 nm). We studied the temporal change of its particle size distribution in detail. The method was the same as used in Chapter 3, i.e. we measured the wavelength- and polarization-dependence of the light scattering by aerosol particles, then determined the adjustable parameters of the assumed size distribution function so that the measured dependence and the theoretically calculated dependence would agree well.

Unlike the experiment reported in Chapter 3, where we produced aerosol by continuous exposure to UV radiation, we initially produced the large amount of condensable species in a brief time by applying the 40 pulses of UV radiation from the KrF excimer laser into the vapor of p-dichlorobenzene, then observed the change of the size distribution of particles which were condensed from the species without any more production of them.

Under such a condition, it is expected that the monodispersed distribution composed of initially produced condensable species is first built up, then it is developed into broadly dispersed distribution by condensation or other aerosol growth processes.

Contrary to our expectation, we could not observe the process because the process was very quick and was completed

during the brief time of applying UV radiation pulses. At the beginning of measurement, the size distribution was already developed. It is desirable to produce the initial aerosol by exposure to a single UV radiation pulse. Considering the fear that the latter one of series of pulses may destroy the condensable species produced by the former pulses, production by single pulse is desirable, too.

For that attempt, it is necessary to rise the power of the excimer laser or the sensitivity of the detection of the scattered light. The former may destroy the products, so the latter is better.

The measured size distribution was different in some respects from the results obtained in the case that aerosol was produced by continuous exposure to UV radiation as in Chapter 3. The sharpening of the distribution for large T is not found. The distribution was developed rapidly in the initial brief time (about less than 30 sec), then it was spread broadly and its wing reached the radii no less than 0.3 μm.

The comparison with the Brownian condensation theory is not achieved, for the quantitative discussion is difficult because of the convection. As the power of the KrF laser is concentrated in narrow wavelength range, the convection caused by the heating up of the wall of the cell or that of the air in the cell is effectively suppressed compared with the case that the radiation from the D_2-lamp is applied directly without filtering. However the suppression seems to be not enough for the experiment of this type. The measure to suppress the convection is necessary. The cell with temperature gradient may be effective.

CHAPTER 5

INFLUENCE OF OXYGEN IN SURROUNDING GAS AND CHLORINE IN RAW MATERIAL ORGANIC COMPOUND ON AEROSOL FORMATION

5.1 Introduction

In Chapter 2, we studied the aerosol formation from twenty kinds of organic compounds under three different experimental conditions: (1) exposure to UV radiation from a D_2-lamp, which radiates UV radiation of continuous spectrum from 180 to 400 nm in wavelength; (2) exposure to UV radiation from a KrF excimer pulse laser, which radiates UV radiation of monochromatic spectrum with wavelength 249 nm; (3) exposure to ozone (O_3) in the absence of UV radiation.[51] According to the experimental results obtained in Chapter 2, we can classify the compounds into four types.

Type 1 is active to both UV radiation from the KrF laser and ozone. Aniline, phenol, styrene, α- and β-pinene, isoprene and limonene belong to this type. In this case, not only the process related to ozone but also the process related to UV light absorption concurrently proceed.

Type 2 is active to UV radiation from the KrF laser but inactive to ozone. This type consists of benzene, chlorobenzene, o- , m- and p-dichlorobenzene, naphthalene, toluene and xylene. They are aromatics. There is no compound of this type belonging to terpenes. In this case, the process related to ozone is not dominant. The process related to UV light absorption including the wavelength of 249 nm must be essential.

Type 3 is inactive to the KrF laser but active to ozone. In this case, the absorption of UV light by organic compounds is not essential. The reaction with ozone produce aerosol. However, as far as we know, there is no compound belonging to this type.

Type 4 is inactive to both UV radiation from the KrF laser and ozone. This group consists of benzoic acid, diphenyl, cyclohexane, camphene and camphor. The process related to the UV light absorption with wavelengths shorter than 249 nm must be essential. Ozone has nothing to do with aerosol production at least in the beginning.

It must be possible to determine more directly and more clearly whether the presence of oxygen (O_2), which is also the origin of O_3, plays major roles in the photochemical aerosol formation or not.

In this chapter, we attempt to answer the question more directly than in Chapter 2. We will report on the aerosol formation experiments using a fully airtight cell filled with pure argon (Ar) gas. In the cell, the pressure of remaining O_2 is less than about 10^{-5} torr. We test p-dichlorobenzene and α-pinene, and observe whether the aerosol is produced or not. The UV radiation source used here is the D_2-lamp.

In addition to the experiment above, we try to identify the products from p-dichlorobenzene and α-pinene by gas-chromatograph-mass-spectroscopy (GCMS) and infrared-spectroscopy (IR). If O_2 is indispensable in aerosol formation, the traces of O_2 must be found in the products.

One more experiment will we present here. The aerosol producibility of p-dichlorobenzene is the highest among the compounds we tested in Chapter 2. From the observation by eyes, it

seems that aerosol producibility of p-dichlorobenzene is excellent compared with other compounds when exposed to UV radiation. However, as far as we know, there is no report which refers to the high aerosol producibility of p-dichlorobenzene so far.[14)]

Comparing p-dichlorobenzene with other compounds, we notice that the peculiar feature of p-dichlorobenzene is to include chlorine (Cl) in the molecule.

As to the role of Cl in photochemical reactions, a interesting and significant problem is recently presented recently. Freons ($CFCl_3$, CF_2Cl_2), which are very stable compounds and are widely used as a coolant of refrigerator or a gas of splay, go into the upper atmosphere of 30~40 km in altitude, where they absorb UV radiation of short wavelengths in solar radiation and dissociate to be ClO_x (x=0,1), i.e.

$$\text{Freons} + h\nu \cdots\rangle ClO_x . \qquad (5.1)$$

The Cl radical produced in this way reacts with O_3 in the ozone layer as

$$O_3 + Cl \text{ ---}\rangle O_2 + ClO \qquad (5.2)$$

and

$$O + ClO \text{ ---}\rangle O_2 + Cl . \qquad (5.3)$$

As Cl plays a role of catalysis, there is a fear that Cl effectively destroys the ozone layer in spite of its very small amount. As a result of destroy of ozone layer, injurious UV radiation of short wavelengths may reach the ground and/or the heat balance of the earth may be broken.[20)]

It may be possible that the Cl in the compound such as p-dichlorobenzene also plays a similar significant role and con-

tributes largely to aerosol formation in the organic aerosol formation.

To study the aerosol producibilities of chlorides, we examined the aerosol formation from mono-(C_6H_5Cl), di-($C_6H_4Cl_2$), tri-($C_6H_3Cl_3$), tetra-($C_6H_2Cl_4$) and hexachlorobenzene (C_6Cl_6) by UV radiation. The aerosol producibility of each compound is evaluated by the measurement of light scattering from produced particles. The method to measure light scattering is the same as used in Chapter 3 and 4.

5.2 Aerosol Formation Experiments under Several Conditions

5.2.1 Aerosol Formation from p-Dichlorobenzene and α-Pinene in Pure Argon Gas

The experimental setup is shown in Fig. 5.1. All tubing is made of pyrex glass except for the window of the cell, which is made of quartz transparent to UV radiation of wavelengths longer than 180 nm. The cell volume is about 100 cc. All removable joints keep airtightness by viton O-rings, and all stopcocks C1~C4 are teflon cocks in order to avoid the use of stopcock grease. There is a report that even silicon grease has an influence upon the aerosol formation.[31] We assured in the preliminary experiment that the vapor of silicon grease produced aerosol in spite of its very low vapor pressure when exposed to UV radiation from the D_2-lamp. In addition, liquid of α-pinene, which we will test in this experiment, dissolves silicon grease, as a result, the stopcocks become fixed, and the experiment becomes impossible.

First all the tubing and the cell are pumped down and baked. Especially the inner wall of the cell is exposed to the UV

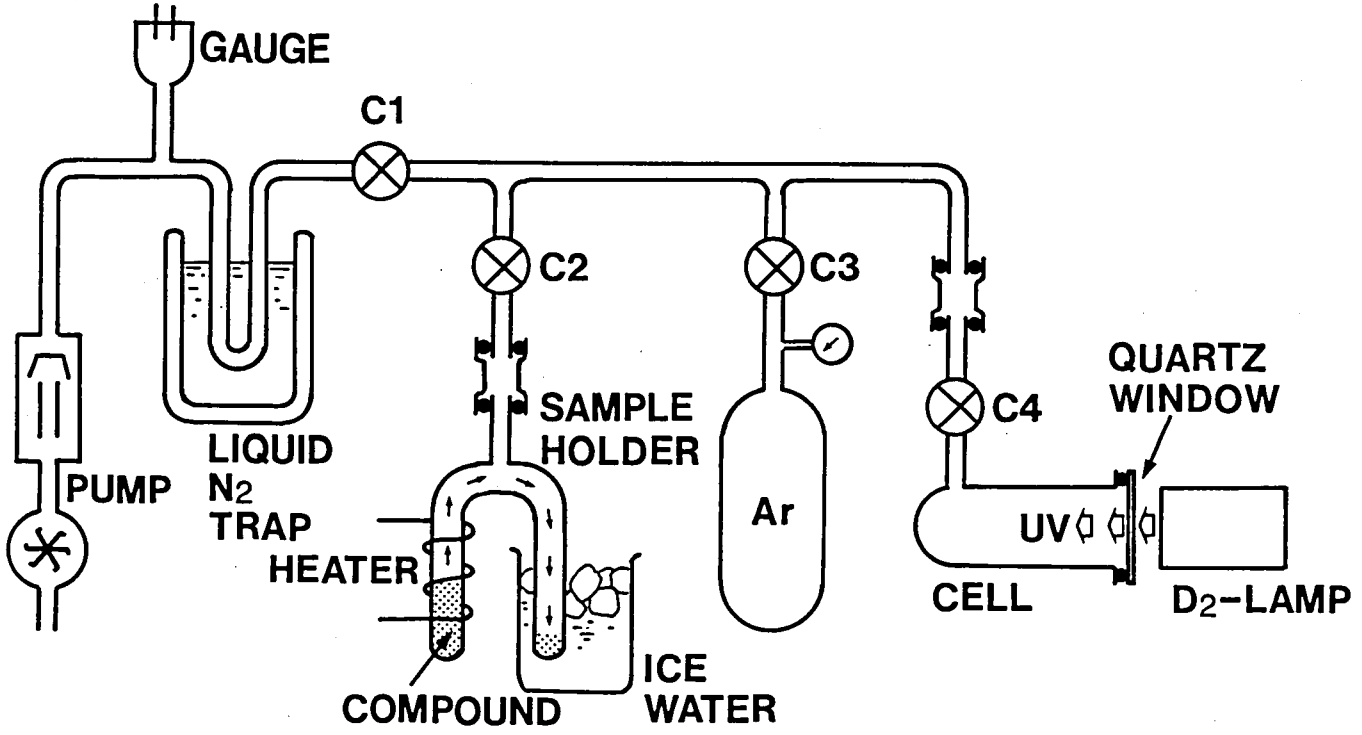

Fig. 5.1 Experimental setup for aerosol formation in pure argon gas. Symbols C1~C4 represent stopcocks.

radiation applied through the quartz window from the D_2-lamp, and cleaned. The pressure of remaining gas finally reaches 4×10^{-6} torr.

Then we shut C3 and C4, leak the air into the sample holder and remove it. We first put p-dichlorobenzene of about 5 g in the sample holder, then install it again. Opening C1 and C2, we exhaust the air from p-dichlorobenzene. After fully pumping down, we close C2, cool the empty branch of sample holder by ice water and heat the branch containing p-dichlorobenzene by ribbon heater. Then p-dichlorobenzene becomes to move to the cooled branch by sublimation. During the movement, the air in the solid of p-dichlorobenzene is released. When the movement is completed, we open C2 and pump down the sample holder. Repeating this operation 5~10 times, we can make the pressure of remaining gas about 4×10^{-6} torr.

Then we close C1 and open the C2 and C4. Cooling the wall of the cell by ice, we condense a small amount of p-dichlorobenzene onto the wall of the cell. Then we close C2, open C3 and fill the cell with pure Ar gas at about 1 atm, at room temperature. After closing C4, we apply UV radiation from the D_2-lamp into the cell and observe whether aerosol is produced or not.

After testing p-dichlorobenzene, we disassemble the tubing to pieces. In order to remove p-dichlorobenzene we wash the cocks, the joints, the cell and the sample holder by acetone, ethanol and pure water, then fully dry them. We dispose other glass tubing off and reconstruct the system with new pyrex glass tube, for it is difficult to remove the p-dichlorobenzene deposited on the wall of the tubing glass. Using the newly con-

structed system, we next test α-pinene similarly.

5.2.2 Identification of Products from p-Dichlorobenzene and α-Pinene

To identify the products, we prepare the sample for analysis by the procedure shown in Fig 5.2. We put a sample (p-dichlorobenzene or α-pinene) in the 50 cc beaker and apply UV

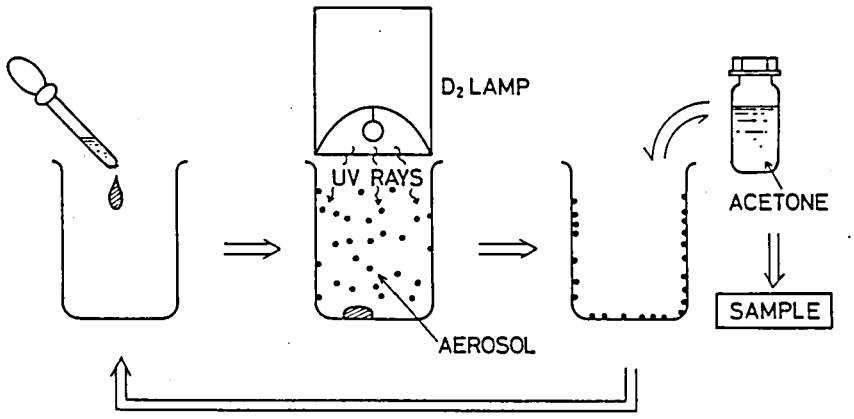

Fig. 5.2 Preparation of sample for gas-chromatograph-mass-spectroscopy.

radiation from the D_2-lamp. After an hour exposure to UV, we wash out the products deposited on the wall of the cell by acetone. Repeating this operation, we condense the products in the acetone. The sample is analyzed by GCMS. The preparation of the sample for GCMS is not done in the pure Ar, but in the usual air.

5.2.3 Aerosol Formations from Mono-, Di-, Tri-, Tetra- and Hexachlorobenzene

In order to evaluate the aerosol producibilities of kinds of

chlorobenzenes, we measure the intensities of the light scattered by aerosol particles which are produced from mono-; 1,4 di-(para-); 1,2,3 tri-; 1,2,4,5 tetra- and hexachlorobenzene by UV radiation.

The experimental setup is the same as used in Chapter 3 (Fig. 3.7). The UV radiation from the D_2-lamp is made monochromatic through the monochromator tuned at 220 nm in wavelength, then applied into the call, which contains a small amount of compound in it. The monitor beams from the Ar^+ laser (λ=457.9 nm) and the He-Ne laser (λ=632.8 nm) are applied into the cell from the antiparallel direction of the UV radiation irradiation. The intensities of the scattered light are detected by photomultiplier from the direction with the angle 90° from the direction of the propagation of monitor beams, and recorded.

We compare the aerosol producibility of each compound based on the intensity of the scattered light. This time, we do not attempt to estimate the particle size distribution.

5.3 Experimental Results and Discussions

5.3.1 Influence of the Presence of Oxygen on Aerosol Formation and Constituents of Products

As to the results of experiments with pure argon gas, the aerosol formation from p-dichlorobenzene was observed. A large amount of aerosol was produced in a few minutes after the D_2-lamp on. After two hours exposure to UV light, a large amount of aerosol was observed floating in Ar gas in the cell.

On the other hand, for the case of the aerosol formation from α-pinene, a large amount of aerosol was similarly produced within a few minutes after the beginning of UV irradiation, but

most of it disappeared in thirty minutes in spite of continuous exposure to UV radiation. After two hours exposure of UV, only small amount of aerosol was observed floating in the cell. Then we turned the D_2-lamp off. An hour later, after assuring that there is no aerosol observed in the cell, we again turned the D_2-lamp on. Then a large amount of aerosol was reproduced within a few minutes. However, one hour later, the aerosol disappeared again in spite of continuous exposure to UV radiation. When the most of aerosol disappeared, we leaked the cell and introduced air in it. Then the aerosol appeared again and it did no longer disappear after two hours exposure to UV radiation.

The results from GCMS shows two kinds of pinene-monoxides, α-campholene aldehyde and iso-pinocamphene (both are $C_{10}H_{16}O$) are found in the products from α-pinene. From the preliminary analysis by IR, >C=O and -O-H bonds were found in the products from α-pinene, which supports the results from GCMS.

As to the products from p-dichlorobenzene, we could not separate the constituents from the sample except for the raw material by gas-chromatography (GC).

Based on the results obtained above, we conclude as follows. As to the aerosol from p-dichlorobenzene, the presence of O_2 is not indispensable for aerosol formation, which is consistent with the conclusion in Chapter 2, that is, the UV light absorption of p-dichlorobenzene mast be the beginning of aerosol formation and O_2 or O_3 plays no significant role.

To the contrary, as to the aerosol formation from α-pinene, the presence of O_2 seems to be essential. According to the conclusion in Chapter 2, the aerosol formation from α-pinene includes two processes, the one related to O_3 and the other having

no concern with O_3 but related to UV light absorption. The results obtained here that the aerosol is produced in the absence of O_2 is consistent with the conclusion in Chapter 2, i.e. there is a process which proceeds without O_3 in addition to the process related to O_3. However, the products produced in the absence of O_2 seems not to be stable, for the aerosol produced in the absence of O_2 disappears soon. To obtain the stable products, the presence of O_2 is necessary. The products may be stabilized by oxidation.

The reaction in the absence of O_2 seems to be reversible, for the aerosol becomes reproducible after an hour lights-out. The aerosol in the absence of O_2 may be stable only under a thermal unequilibrium state, for example, under a large gradient of temperature in the cell. When the cell is uniformly heated up by the radiation from the D_2-lamp, the aerosol is no longer stable and disappears.

Though there is a report that pinene trioxides are found in the smog chamber experiments with pinene simulating photochemical smog,[14] this work is the first report of monoxide of α-pinene as far as we know. Anyway the stable constituents of products from α-pinene are oxides.

To the contrary, we failed in identifying the products from p-dichlorobenzene. The solution of p-dichlorobenzene in acetone is colorless and transparent, whereas the acetone which dissolves the products from p-dichlorobenzene is colored a little brown, which shows some constituents of products are in solution. However we could not separate them by GC. The constituents may be too heavy to be analyzed by GC.

We will present one more remark as to the influence of sur-

rounding gas on aerosol formation. Results from Chapter 3, especially from Sec. 3.4.8, suggests that the influence of surrounding gas is as pure N_2, air, pure O_2 in order of the amount of produced aerosol or the velocity of aerosol growth. Though the experiment in Chapter 3 is devoted to aerosol from p-dichlorobenzene, this tendency is general for any compound, and is independent of the types of compounds. Even when the compound to be tested is α-pinene, the velocity of aerosol production in pure O_2 (~ 1 atm in pressure) is much slower than in air or in pure N_2. It is easily assured by eyes without any quantitative measurement that the aerosol production is extremely delayed in pure O_2. As shown in Fig. 3.13, where (a), (b) and (c) are respectively in the cases that the surrounding gas is air, N_2 and O_2, the total volume of aerosol which is finally produced does not differ for each case of pure N_2, air and pure O_2. The effect of the presence of O_2 seems to delay the aerosol growth.

The scattering cross section of O_2 or O_3 in the wavelength range we concerned is too small to explain the delay by UV light absorption. IN other words, it is unlikely that UV light absorption of O_2 or O_3 weakens the intensity of UV, as a result, the photochemical reaction to produce aerosol is suppressed. Therefore, in the aerosol production system containing dense O_2 (~ 1 atm in pressure), there must be a certain photochemical mechanism to delay aerosol growth. For example, O radical produced photochemically from O_2 (see Eq. (2.4)) may destroys the products or other indispensable species such as OH.

5.3.2 Influence of Chlorine in Benzene Chlorides on Aerosol Formation

The temporal change of the light intensities scattered by aerosol particles produced from mono-, di-, tri-, tetra- and hexachlorobenzene are shown in Fig. 5.3. The scattered light intensity $I^{Obs}_{\mu,\lambda}$ in Fig. 5.3 are defined as same as in Chapter 3 (see Eq. (3.20)), but the unit is arbitrary one, for we could not compare these five cases quantitatively. When the experimental condition for 1,4 dichlorobenzene was as same as for other compounds, the scattered light was too strong to be measured. Then we unwillingly made the slit width of the monochromator narrower in order to decrease the power of incident UV radiation. Other experimental conditions are same for each case. The slit width was 1.0 mm for 1,4 dichlorobenzene and 1.5 mm for others. Even with such a handicap, aerosol producibility of dichlorobenzene is excellent. We conclude that the aerosol producibilities of these compounds are as follows. The aerosol producibility of dichlorobenzene is excellent. Then those of mono- and trichlorobenzene follow in this order. The producibilities of tetra- and hexachlorobenzene are much inferior compared with those of other three. In the cases of tetra- and hexachlorobenzene in Fig. 5.3, $I^{Obs}_{\mu,\lambda}$ randomly fluctuates, which suggests that little amount of aerosol was produced and the signal of the scattered light is buried in the noise. However, when the UV radiation from the D_2-lamp is applied directly without any filtering large amount of aerosol is also produced from tetra- and hexachlorobenzene.

The compound that includes more number of Cl atoms in its

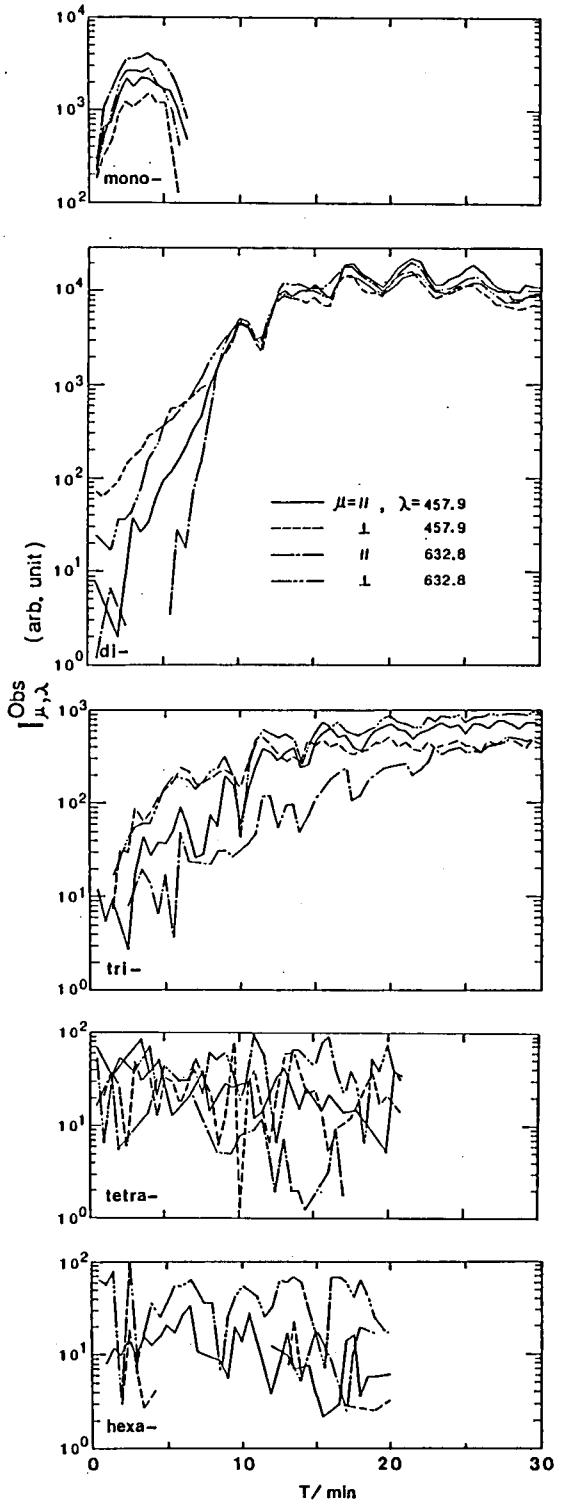

Fig. 5.3 Temporal changes in scattered light intensities $I^{Obs}_{\mu,\lambda}$ for aerosols produced from mono-, di-, tri-, tetra- and hexachlorobenzene by ultraviolrt radiation with wavelength 220 nm.

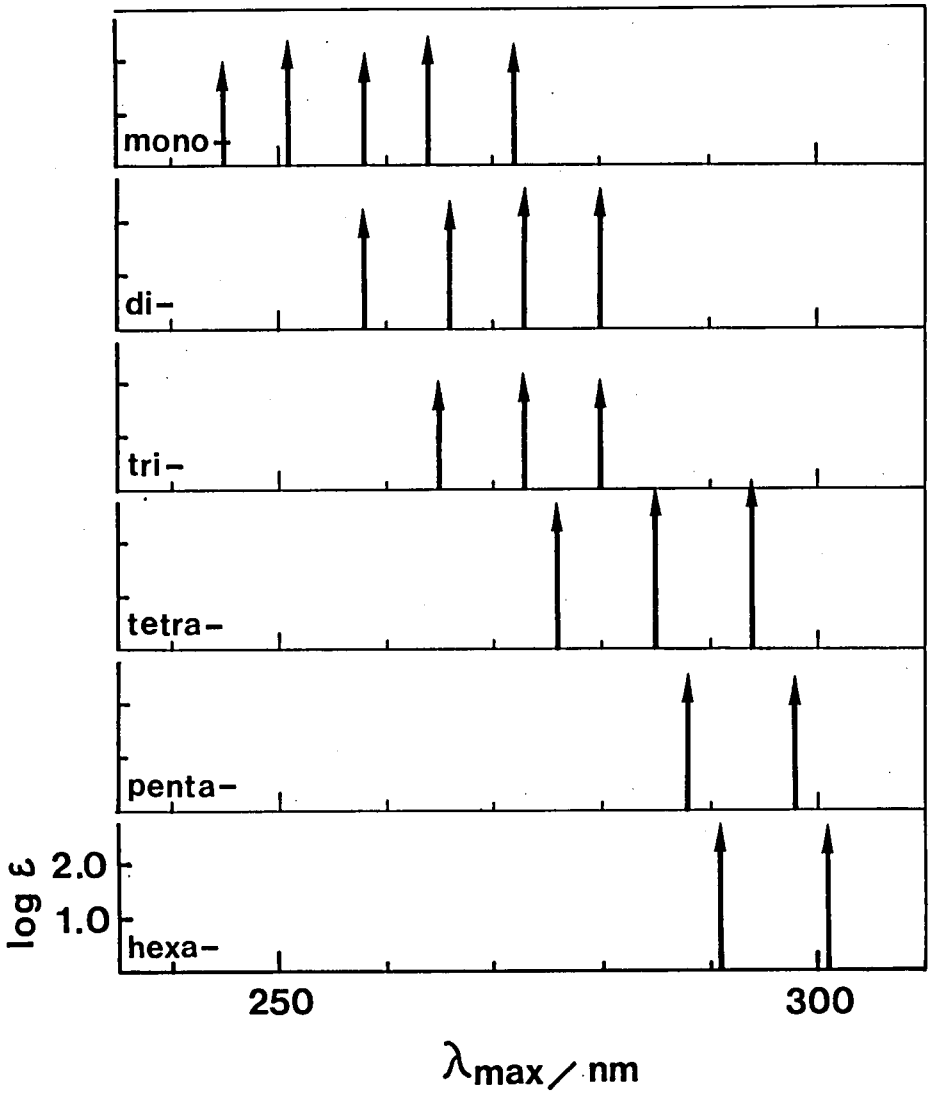

Fig. 5.4 Light absorption of kinds of benzene chlorides (mono-, di-, tri-, tetra-, penta- and hexachlorobenzene) in ultravioret range, which shows that the logarithm of molar absorption coefficient ε takes the maximum value log ε at wavelength λ_{max}.

molecule do not necessarily produce larger amount of aerosol. Figure 5.4 shows the λ_{max} and log ε for each compound, which represents that the logarithm of molar absorption coefficient ε takes the maximum value log ε at wavelength λ_{max}. As the number of Cl included in a molecule increases, the band of UV light absorption shifts to longer wavelengths. Under our experimental conditions, the wavelength of incident UV radiation is fixed at 220 nm. If the distance between λ_{max} and the wavelength of incident UV is dominant, monochlorobenzene must give the highest aerosol producibility. However, the log ε and λ_{max} do not mean the true maximum but the local maximum. In general, strong UV light absorption of aromatics such as chlorobenzenes spreads broadly at about 200 nm in wavelength. Therefore the low aerosol producibility of the compound which contains many Cl atoms in its molecule cannot be explained from the position of λ_{max}. The geometrical feature of dichlorobenzene must give the high aerosol producibility. Therefore it may be interesting to study aerosol producibilities of o-, m- and p-dichlorobenzene quantitatively. On the other hand, the role of Cl dose not clear yet.

5.4 Conclusions

In the aerosol formation from p-dichlorobenzene, the presence of O_2 plays no significant role. In the absence of O_2, a large amount of aerosol is produced and the products are fully stable.

On the other hand, the aerosol produced from α-pinene in the absence of O_2 is not stable and disappears soon. To stabilize it, the presence of O_2 in the surrounding gas is indispensable. The stability of products may be caused by oxidation.

Two kinds of pinene-monoxide, α-campholene aldehyde and iso-pinocamphene were found in the products from α-pinene, which is consistent with the the conclusion obtained above. On the other hand, we could not identify the constituents of products from p-dichlorobenzene.

The aerosol producibility of dichlorobenzene is the highest among five chlorobenzenes tested here. Then those of mono- and trichlorobenzene follow. The aerosol producibilities of tetra- and hexachlorobenzene are much lower than those of previous three. The number of Cl in a molecule seems not to correlate the aerosol producibility. The geometrical feature of molecule may be more dominant.

CHAPTER 6

CONCLUSIONS

In this thesis, we have reported on the aerosol formation from organic compounds by ultraviolet (UV) radiation. Twenty kinds of organic gases produce aerosol when exposed to UV radiation. Typical compound is, for example, p-dichlorobenzene. The effective wavelengths of UV radiation are shorter than about 310 nm, and their long limits differ a little for each compound. These effective wavelengths are much shorter than that of photochemical smog.

We have used a UV light source of continuous spectrum (a D_2-lamp; $180<\lambda<400$ nm) and a monochromatic source (a KrF excimer laser; $\lambda=249$ nm), then compared the difference of aerosol formation in each case. We have also studied the aerosol producibility of each compound with ozone in the absence of UV radiation.

As to the aerosol produced from p-dichlorobenzene, we have studied in detail the particle size distribution and its temporal change in both cases of continuous exposure to UV radiation (from the D_2-lamp) and brief exposure at the beginning (from the KrF laser).

We have also examined the aerosol formation from p-dichlorobenzene and α-pinene in pure argon gas to study the role of O_2 in photochemical process.

Then we have tried to identify the products in aerosol produced from p-dichlorobenzene and α-pinene. In addition, in order to study the role of chlorine in raw material molecule, we

have studied the aerosol producibilities of several kinds of benzene chlorides (mono-, di-, tri-, tetra- and hexachlorobenzene).

In Chapter 1, we have presented a brief review of the natural and artificial aerosols. We have introduced the aerosol of our main interest, the aerosol formation from organic gases by UV radiation. The outline of this thesis has been explained.

In Chapter 2, we have reported on the aerosol formation experiments using a D_2-lamp and a KrF laser. In addition to the experiments using these sources of UV light, we have studied whether aerosol was produced or not by reaction with O_3 in the absence of UV radiation. As a result, we found that twenty kinds of organic compounds produced aerosols when exposed to UV radiation of continuous spectrum from the D_2-lamp. The effective wavelengths of UV radiation are different for each compound, but their long limits are not longer than about 310 nm. We have presented the classification of them according to the activity to O_3 and UV radiation from the KrF laser, and discussed the difference of process in each case.

Type 1 is active to both UV radiation from the KrF laser and O_3. Aniline, phenol, styrene, α- and β-pinene, isoprene and limonene belong to this type. The aerosol formation of this type includes two different processes, the one is that the UV light absorption of organic compound is essential, and the other is that O_3 produced photochemically from O_2 in the air reacts with organic compound and produces aerosol.

Type 2 is active to UV radiation from the KrF laser but inactive to O_3. The absorption band of organic compound including 249 nm, the wavelength of the KrF laser, must be essen-

tial. This type consists of benzene, chlorobenzene, o- , m- and p-dichlorobenzene, naphthalene, toluene and xylene. They are aromatics. There is no compound of this type belonging to terpenes.

Type 3 is inactive to the KrF laser but active to O_3. However, as far as we tested, there is no compound belonging to this type.

Type 4 is inactive to both the KrF laser and O_3. This group consists of benzoic acid, diphenyl, cyclohexane, camphene and camphor. The UV absorption band of wavelengths shorter than 249 nm must play major role. Ozone has nothing to do with aerosol production at least in the beginning.

In Chapter 3, we have reported on the optical measurements for the particle size distribution of aerosol produced from p-dichlorobenzene by UV radiation with wavelength 220 nm (almost monochromatic), with power density about 1 mW/cm^2. The method is based on the measurement of the wavelength- and polarization-dependence of the light scattered by particles.

Generally the assumed functions such as the Gauss, the Log-normal and the Stevenson seem to be superior in giving good fitting to particle size distribution and in estimating several moments of distribution function such as total number, radius, surface and volume. The Junge and the Modified exponential are also useful partially.

The illustration of aerosol formation in the air is as follows. For $T<6$ min, where T represents the time after the beginning of UV light irradiation, the aerosol formation is homogeneous. The number of particles rapidly rises up until it reaches the peak at $T\sim6$ min. At the peak, the number density of

particles, most of which consists of particles of radii smaller than 0.1 μm, is more than about 3×10^6 particles/cm^3. For T>6 min, particles grow mainly by coalescence. The total number density of particles decreases, whereas the total volume density increases until T~13 min. It is due to the deposition of products onto surface of particles, that is, the growth of particles is partially heterogeneous. The distribution function becomes broader and broader until T~10 min, then it becomes narrower again. For T~13 min, the increase of total volume is saturated at 1.7×10^4 μm^3/cm^3, where the most frequent radius is about 0.2 μm and the total number is about 7×10^5 particles/cm^3. The breadth of distribution becomes narrower and narrower. For large T, the distribution is near monodisperse, where most frequent radius is about 0.2 μm, the total number and volume are 5×10^5 particles/cm^3 and 1.5×10^4 μm^3/cm^3 respectively. The largest radius seems to be restricted by gravitational settling. At this stage, the loss by gravitational settling and the gain by photochemical production of particles almost balance.

In Chapter 4, we have reported on the aerosol formation from p-dichlorobenzene induced by brief exposure to UV radiation from a KrF excimer laser. We studied the temporal change of its particle size distribution in detail. The method was the same as used in Chapter 3.

Unlike the experiment reported in Chapter 3, we initially produced the condensable species in a brief time by applying the several pulses of UV light from the KrF excimer laser into the vapor of p-dichlorobenzene, then observed the change of scattered light intensity without any more applying UV radiation.

Under such a condition, it was expected that the

monodispersed distribution which was composed of initially produced condensable species was first built up, then it was developed into broadly dispersed distribution by condensation or other mechanisms of aerosol growth.

Contrary to our expectation, we could not observe the process because the process was very quick and was completed during the brief time of applying UV radiation. At the beginning of measurement, the size distribution had been already heterodispersed.

The measured size distribution was different from that obtained in Chapter 3 in some respects. The sharpening of the distribution for large T was not found. The distribution developed rapidly in the initial brief time (about less than 30 sec), then it spread broadly and its wing reached the radii of 0.3 μm. The distribution observed was fluctuated due to convection.

In Chapter 5, we have reported on the several experiments in order to study the influences of the presence of O_2 in surrounding gas and the presence of chlorine in row material molecule on aerosol formation. We have performed the aerosol formation experiments by UV radiation with p-dichlorobenzene and α-pinene in pure argon gas of about 1 atm in pressure in order to study the influence of O_2. We have also produced aerosol from several kinds of benzene chlorides (mono-, di-, tri-, tetra- and hexachlorobenzene) by UV radiation and have evaluated their aerosol producibilities by measuring the light scattering intensities from aerosol particles. In addition to these experiments, we have tried to identify the constituents of products from p-dichlorobenzene and α-pinene be gas-chromatograph-mass-

spectroscopy.

For the aerosol formation from p-dichlorobenzene, the presence of O_2 plays no significant role. In spite of the absence of O_2, a large amount of aerosol was produced and the products were fully stable. On the other hand, the aerosol produced from α-pinene in the absence of O_2 was not stable and disappeared soon. To stabilize it, O_2 is necessary and the stability of products may be caused by oxidation for the case of α-pinene.

Two kinds of pinene-monoxide, α-campholene aldehyde and iso-pinocamphene were found in the products from α-pinene. On the other hand, we could not identify the constituents of products from p-dichlorobenzene.

The aerosol producibility of dichlorobenzene is the highest among five kinds of benzene chlorides tested here. Then those of mono- and trichlorobenzene follow. The aerosol producibilities of tetra- and hexachlorobenzene are much lower than those of previous three. The number of Cl in a molecule seems not to correlate the aerosol producibility. The geometrical feature of molecule may be more dominant.

REFERENCES

1) U. S. Standerd Atmosphere, 1976, ed. by National Oceanic and Atmospheric Administration, National Aeronautics and Space Administration, United States Air Force (Washington, D. C., October 1976) p. 46.

2) K. Willeke and K. T. Whitby, J. Air Pollution Control Assoc. **25**, 529 (1975).

3) S. K. Friedlander, Smork, Dust and Haze (John Wiley & Sons, Inc., 1977).

4) K. Takahashi, Kiso Earozoru Kogaku (Yokendo, Tokyo, 1978) [in Japanese].

5) Y. Misaki, S. Nakatani, and K. Naito, Kisho Kenkyu Noto (Nippon Kisho Gakkai, Tokyo, 1982) No. 142 [in Japanise].

6) E. K. Bigg, J. Atmos. Sci. **33**, 1080 (1976).

7) S. C. Mossop, Nature **199**, 325 (1963).

8) F. W. Went, Nature **187**, 641 (1960).

9) D. R. Fitz, M. C. Dodd and A. M. Winer, Proceedings of the 74th Annual Meeting of the Air Pollution Control Association, 81-27.3, Philadelphia, Pennsylvania, June 21-26, 1981.

10) R. R. Arnts, W. B. Petersen, R. L. Seila and B. W. Gay, Proceedings of the 74th Annual Meeting of the Air Pollution Control Association, 81-27.4, Philadelphia, Pennsylvania, June 21-26, 1981.

11) R. A. Rasmussen and F. W. Went, Proc. Nat. Acad. Sci. **53**, 215 (1965).

12) F. W. Went, Tellus **18**, 549 (1966).

13) K. Kamiyama, T. Takai and Y. Yamanaka, Proceedings of the International Clean Air Conference, Brisbane, Australia, May

15-19 (Ann Arbor Science Publishers, Inc., Michigan, 1978) p. 365

14) Ozone and Other Photochemical Oxidants, ed. by National Research Council, Div. Medical Science, Medical and Biologic Effects of Environmental Pollutants. (Natl. Acad. Press, Washington, 1977) Chap. 3.

15) Wm. E. Wilson, Jr., D. F. Miller, A. Levy and R. K. Stone, J. Air Poll. Control Assoc. **23**, 949 (1973).

16) G. M. Hidy with B. R. Appel, R. J. Charlson, W. E. Clark, S. K. Friedlander, D. H. Hutchison, T. B. Smith, J. Suder, J. J. Wesolowski, K. T. Whitby, J. Air Poll. Control Assoc. **25**, 1106 (1975).

17) T. Ohen, Sci. Am. (Apr. 1982).

18) T. Sato, T. Yabuzaki and T. Ogawa, Jpn. J. Appl. Phys. **21**, 1599 (1982).

19) M. Born and E. Wolf, Principles of Optics, (Pergamon, Oxford, 1962) p. 633~664.

20) T. Shimasaki, Sci. Am. (Aug. 1977).

21) Taiki no Hikari Kagaku, ed. by S. Suzuki (Tokyo Daigaku Syuppan, Tokyo, 1979) [in Japanese].

22) R. D. Cadle, J. Colloid Interface Sci. **39**, 25 (1972).

23) A. C. Tam, G. Moe, and W. Happer, Phys. Rev. Lett. **35**, 1630 (1975).

24) A. C. Tam, W. happer and D. Siano, Chem. Phys. Lett. **49**, 320 (1977).

25) T. Yabuzaki, T. Sato, and T. Ogawa, J. Chem. Phys. **73**, 2780 (1980).

26) N. Nakashima, H. Inoue, M. Sumitani and K. Yoshihara, J. Chem. Phys. **73**, 4693 (1980).

27) N. Nakashima, H. Inoue, M. Sumitani and K. Yoshihara, J. Chem. Phys. **73**, 5976 (1980).

28) N. Nakashima and K. Yoshihara, Bull. Chem. Soc. Jpn. **55**, 2783 (1982).

29) N. Nakashima and K. Yoshihara, J. Chem. Phys. **79**, 2727 (1983).

30) Y. K. Wei and R. J. Cvetanović, Can. J. Chem. **41**, 913 (1963).

31) J. P. Friend, R. Leifer and M. Trichon, J. Atmos. Sci. **30**, 465 (1973).

32) R. B. Husar and K. T. Whitby, Environ. Sci. Technol. **7**, 241 (1973).

33) M. J. Prager, E. R. Stephens, and W. E. Scott, Ind. Eng. Chem. **52**, 521 (1960).

34) Wm. E. Wilson, Jr., E. L. Merryman, A. Levy and H. R. Taliaferro, J. Air Poll. Control Assoc. **21**, 128 (1971).

35) L. A. Ripperton and D.Lillian, J. Air Poll. Control Assoc. **21**, 629 (1971).

36) Wm. E. Wilson, Jr., A. Levy and D. B. Wimmer, J. Air Poll. Control Assoc. **22**, 27 (1972).

37) R. B. Husar, K. T. Whitby, and B. Y. H. Liu, J. Colloid Interface Sci. **39**, 211 (1972).

38) T. Yabuzaki, M. Watanabe, M. Kitano, and T. Ogawa, Rev. Laser Eng. **6**, 305 (1978) [in Japanese].

39) J. Rosinski and F. Parungo, J. Appl. Meteor. **5**, 119 (1966).

40) J. J. Bufalini and A. P. Altshuller, Can. J. Chem. **43**, 2243 (1965).

41) D. H. Stedman and H. Niki, Environ. Lett. **4**, 303 (1973).

42) S. Iwata and K. Koike, Toranjisuta Gijutsu, 312 (Sep. 1981)

[in Japanese].

43) W. N. Stasiuk, Jr. and P. E. Coffey, J. Air Poll. Control Assoc. **24**, 564 (1974).

44) S. M. Japar, C. H. Wu, and H. Niki, J. Phys. Chem. **78**, 2318 (1974).

45) T. Vrbaski and R. J. Cvetanović, Can. J. Chem. **38**, 1063 (1960).

46) I. D. Clark and J. F. Noxon, Science **174**, 941 (1971).

47) H.-R. Schulten and U. Schurath, J. Phys. Chem. **79**, 51 (1975).

48) G. Boocock and R. J. Cvetanović, Can. J. Chem. **39**, 2436 (1961).

49) G. R. H. Jones and R. J. Cvetanović, Can. J. Chem. **39**, 2444 (1961).

50) D. D. Davis, W. Bollinger and S. Fischer, J. Phys. Chem. **79**, 293 (1975).

51) T. Sekiya, T. Yabuzaki and T.Ogawa, J. Atmos. Sci. [to be published].

52) C. H. Keith and J. C. Derrick, J. Colloid Sci. **15**, 340 (1960).

53) S. E. Devir, J. Colloid Interface Sci. **21**, 9 (1966).

54) E. Willis, M. Kerker, and E. Matijević, J. Colloid Interface Sci. **23**, 182 (1967).

55) E. Matijević, K. F. Schulz, and M. Kerker, J. Colloid Sci. **17**, 26 (1962).

56) W. Heller and M. L. Wallach, J. Phys. Chem. **67**, 2577 (1963).

57) K. Takahashi, Techn. Rep. Eng. Res. Ins. Kyoto Univ. **149**, 1 (1970).

58) M. Kerker, E. Matijević, W. F. Espenscheid, W. A. Farone, and S. Kitani, J. Colloid Sci. **19**, 213 (1964).

59) E. Matijević, S. Kitani, and M. Kerker, J. Colloid Sci. **19**, 223 (1964).

60) W. F. Espenscheid, E. Matijević, and M. Kerker, J. Phys. Chem. **68**, 2831 (1964).

61) M. Kerker, E. Daby, G. L. Cohen, J. P. Kratohvil, and E. Matijević, J. Phys. Chem. **67**, 2105 (1963).

62) W. Heller and W. J. Pangonis, J. Chem. Phys. **26**, 498 (1957).

63) W. Heller, M. Nakagaki, and M. L. Wallach, J. Chem. Phys. **30**, 444 (1959).

64) M. Nakagaki and W. Heller, J. Chem. Phys. **30**, 783 (1959).

65) W. Heller and M. Nakagaki, J. Chem. Phys. **31**, 1188 (1959).

66) W. J. Pangonis, W. Heller, and N. A. Economou, J. Chem. Phys. **34**, 960 (1961).

67) H. Shimizu, T. Kobayashi, and H. Inaba, Oyo Buturi **47**, 30 (1978) [in Japanese].

68) C. E. Junge, C. W. Chagnon, and J. E. Manson, J. Meteor. **18**, 81 (1961).

69) A. F. Stevenson, W. Heller, and M. L. Wallach, J. Chem. Phys. **34**, 1789 (1961).

70) K. Shimizu and A. Ishimaru, Oyo Buturi **52**, 354 (1983) [in Japanese].

71) T. Sekiya, T. Yabuzaki and T.Ogawa, Jap. J. Appl. Phys. [to be published].

72) D. T. Gillespie, J. Atmos. Sci. **29**, 1496 (1972).

73) D. J. Jeffrey, J. Atmos. Sci. **38**, 2440 (1981).

74) C. S. Kiang, D. Stauffer, G. H. Walker, O. P. Puri, J. D.

Wise, Jr. and E. M. Patterson, J. Atmos. Sci. **28**, 1222 (1971).

75) C. S. Kiang, D. Stauffer, V. A. Mohnen, J. Bricard and D. Vigla, Atmos. Environ. **7**, 1279 (1973).

76) P. Mirabel and J. L. Katz, J. Chem. Phys. **60**, 1138 (1974).

77) J. L. Katz, C. J. Scoppa II, N. G. Kumar, and P. Mirabel, J. Chem. Phys. **62**, 448 (1975).

78) H. E. Gerber, Atmos. Environ. **2**, 117 (1968).

79) K. T. Whitby and B. Y. H. Liu, Atmos. Environ. **2**, 103 (1968).